

**Optimising the output power available from a photovoltaic panel through
empirical testing**

Asowata Osamede

210137207

**Dissertation submitted in fulfilment of the requirement for the
Magister Technologiae: Engineering: Electrical**



**Department: Electronic Engineering
Faculty of Engineering and Technology**

Vaal University of Technology

Vanderbijlpark

South Africa

Supervisor: Prof James Swart

Co-supervisor: Prof H C vZ Pienaar

Date: September 2013

Declaration

I Asowata Osamede hereby declare that the following research information is solely my own work. This dissertation is submitted for the requirement of the degree of Magister Technologiae: Engineering: Electrical to the Department of Electronic Engineering at the Vaal University of Technology, Vanderbijlpark. This dissertation has never been submitted for the evaluation at any educational institution.

Signed.....

Date.....

Acknowledgements

I hereby wish to express my gratitude to the following persons and individuals who facilitated my research and enabled this document to be completed successfully on time.

- Prof H C vZ Pienaar
- Prof James Swart

Your encouragement, motivation, guidance and support helped me in the course of this new endeavour on Photovoltaic panels (Solar Energy). Your discipline and supervision helped me to be focused and brought out the untapped ability in me.

The financial assistance of the following institutions towards this research is also hereby acknowledged.

- Research Department of Vaal University of Technology
- Telkom South Africa Ltd, TFMC Pty LTD, M-TEC and THRIP
- Staff and personnel of the Department of Electronic Engineering for the support and encouragement

Dedication

This dissertation is dedicated to God Almighty for keeping me alive and making this work a success. Also on the list are my family and my son Eniosasere Asowata.

Abstract

Einstein said, “the release of energy has not created a new problem, but has made more urgent the necessity of solving an existing one”. This dissertation presents a method of optimising the available output power from a photovoltaic (PV) panel through empirical testing as this will enable a higher yield of solar energy thereby reducing dependence on traditional energy sources such as fossil fuels. The proposed study intends using existing equations of latitude, mathematical models and simulation packages in combination with the experimental data to analyse the optimum tilt and orientation angles for PV panels. This will assist in identifying ways to improve the installation of PV panels for optimum output power in the Vaal Triangle.

Photovoltaic panels are semiconductor devices that convert incident direct beam radiation to electrical energy and the panel is composed of several unitary cells connected in series and/or in parallel. The optimisation process involves the empirical testing of the entire system with the use of existing equations of latitude as suggested by literature for PV installation in the southern hemisphere, power conditioning devices (such as an DC-DC converter, solar charger with MPPT) in order to validate results as well as the correlation of empirical results with a simulation package.

The first objective was to have an overview of the types of PV panels that exist; this was done in order to be able to make a right choice of PV panel to be used in this research. A concise literature review was carried to enable this research to have a background of existing information in the areas of optimisation of power from PV panels. The next objective was to carry out a pilot study, this was done to form the foundation for the main study. A data-logging interface circuit (DLIC) was incorporated in the system for some reasons presented in subsequent chapters of this dissertation. At the end of this study data were taken over a two year period, the data were analysed and conclusions were drawn and some recommendation in optimising available output power from a PV panel are suggested.

TABLE OF CONTENTS

Declaration	ii
Acknowledgements	iii
Dedication	iv
Abstract	v
List of Figures	ix
List of Tables	xii
Glossary of acronyms, abbreviations and symbols	xiv
Chapter 1 Introduction	1
1.1 Background	1
1.2 Problem statement	3
1.3 Objective of the research	4
1.4 Methodology	4
1.5 Delimitation	6
1.6 Significance of research	6
1.7 Overview of the report	6
1.8 Summary	8
Chapter 2 PV panels, power regulation circuits and energy storage devices	9
2.1 Introduction	9
2.2 PV systems	9

2.3	PV systems (principle of operation of photovoltaic cells)	10
2.3.1	Mono-crystalline (manufacturing process)	15
2.3.2	Poly-crystalline (manufacturing process)	18
2.3.3	Amorphous (manufacturing process)	21
2.3.4	Summary of PV cells (advantages, disadvantages and applications)	23
2.4	Power regulation circuits	25
2.4.1	Maximum power point tracker (principle of operation)	25
2.4.2	Solar chargers (principle of operation)	28
2.4.3	DC-DC converters (principle of operation)	28
2.4.4	Summary of power regulation circuits (advantages, disadvantages and application)	29
2.5	Energy storage devices	31
2.5.1	Lead acid deep discharge batteries	32
2.5.2	Nickel-Cadmium (NiCad) batteries	33
2.5.3	Nickel-Zinc Battery	34
2.5.4	Summary of power regulation circuits (advantages, disadvantages and application)	35
2.6	Summary	37
Chapter 3 Research design and experimental set-up		39
3.1	Introduction	39
3.2	Research design	39

3.3	Sampling, validity and data analysis	40
3.4	Software simulation packages for PV system designs	42
3.5	Mathematical models and equations of latitude for PV panel installations	43
3.6	Pilot Study	44
3.7	Main Study	49
3.8	Summary	52
	Chapter 4 Measurement and results	53
4.1	Introduction	53
4.2	Pilot study results	53
4.3	Main study results	66
4.4	Simulation model results	77
4.5	Summary	81
	Chapter 5 Recommendations and conclusions	82
5.1	Introduction	82
5.2	Brief overview	82
5.3	Conclusions	83
5.4	Recommendations	86
	BIBLIOGRAPHY	87
	ANNEXURE PAGE NUMBERS	100

List of Figures

Figure 1	Flow diagram of the research	7
Figure 2	A typical PV system	10
Figure 3	Schematic of a silicon crystal lattice doped with impurities to produce n-type and p-type semiconductor material	11
Figure 4	The basic model for a photovoltaic module	14
Figure 5	Types of solar cell	14
Figure 6	The Czochralski and the Float-zone (FZ) process	16
Figure 7	A cell of a mono-crystalline PV panel	17
Figure 8	Ingot-casting methods and Ribbon technique methods	19
Figure 9	A cell of a poly-crystalline PV panel	21
Figure 10	A cell of an amorphous silicon PV panel	23
Figure 11	Symbolic representation of the non-even power generation	31
Figure 12	A RITAR RA12-100 (100 Ah) LADDB	35
Figure 13	Depth of discharge for a LADDB (lead acid deep discharge battery)	37
Figure 14	Practical set-up for pilot study	48
Figure 15	SW220 poly-crystalline PV panel used in the pilot study	48
Figure 16	Practical set-up for the main study	50
Figure 17	Electrical design of the main study	51
Figure 18	Radiation conditions for the output of the DC-DC converter	54

Figure 19	Average work-time per day of the DC-DC converter (an example)	55
Figure 20	Regression analysis (linear) of the data obtained for 8 – 15 July, 2011, (12 V DC-DC converter/PV panel placed at tilt angle = 16°)	56
Figure 21	Average work-time per day 8 – 15 July, 2011 (12V DC-DC converter/PV panel placed at tilt angle = 16°)	57
Figure 22	Regression analysis (linear) of the data obtained for 17 – 24 June, 2011 (12 V DC-DC converter/PV panel placed at tilt angle = 26°)	59
Figure 23	Regression analysis (linear) of the data obtained for 10 – 17 June, 2011 (12 V DC-DC converter/PV panel placed at tilt angle = 36°)	59
Figure 24	Average work-time per day 17 – 24 June, 2011 (12V DC-DC converter/PV panel placed at tilt angle = 26°)	61
Figure 25	Average work-time per day 10 – 17 June, 2011 (12V DC-DC converter/PV panel placed at tilt angle = 36°)	61
Figure 26	Data showing reference voltages of 10 V and 18 V for the 19 February 2012	68
Figure 27	Average percentage when the system was fully charged (January – March 2012)	69
Figure 28	Average percentage when the system was fully charged (April – June 2012)	70
Figure 29	Average percentage when the system was fully charged (July – September 2012)	71
Figure 30	Average percentage when the system was fully charged (October – December 2012)	72

Figure 31	Regression analysis (linear) for 1 – 7 January, 2012 (tilt angle = 36°)	74
Figure 32	Regression analysis (linear) for 1–7 January, 2012 (tilt angle = 26°)	75
Figure 33	Regression analysis (linear) for 1 –7 January, 2012 (tilt angle = 16°)	75
Figure 34	A comparison of +15°, - 15° and 0° orientation angles with the tilt angle placed at 36°	76
Figure 35	Simulation results of 16°, 26° and 36° tilt angles obtained from the METEONORM software for the 1996 – 2005 time period	78
Figure 36	Correlation between the simulation data obtained from METEONORM and the empirical data obtained from the practical set-up	80

List of Tables

Table 1	ZKX-160D-2 module/160Wp-180Wp mono-crystalline PV panel	17
Table 2	SOLARWORLD SW 220 poly-crystalline PV panel	21
Table 3	Amorphous silicon thin film PV Panel (a-Si PV module)	23
Table 4	Advantages and disadvantages of the different types of PV panels	24
Table 5	Power regulation devices (MPPT, solar chargers, DC-DC converters)	30
Table 6	Types of batteries	36
Table 7	Simulation packages	43
Table 8	Mathematical models	44
Table 9	Suggested equations of latitude	45
Table 10	Calculation of tilt angles	45
Table 11	Tilt and orientation angles of the PV panels used in the pilot and main studies of this research	46
Table 12	Set of data for the months of April 2011 through July 2011 using 12 V, 24 V and 48 V DC-DC converters	62
Table 13	Data for a 48 V DC-DC converter	64
Table 14	Data for a 24 V DC-DC converter	64
Table 15	Data for a 12 V DC-DC converter	64
Table 16	Quarters of the year as structured for the main study	66
Table 17	Charge conditions of data taken for the week starting 19 January 2012	68

Table 18	The average fully charged percentages for the five PV systems	69
Table 19	R^2 values and PV voltages for the start of the PWM stage for each week of 2012	73
Table 20	Average of the 0° , $+15^\circ$ and -15° orientation using 36° tilt angle	76
Table 21	Set of average data from the experimental results and the solar irradiation results for the months of April through December	79

Glossary of acronyms, abbreviations and symbols

A

Ah – Amp hour

A – Amps

a-Si – Amorphous silicon

Φ – Alpha

C

$^{\circ}\text{C}$ – Degrees Centigrade

CZ – Czochralski

CO – Carbon monoxide gas

CO₂ – Carbon dioxide

cm² – Centimetre squared

cm – Centimetre

Cd – Cadmium

D

DC – Direct current

DLIC – Data Logging Interface Circuit

DOD – Depth of discharge

$^{\circ}$ – Degrees

E

EFG – Edge-film-growth

eV – Electron volts

e⁻ – Electron

exp – Exponential

F

FZ – Float Zone

H

H₂SO₄ – Sulphuric acid

I

I – Current

I_L – Light generated current

I₀ – Reverse saturation current

I_{mp} – Current at maximum power

IPA – Isopropyl alcohol

I/O – Input/output

K

KOH – Potassium hydroxide

kWh/m² – Kilowatt-hours per metres square

L

LADDB – Lead Acid Deep Discharge Battery

L.E.D – Light Emitting Diode

M

m – Metre

mm – Millimetre

mA – Milliamps

MW – Megawatt

mW – Milliwatt

MPPT – Maximum power point tracker

N

NiOOH – Nickel hydrate

NiCad – Nickel-cadmium

Na OH – Sodium hydroxide

O

Ω – Ohms

α – Orientation angle/Azimuth

P

PV – Photovoltaic

P – Power

P_{max} – Maximum power

Δp – Derivative of power

% – Percentage

PbO₂ – Lead dioxide

Pb – Sponge lead

R

R_s – Shunt resistance of the cells

R_{sh} – Series resistance of the cells

RGS – Ribbon growth on substrate

R² – R-squared

S

SiO₂ – Silicon Oxide

SWE – Staebler Wronski Effect

SOC – State of charge

T

T – Temperature

T_c – Cell temperature

U

μm – Micrometre

V

V – Volt

V_t – Thermal voltage

V_{mp} – Voltage at maximum power

Δv – Derivative of voltage

W

Wh/kg – Watt hours per kilogram

W – Watt

XY

y – Tilt angle

Z

ZnO – Zinc oxide

Chapter 1 Introduction

1.1 Background

Electrical power usage can be traced back to 1878, when Thomas Edison began work on an electric light and formulated the concept of a centrally-located power station (Sarma & Glover, 2002:5). In the United States, for example, electric energy sales have grown well over 400 times between the turn of the century and the early 1970s through the construction of power stations. Since the deregulation of the telecommunication, gas and other industries, electric power industries have undergone fundamental changes which have contributed to the welfare, progress and technological advances of mankind (El-Hawary, 2008:1-3).

Albert Einstein once stated “The release of energy has not created a new problem, it has merely made more urgent the necessity of solving an existing one” (Einstein, A. 1879 - 1955). These new problems include limited resources and greenhouse gases. The most acknowledged greenhouse gases in the production of energy from fossil fuels is carbon dioxide (CO₂) and carbon monoxide (CO) from fossil fuel combustion, leakage of methane (CH₄), and an increase in carbonaceous (soot) particles which can produce ‘Greenhouse warming’ (Bartels, Pate & Olson, 2010:8371–8384).

According to the data from the United States Department of Energy (USDOE, 2008), world population has increased over the past decades, which has led to an increase in fossil fuel consumption and CO₂ emission. Given the magnitude of US energy consumption and CO₂ emissions, federal and state policymakers have worked and are still working on climate change mitigation and renewable energy investment policies which need to be incorporated into energy and environmental legislation. Their efforts complement existing energy conservation and efficiency measures which have been the cornerstones of US energy policies since the oil embargo and price spikes of the 1970s (Dixon, McGowan, Onysko & Scheer, 2010:6398-6408).

Another policy for the reduction of carbon emission is the Energy Policy and Conservation Act of 1975 (EPCA) which marked the first significant federal policy initiative aimed at addressing rising energy prices and imports through energy conservation and efficiency measures. The Energy Independence and Security Act of 2007 (EISA) is the latest in a series of energy legislation that builds on previous laws, updates EPCA and its proponents, and puts forth new federal policies for expanding US energy conservation and efficiency technologies, tools and techniques.

The signing of a climate change memorandum of understanding between key stakeholders representing hundreds of electric utilities was the first step for electric utilities to make specific commitments to reduce greenhouse gas emissions (Sturges & Hewitt, 1995:60-70). Most of the energy used in South Africa is produced by fossil fuel power plants. It has been estimated that South Africa is responsible for 45.17% of total CO₂ emission in Africa and about 0.85% of the world CO₂ emission owing to burning of petroleum, natural gas and coal (USDOE, 2008).

The majority of stakeholders powerfully choose the improvement of a renewable energy developed cluster, in which government improves corresponding plan mechanisms that attract renewable energy companies (Krupa & Burch, 2011: 6254-6261). In recent years, the world economic growth and population increase has necessitated the need for more energy (Furkan, 2010:713-720). Energy is essentially important for the socio -economic development of developing countries, solving current energy generation problems calls for more than legislative changes, it really requires the usage of alternative energy sources.

Renewable energy sources are inexhaustible, intrinsically clean, replenishing themselves and allowing energy harvesting at a rate decided by nature (Grimmes, Ooman & Sudhir, 2008:10). Among the many types of renewable energy sources, solar energy obtained from sun is considered promising since it is comparatively more evenly distributed geographically (Chang, 2010:1954-1963). Energy from the sun, known as solar energy, drives the entire natural ecosystem on the earth and is transmitted by means of radiation through the electromagnetic spectrum (Incropera

& Dewitt, 2002:771-773). The sun has a temperature close to 5500°C at its surface and emits radiation at a rate of 3.8×10^{23} kW per second (Lovegrove & Dennis, 2006:791-802). In the quest to harness clean and cheap energy supply from the sun, a phenomenon was discovered in the early 19th century where electrical energy was generated using the photovoltaic (PV) effect (Boxwell, 2010:3).

Solar energy is converted directly into electrical energy with modules consisting of many PV cells, usually manufactured from fine films or wafers. They are semiconductor devices adept of converting incident solar energy into DC current, with efficiencies changing from 3 to 31%, depending on the light spectrum, temperature, design and the material used in the PV cell, (Farret & Simoes, 2006:129). According to Krauter (2006:2), solar cells derive their origin from one of the most important scientific developments of the 20th century which includes the winning of the Nobel Prize for the work of several of the most important scientists of that century. Max Planck, the German scientist, began the century engrossed in the problem of trying to explain the nature of light-emitting hot bodies, such as the sun. This was followed by the works of Albert Einstein, who in 1905 postulated that light was made of small ‘particles’, later called photons, each with a tiny amount of energy that depends on the photon's colour. Blue photons have about twice the energy of red photons. (Grimes *et al.*, 2008:10). PV history started in 1839, when Alexandre-Edmund Becquerel (physicist) observed that “electrical currents arose from certain light-induced chemical reactions” and similar effects were observed by other scientists several decades later (El chaar, Lamont & El Zein, 2011:2165-2175). The fall of the late 1940s saw the development of the first solid state devices in the industry this surface way for the first silicon solar cell to be developed with an efficiency of 6%.

1.2 Problem statement

There are numerous isotropic and anisotropic mathematical models, equations of latitude and simulation packages that can estimate the optimum tilt and orientation angle of a PV panel for a given latitude on earth. However, little real experimental

data or no real consistency exists with which to verify the suggested values from the mathematical models, equations of latitude and simulation packages. This at times proves problematic in the successful installation of PV panels for optimum output power. The problem therefore exists that there is no real consistency between the mathematical models, the simulation packages and experimental data for specified locations of latitude.

1.3 Objective of the research

The purpose of this study is to optimize the available output power from a stationary PV panel. This will assist in identifying ways to improve the installation of PV panels for optimum output power as well as enable a higher yield of solar energy particularly in South Africa, thereby reducing dependence on traditional energy sources, such as fossil fuels. Certain essential parameters in a PV panel must be set for optimal operating conditions. This research will address the problem of optimising the output power from a PV panel system by:

- Determining the tilt and orientation angle for optimal output power from a PV panel.
- Providing the correct power regulation of the PV system, using either a solar charger, DC-DC converter or a maximum power point tracker (MPPT).
- Analysing and evaluating the results of the experimental data with that from existing equations of latitude, mathematical models and simulation packages, to establish validity.

1.4 Methodology

In this research, the optimum power available from a PV panel would be achieved through empirical testing using software simulation packages in PV system designs, mathematical models and equations of latitude in combination with the experimental data obtained to evaluate the optimum orientation and tilt angles. Firstly, an in-depth

literature study of different types of PV panels along with their mode of operation and application is presented. Power regulation devices which include maximum power point trackers (MPPT), solar chargers and DC-DC converters are addressed. Energy storage devices which include lead acid deep discharge batteries (LADDB), Nickel-Cadmium (NiCad) batteries and Nickel-Zinc batteries are also discussed.

This will help in the selection of an appropriate PV panel, power regulation circuit, and energy storage system for the experimental setup where the empirical data will be collected. Secondly, simulation packages, mathematical models and equations of latitude used in determining optimum tilt and orientation angles for PV panels are addressed. This will be followed by the research methodology employed in the pilot study and main study.

The data logger is used for collecting voltage and current measurements which will serve as the empirical data. Quantitative data analysis will be used to measure a set of variables using a large population of randomly sampled objects as it deals with time-tested statistical tools (Hahn, 2008:1). To be quantitative, a text analysis must address the scientific question of a well-defined text population. It should also provide an answer to the question having a known probability of inaccurate aspects of the text population (Benchmarks, 2007:368).

The optimum tilt and orientation angles will be achieved by taking a number of samples for each of the tilt angles of the PV panel when placed at 16° , 26° and 36° in relation to three different orientation angles (0° , $+15^\circ$ and -15°). Rationale for these angles is presented in Chapter 3. Empirical data will be taken over a minimum period of two years and a regression analysis will be used to determine the best tilt and orientation angles for optimal output power from a stationary PV panel.

Regression analysis can be used to build models for process optimisation (Montgomery & Runger, 2011:402). Finally the results gathered from the experiments would be compared to existing simulation packages, mathematical models in combination with existing equations of latitude to establish validity.

1.5 Delimitation

This research does not involve the construction of a PV panel as well as the application of its output power to specific environments.

1.6 Significance of this research

This research will address the current need of the use of renewable energy, as this will enable a higher yield of solar energy, thereby reducing dependency on traditional energy such as fossil fuels. The future of the environment is dependent on the availability of low cost and environmentally-friendly sources of energy. Presently, non-renewable energy sources release greenhouse gases during the production of energy and have a limited supply.

Therefore, for both environmental and economic reasons, alternative energy sources must be pursued for the purposes of producing energy (Bartels, *et al.*, 2010:8371-8384). The proposed study intends using the mathematical models and simulation packages in combination with experimental data to determine the optimum tilt and orientation angles for PV panels. This will assist in identifying ways to improve the installation of PV panels for optimum output power for specific areas of latitude.

1.7 Overview of the report

This research can be divided into the literature review and the empirical test. The design of a DLIC falls under the practical set-up. Figure 1 illustrates the two stages and their relevant sections by means of a flow diagram. Chapter 2 contains an in-depth literature review of PV panels, solar chargers, DC-DC converters, MPPT and energy storage devices. The manufacturing process, mode of operation, applications, advantages and disadvantages of the aforementioned devices in terms of their application in electrical engineering and solar systems is discussed.

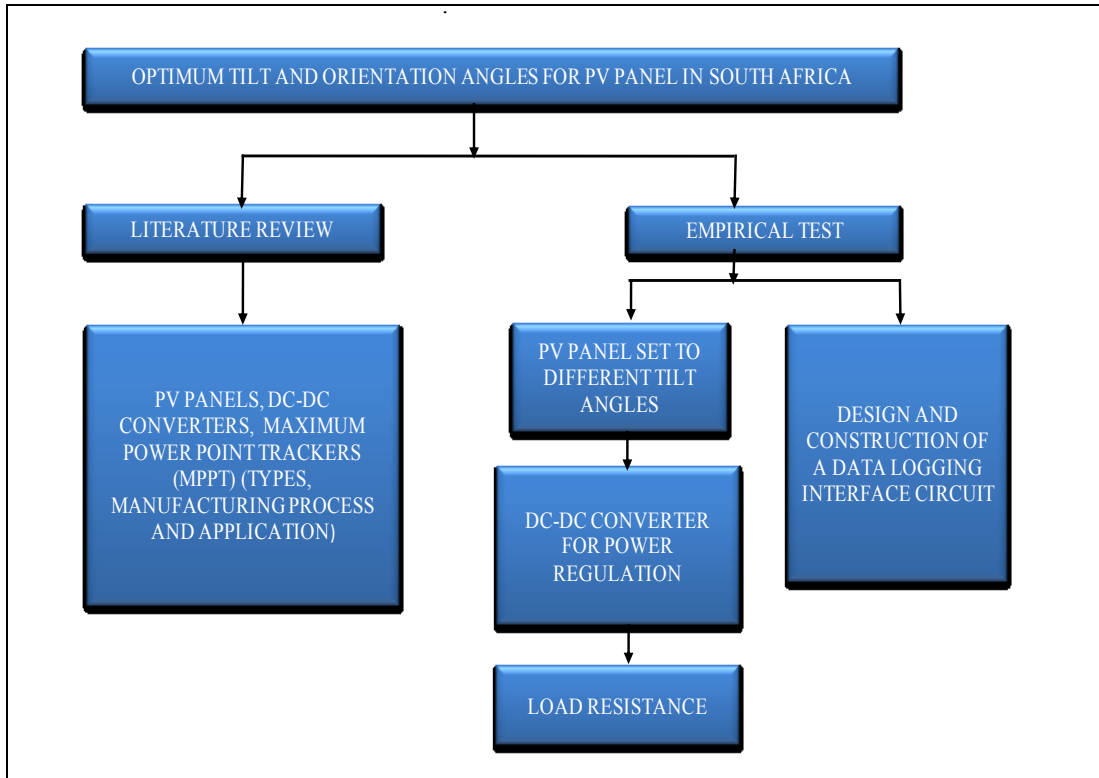


Figure 1: Flow diagram of the research

Chapter 3 contains the research methodology. Methods of optimising the output power from a stationary PV panel are addressed in this chapter. Existing equations of latitude, mathematical models and simulation packages for optimum tilt are introduced. An experimental analysis of the equation of latitude that affects the southern hemisphere as suggested by Heywood and Chinnery is done to verify the suggested values. A simulation package METEONORM is used to correlate the experimental results for specific areas of latitude. A brief overview of a DLIC is also done in Chapter 3. The experimental set-up is also validated. Analysis of data collected from the experimental setup is presented in Chapter 4. The data collected is represented in graphs and normal probability plots and is interpreted according to:

- Average on-time per week for the DC-DC converter (clear sky and no clear sky condition).
- Average on-time per day for the DC-DC converter.
- Average voltage, current, power and efficiency per week.

- A regression trend line value (linear) for the normal probability plot.
- A regression trend line value (polynomial 6) for the residual plot.

A regression analysis is done to sample a dependent variable (voltage) and an independent variable (time) between two models. The reliability of the different data with regards to the equations of latitude, the mathematical models and the simulation packages will be analysed. The final results of this analysis will be presented in Chapter 5, which will further present succinct recommendations with regard to the best tilt and orientation angles for a stationary PV panel for a specified area of latitude.

1.8 Summary

The background to this research project has been given. This research will attempt to optimise the available output power from a PV panel, thereby reducing dependence on traditional energy sources such as fossil fuels. Presently, non-renewable energy sources have a limited supply, and in addition, release greenhouse gases during the production of energy. Therefore, for both environmental and economic reasons, alternative energy sources must be pursued for the purposes of producing energy. The problem statement, objective, methodology, significance was reviewed as well as the delimitations of the research. The overview of the report completed this chapter. The next chapter will introduce the main types of PV panels, power regulation circuits and energy storage devices.

Chapter 2 PV panels, power regulation circuits and energy storage devices

2.1 Introduction

This chapter will focus on PV systems, power regulation and energy storage devices that can be employed to generate maximum power. The components that form a basic PV system according to literature will firstly be presented. This would be followed closely with the principle of operation of PV cells. The three main types of PV panel will be discussed and a particular specification for each of the types of PV panel will be presented. Also the types of PV panels with respect to their manufacturing process will be addressed and a summary of their advantages, disadvantages and application will be presented. A discussion of power regulations devices (Maximum power point trackers, solar chargers and DC-DC converters) as employed in PV systems will then follow along with an explanation of energy storage devices. This will be done in order to understand their manufacturing process, advantages, disadvantages and respective applications better so that the right equipment may be selected and used for this research.

2.2 PV systems

According to Yafaoui and Cheung (2007:1-5), a typical PV system (see Figure 2) usually consists of the following:

- A PV panel that converts solar energy to electrical energy, from a phenomenon called photovoltaic effect.
- A power regulation device/charge controller (DC-DC converter, maximum power point tracker (MPPT), solar charger) that converts the PV panel voltage to a constant DC voltage while optimizing the power transfer from the PV panel to the storage device.
- Energy storage device that stores the power from the PV panel owing to the

fluctuating nature of the PV voltage caused by climatic conditions.

- A load that uses the stored energy from the energy storage device (Chen, Shen, Shu, Qin, & Deng, 2007:1611-1622). An example of the load can be a DC light bulb (fluorescent or light emitting diodes popularly called L.E.D).

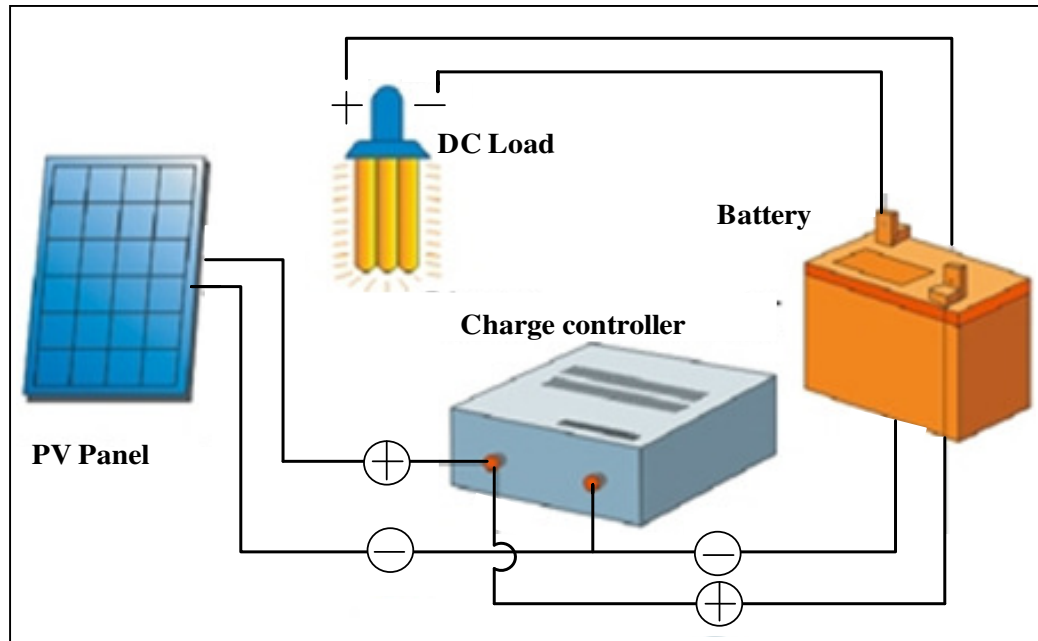


Figure 2: A typical PV system

2.3 PV systems (principle of operation of photovoltaic cells)

Solar energy can be converted to electrical energy by means of two methods: the first one is a direct method with PV systems and the second is an indirect one by solar thermal power generation (Nassar & Salem, 2007:86-90). PV modules provide direct conversion of solar radiation into electrical energy and play an important role in the field of renewable energies (Krauter, 2006:19) at standard connections of 12, 24 or 48 V (Farret & Simoes, 2006:146). The manufacturing process involves sophisticated technology that is used to build efficient solar cells, which are the key components of a PV system (Luis & Santiago, 2002:1). A solar cell is essentially a low-voltage, high-current device with a typical open-circuit voltage of about 0.5 V, far lower than the operating voltage of most electrical loads and systems. So it is

normal for a PV module to contain many series-connected cells raising the voltage to a more useful level (Lynn, 2010:76). PV systems are found in the MW range, and in the mW range, producing electrical energy for very different uses and applications (Saloux, Teysseidou & Sorin, 2010:713-722). PV cells are manufactured from semiconductor materials; that is, materials that act as insulators at low temperatures, but as conductors when energy or heat is available. Conduction in PV cells occurs through two main processes and this is shown in Figure 3:

- Electrons from broken bonds are free to move
- Electrons from neighboring bonds can move into the 'hole' created in the broken bond, allowing the broken bond or hole to propagate as if it had a positive charge (Stuart, Martin, Muriel & Richard, 2007:33).

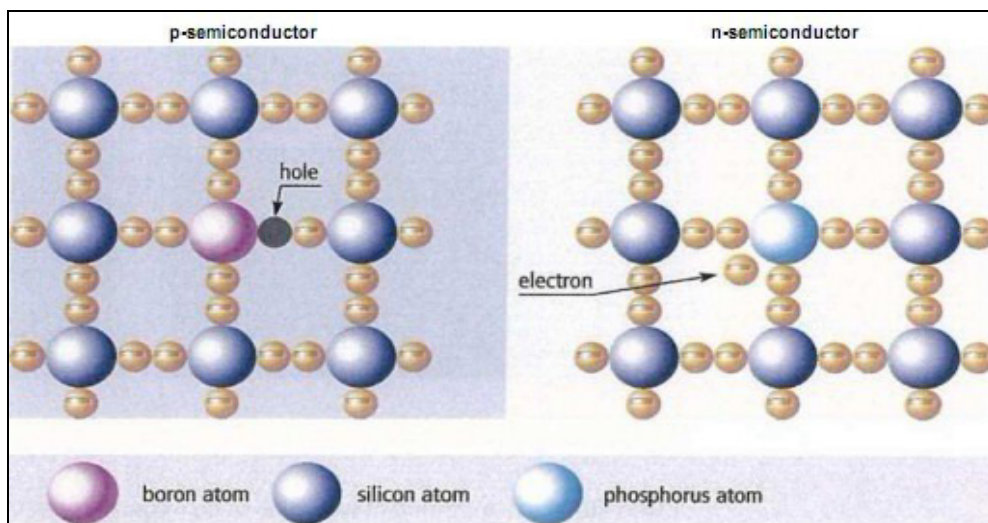


Figure 3: Schematic of a silicon crystal lattice doped with impurities to produce *n-type* and *p-type* semiconductor material (The German Solar Energy Society, 2005:19)

A PV cell is a large area semiconductor diode. It consists of a p-n junction created by an impurity addition (*doping*) into the semiconductor crystal (Lynn, 2010:32). The semiconductor crystal, in the most commonly used silicon solar cells, consists of four covalent bonds to the neighboring atoms (The German Solar Energy Society,

2005:19). Photovoltaic energy conversion in solar cells consists of two essential steps. Firstly, the absorption of light generates an electron-hole pair. The electrons flow to the negative terminal and holes to the positive terminal, in effect generating electrical energy (Abdelkader, Al-salaymeh, Al-hamamre & Sharaf, 2010:543-552). There are different semiconductor materials that can be used in the manufacture of solar cells such as silicon, gallium arsenide, cadmium telluride or copper indium diselenide (The German Solar Energy Society, 2005:18). Currently 95% of all solar cells worldwide are made of silicon which does not exist as a chemical element, but exists primarily in the form of silicate sand (SiO_2). Its principal advantage is its availability in the earth crust (Abdelkader *et al.*, 2010:543-552). Silicon has a stable crystalline structure, so the cells have a very high lifetime (>25 years). The band gap of silicon is relatively well-suited to convert solar energy to electrical energy (Krauter, 2006:95). In order to enable silicon material to work as an energy generator, an element that possesses one or more electrons (phosphorus), or one less electron (boron) than silicon in its outer electron shell, is paired with the silicon crystal atoms and is called '*doping*'. It is possible to shift the balance of electrons and holes in a silicon crystal lattice by doping it with other atoms (Stuart *et al.*, 2007:33). Basically atoms with one less valence electron results in a '*p-type*' while atoms with one more valence electron produces an '*n-type*' material.

These atoms possess either one or more electrons (phosphorus), or one fewer electron (boron) than silicon, in its outer electron shell. Due to this, the doped atoms cause defects within the crystal lattice. If the lattice is doped with phosphorus it is called *n-doping*, when it's doped with boron it's called (*p-doping*) (The German Solar Energy Society, 2005:19). If a p-n semiconductor (solar cell) is exposed to light, photons are absorbed by the electrons. The electrons that are set free are pulled through the electric field and into the n-area. The holes created move in the other direction, into the p-area. This whole process is called the *photovoltaic effect*. The electrical characteristics of a PV module can be analyzed by a photovoltaic cell model. The primary solar cell equivalent circuit is modeled as a current source with a parallel diode. The Shockley equation provides the diode current (Elchaar *et al.*,

2011: 2165-2175). The current–voltage (I – V) characteristic of the photovoltaic modules can be described as:

$$I = I_L - I_o \left[\exp\left(\frac{V + IR_s}{V_t}\right) - 1 \right] - \frac{V + IR_s}{R_{sh}} \quad (1)$$

Where: I_L is the light generated current (A), I_o is the reverse saturation current of the p–n diodes (A), R_s is the series resistance of the cells (Ohms), R_{sh} is the shunt resistance of the cells (Ohms) and V_t is the thermal voltage depending on the cell temperature, defined as:

$$V_t = kT_c/q \quad (2)$$

In Equation 2, T_c is the cell temperature (K) and k and q are constants. The short circuit current can be found when $V = 0$, i.e. $I_{sc} = I_L - \frac{IR_s}{R_{sh}}$ is usually ignored, as it is very large for mono-crystalline cells as compared to R_s , Equation 1 is then reduced to

$$I = I_L - I_o \left[\exp\left(\frac{V + IR_s}{V_t}\right) - 1 \right] \quad (3)$$

The simple relationship of power for a photovoltaic module is:

$$P = IV \quad (4)$$

Introducing Equation 3 into Equation 4 results in:

$$P = IV = \left\{ I_L - I_o \left[\exp\left(\frac{V + IR_s}{V_t}\right) - 1 \right] \right\} V \quad (5)$$

Finally the maximum power of a corresponding cell is given as:

$$P_{\max} = I_{mp} V_{mp} = (I_L + I_o) \left[I - \frac{V_t}{(V_t + V_{mp})} \right] V_{mp} \quad (6)$$

The basic model for a PV module is presented in Figure 4 where all the parameters are well represented.

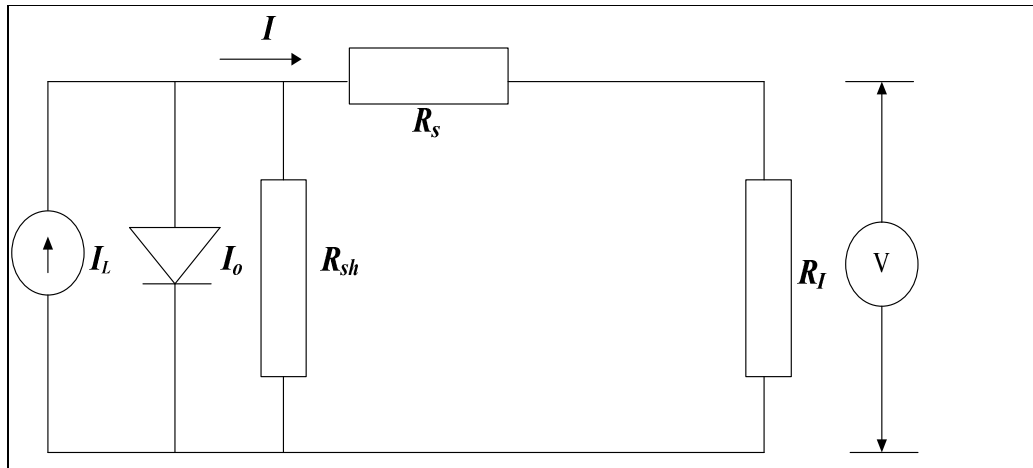


Figure 4: The basic model for a photovoltaic module (Ali, 2006:370-387)

Figure 5 represents an organogram of the different PV panels arranged according to cells types

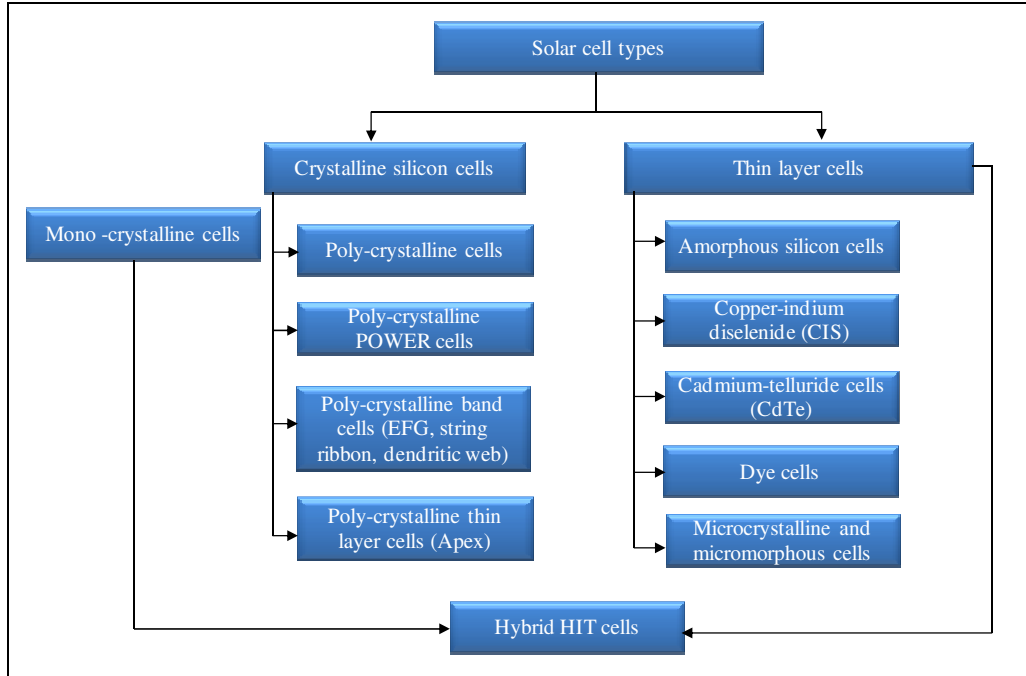


Figure 5: Types of solar cell (The German Solar Energy Society, 2005:21)

Three main PV panel modules exist, namely the mono-crystalline, the poly-crystalline and the thin film panels. The manufacturing process of the three main types of PV panels is discussed closely after the diagram. The cell structure is the main characteristic of each PV panel.

2.3.1 Mono-crystalline (manufacturing process)

A mono-crystalline PV panel has an ordered crystal structure with each atom ideally lying in a pre-ordained position (Stuart *et al.*, 2007:34). Most experts consider mono-crystalline PV panels to be the most efficient type of solar panel, as they employ crystalline-based silicon that can be incorporated into the panel as one sheet (Solar-always, 2011). This type of cell is the most commonly used, constituting about 80% of the market (El Chaar *et al.*, 2011:2165-2175). It has a smooth surface which makes the width of the slice visible. In order to protect them they must be mounted on a secure frame owing to their inflexibility. To conduct the electrons, metal strips are laid across the entire expanse of the panel. Mono-crystalline PV panels are the most expensive when compared to other technologies owing to the complicated process required to produce them (Abdelkader *et al.*, 2010:543-552).

One of the problems of modern silicon photovoltaics is a decrease in optical losses in mono-crystalline silicon cells. In order to attain uniformity a mixture of sodium hydroxide (NaOH) or potassium hydroxide (KOH) and isopropyl alcohol (IPA) is generally used during texturization on the silicon surface. (Gangopadhyay, Kim, Dhungel, Basu & Yi, 2006:1906-1915). The production of mono-crystalline silicon wafers starts with the manufacturing of cylindrical crystal ingots by using the melt growth processes known as Float-zone (FZ) and Czochralski (CZ) process (Jinsu, 2010:1612-1615). Basically the production of highly efficient solar cells is influenced by FZ process (Krauter, 2006:97). The production of FZ-silicon-based cells requires a lot of time and energy which makes them extremely expensive (The German Solar Energy Society, 2005:21). In the CZ process, a seed crystal of silicon is dipped into melted poly-crystalline silicon (Solar cell, 2012). The process involves immersing a central nucleus with a defined orientation in a silicon-melting bath

(melting point 1420°C) and it is slowly turned while taking it out of the bath. Cylindrical single crystals with a diameter of 0.3m and several meters in length are produced. The cylindrical single crystals are made into octagonal bars and then cut into thick slices of 0.33 mm (wafers) (The German Solar Energy Society, 2005:21). These thick slices of 0.33 mm are used to form a solar cell of approximately 35 mA of current for every cm^2 with a voltage of 0.55 V at full illumination (El Chaar *et al.*, 2011:2165-2175).

The FZ process is another process to produce mono-crystalline silicon, which is further used to produce solar cells that are of higher purity and 1-2% more efficient (The German Solar Energy Society, 2005:22). In this process a highly pure crystalline silicon bar is required to achieve this purity. It is melted from the bottom to the top with the help of a high-frequency field. Mono-crystalline silicon is produced while cooling and the impure materials remain in the melting bath (The German Solar Energy Society, 2005:22). Figure 6 presents a diagram of the CZ and FZ process of producing a mono-crystalline cell.

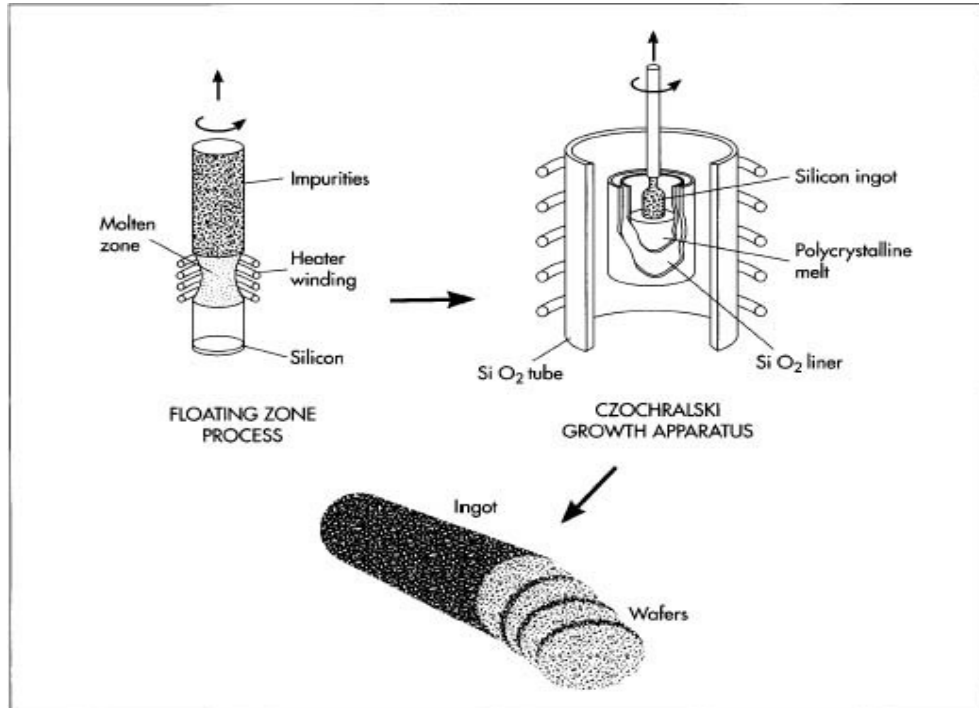


Figure 6: The Czochralski and the Float-zone (FZ) process (Madehow, 2012)

The CZ process is the most commonly used process for ingot pulling as compared to the FZ process. About 90% ingots are pulled using this process (Solanki, 2009:141). The main disadvantage in the CZ process arises from the fact that the high temperature silicon (Si) melt gets in contact with the crucible. The FZ process is more expensive than the CZ process resulting in the FZ process being less commonly used (Solanki, 2009:142).

Figure 7 presents a photograph of a mono-crystalline cell while Table 1 indicates selected parameters for this type of PV panel.

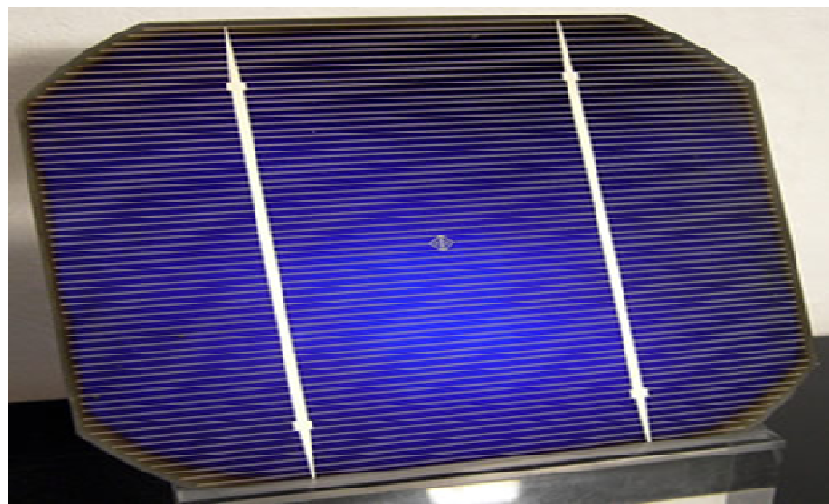


Figure 7: A cell of a mono-crystalline PV panel (M0ukd, 2011)

Table 1: ZKX-160D-2 module/160Wp-180Wp mono-crystalline PV panel

Specification	Abbreviation	Value
Maximum output	P_{MAX}	160 W
Open circuit voltage	V_{OC}	42.8 V
Rated voltage	V_{MPP}	34.9 V
Short circuit current	I_{SC}	5.15 A
Rated current	I_{MPP}	5.03 A

2.3.2 Poly-crystalline (manufacturing process)

Poly-crystalline PV panels are also referred to as multi-crystalline PV panels or simply as *poly-Si* (Lynn, 2010:54). Poly-crystalline silicon is an attractive choice for a low-cost substrate developed for PV cell. Recently, poly-crystalline silicon solar cells have surpassed mono-crystalline silicon solar cells. Efforts of the PV industry to reduce costs and increase production throughout have led to the development of new crystallization techniques (El Chaar *et al.*, 2011:2165-2175). Poly-crystalline PV panels are basically made from an ingot casting or ribbon technique (Möller, Funke, Rinio & Scholz, 2005:179–187). Under the ingot casting is the Ingot Casting/Bridgman method, the heat extraction method and the electromagnetic casting method. The ribbon technique includes the–ribbon-growth-on-substrate method and the edge-defined-film-fed-growth method. In the ingot casting/Bridgman method, the crystallization crucibles are either filled with high purity silicon, which is molten inside, or the silicon is molten in a separate crucible and then poured into the crystallization crucible (casting technique).

The ingots are crystallized either by the Bridgman or gradient-freeze technique and have cross-sections of more than 60 x 60 cm² with a weight of over 300 kg. The crystallization and cooling processes takes about 30 to 40 H. The heat extraction must occur in a very controlled manner to retain a high quality of the crystal. In order to achieve a low dislocation density, the melt interface must be kept planar to ensure low thermal stresses (Möller *et al.*, 2005:179–187). Silicon blocks of 400 mm x 400 mm with a height of 300 mm are created after been heated under vacuum at up to 1500°C and then cooled down towards the base of the crucible which has a temperature of about 800°C (The German Solar Energy Society, 2005:23). A schematic diagram of the different ingot-casting technique methods and ribbon technique are represented in the diagrams below.

- 8(a): Ingot Casting/Bridgman method
- 8(b): Heat Extraction method

- 8(c): Electromagnetic casting method
- 8(d): Ribbon technique/edge-defined-film-fed-growth method

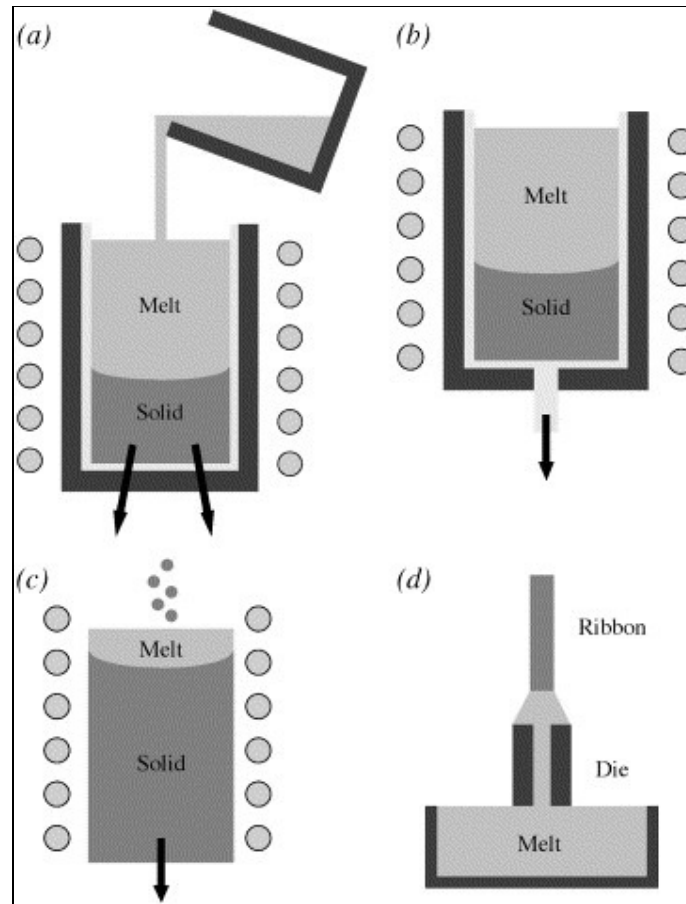


Figure 8: Ingot casting methods and Ribbon technique methods (Möller et al, 2005:179-187)

In the ingot casting/heat extraction method (HEM), as shown in Figure 8(b), heat is extracted locally at the bottom of the crucible, this leads to a coarser homogenous grain structure (Möller *et al.*, 2005:179–187). The electromagnetic casting (EMC) method is another ingot casting method of manufacturing poly-crystalline cells. In this method the contact with the crucible wall is avoided but at the cost of higher stresses and dislocation densities. The melt is kept in place by electromagnetic forces. Considering the final quality of the crystals or solar cells, none of the techniques appears to have a clear advantage. After crystal growth, the ingots are

sliced into columns mainly by band saws and finally into wafers by multi-wire saws using oil or ethylenglycol slurries and SiC abrasive powders. The slicing is an expensive processing step because of the high cost of the abrasives and the loss of about 50% of the silicon (Möller *et al.*, 2005:179–187).

The ribbon technique was introduced to reduce the high loss of silicon and to increase its utilization. (The German Solar Energy Society, 2005:25). The ribbon, or sheet growth techniques, requires a shaping system to determine the final shape (Möller *et al.*, 2005:179–187). The sheet growth techniques differ mainly by the shaping system that is used and can be divided into two categories depending on whether the crystallization direction is parallel or perpendicular to the pulling direction. The RGS method has the potential of very high production speeds but is still in the development stage. The most advanced method is the edge-film-growth (EFG) method. EFG silicon ribbon is a promising alternative for cutting down wafer costs by reducing the poly-silicon consumption and eliminating kerf loss (Jinsu, 2010:1612-1615). Methods to grow shaped silicon ribbon crystals by the EFG method for use as substrate material for solar cells have been under development for over three decades (Mackintosh, Seidl, Ouellette, Bathey, Yates & Kalejs, 2006:428-432). In this process an octagonal tube made of graphite is immersed into a silicon bath (The German Solar Energy Society, 2005:25).

The side faces have a width between 10 cm and 12.5 cm and a wall thickness of about 300 μm , the length of the tube is about 7 m and mainly determined by the height of the production building. The tubes are cut into the final wafer size by high-powered lasers (Möller *et al.*, 2005:179–187). The ready to use wafers are cut out of the eight sides of the octagon. After doping with phosphorus and attaching the rear contact layer the wafers are equipped with electrical leads on the front side and with anti-reflection (AR) layer. Although EFG silicon is poly-crystalline, it has a few nucleus boundaries and crystal defects. Growth of crystalline silicon octagon tubes by the EFG method for production of wafers for solar cells has been brought to a level of large-scale manufacturing and become a significant contributor of material for the PV industry (Mackintosh *et al.*, 2006:428-432).

Figure 9 presents a photograph of a poly-crystalline cell while Table 2 indicates selected parameters for this type of PV panel.

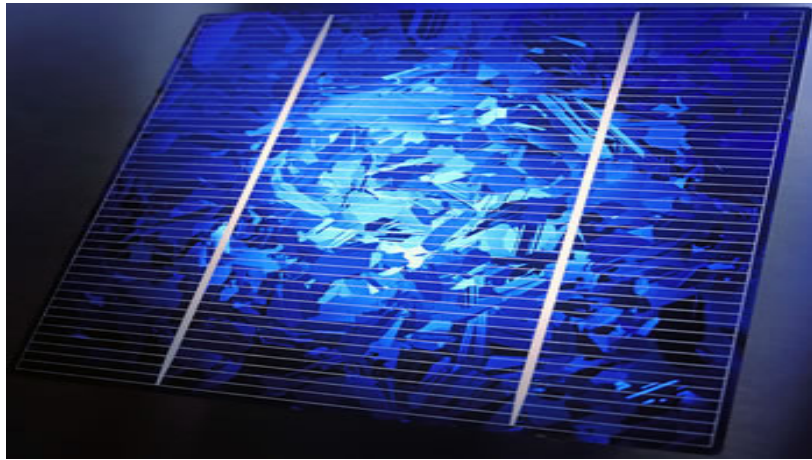


Figure 9: A cell of a poly-crystalline PV panel (M0ukd, 2011)

Table 2: SOLARWORLD SW220 poly-crystalline PV panel

Specification	Abbreviation	Value
Maximum output	P_{MAX}	220 W
Open circuit voltage	V_{OC}	36.6 V
Rated voltage	V_{MPP}	29.2 V
Short circuit current	I_{SC}	8.08 A
Rated current	I_{MPP}	7.54 A

2.3.3 Amorphous (manufacturing process)

The word *amorphous*, derived from ancient Greek, means ‘without form or shape’ (Lynn, 2010:57). Amorphous silicon panels are also known as a-Si PV panels (Markvart & Castaner, 2005:284-289). Amorphous silicon was first deposited from a silane discharge (Carabe & Gandia, 2004:1–6).

They are cells made from thin films of amorphous silicon incorporated with a small percentage of hydrogen (Krauter, 2006:102). This technology diverges from crystalline silicon in the fact that silicon atoms are randomly located from each other. This randomness in the atomic structure has a major effect on the electronic properties of the material causing a higher band-gap (1.7 eV) than crystalline silicon (1.1 eV). The development of a-Si PV technology materials is driven by cost reduction. (AbdelKader *et al.*, 2010:543-552). The addition of small percentages of hydrogen greatly reduces the electrical resistance of the material and allows it to be doped n-type or p-type (Krauter, 2006:102). There are four advanced thin film technologies, their names are derived from the active cell materials: cadmium telluride (CdTe), copper indium diselenide (CIS), amorphous silicon (a-Si) and thin film silicon (thin film-Si). Amorphous silicon is in commercial production while the other three technologies are slowly reaching the market. Thin film modules are made directly on the substrate, without the need for the intermediate solar cell fabrication step (AbdelKader *et al.*, 2010:543-552).

Amorphous silicon PV panels are fabricated in a laboratory with a wide variety of different structures, but most commercial products utilize p-i-n or n-i-p junctions. Multi-junction devices are also being designed to take advantage of a broader spectrum of the sun's rays and to maximize efficiency (Solar-always, 2011). It is mainly because of the large open-circuit voltage available from amorphous silicon p-i-n solar cell that the device has found useful commercial applications (Dhariwal & Smirty, 2006:1254-1272). It is well known that continuous exposure to light degrades amorphous silicon by introducing mid-gap states called the dangling bonds. The larger band-gap allows a-Si cells to absorb the visible part of the solar spectrum more strongly than the infrared portion of the spectrum. However, to promote the widespread use of thin film PV technology; two obstacles have to be overcome. First, a low cost deposition technique must be developed to fabricate high-efficiency thin film PV devices. Secondly, prolonged light exposure induced degradation has to be minimized to further improve long-term reliability of thin film PV devices (Huang, Lin, Shen, Shieh & Dai, 2012:277-282). Amorphous silicon has been studied extensively and is applied both in large-scale electronics and solar cells. The main

drawback of amorphous silicon is the Staebler Wronski Effect (SWE). This effect describes the reversible increase in defect density in amorphous silicon (Muthmann & Gordijn, 2011:573-578). Figure 10 presents a photograph of a mono-crystalline cell while Table 3 indicates selected parameters for this type of PV panel.

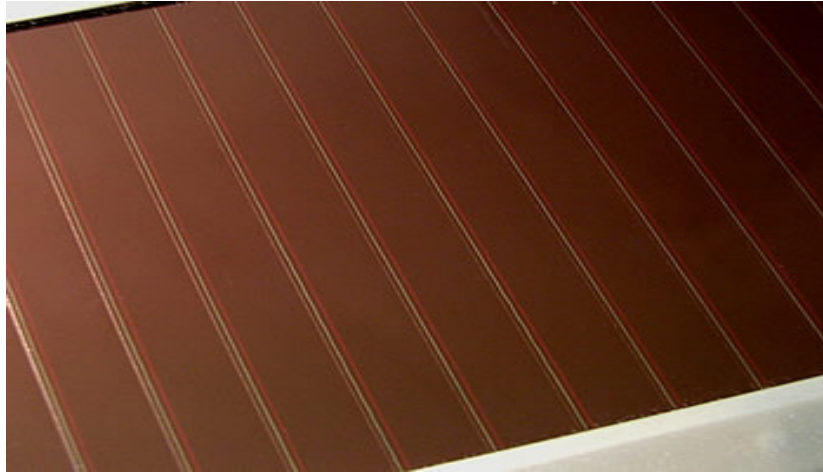


Figure 10: A cell of an amorphous silicon PV panel (M0ukd, 2011)

Table 3: Amorphous silicon thin film PV Panel (a-Si PV module)

Specification	Abbreviation	Value
Maximum output	P_{MAX}	41 W
Open circuit voltage	V_{OC}	58 V
Rated voltage	V_{MPP}	44 V
Short circuit current	I_{SC}	1.20 A
Rated current	I_{MPP}	0.94 A

2.3.4 Summary of PV cells (advantages, disadvantages and applications)

Table 4 is a comparison of the different PV panels that exist with regard to texture, manufacturing process, advantages, disadvantages, efficiency and power ratings.

Table 4: The advantages, disadvantages of the different types of PV panels

	Mono-crystalline	Poly-crystalline	Thin film
Known names	Single-crystalline	Multi-crystalline	Amorphous
Texture	They have a smooth texture which makes the thickness of the slice visible	They have a speckled reflective appearance, making the thickness of the slice visible	Due to the amorphous nature of the thin layer, it is flexible
Manufacturing process	Mono-crystalline PV cells are made using the CZ and the FZ process from a single crystal ingot	Molten silicon is cast into ingots of poly-crystalline silicon; these ingots are then saw-cut into very thin wafers and assembled into complete cells. A ribbon technique may also be used	Amorphous silicon PV cells are fabricated in a laboratory with a wide variety of different structures; most commercial products utilize p-i-n or n-i-p junctions
Advantages	The principle advantage of mono-crystalline cells is their high efficiencies	They are less expensive and have a high durability and longevity	Lower cost and flexibility when compared to the other PV panels
Disadvantages	The manufacturing process required to produce mono-crystalline silicon is complicated, resulting in slightly higher costs than other technologies	The major disadvantage is their lower efficiency when compared to mono-crystalline cells	Due to flexibility and chemical structure, their power output reduces over time, due to Wronski effect (SWE), particularly during the first few months, after which they are basically stable
Application	They can be used for Solar Home Systems (SHS), pumps, research practicals, residential and public illumination	They can be used as building-integrated photovoltaic systems (BIPV), such as for roofing. They can also be used for telecommunication application as well as a desalination plant	GaAs-based cells are mature and space-qualified. High-eta thin Si cells reach impressive performances. They can be applied in calculators and wrist watches
Efficiency	±15%	± 12%	± 6%
Maximum out power (P_{MAX})	± 160 W	± 220 W	± 41 W
Open circuit voltage (V_{OC})	± 42.8 V	± 36.6 V	± 42.8 V
Rated voltage (V_{MPP})	34.9 V	29.2 V	44 V
Short circuit current (I_{SC})	5.15 A	8.08 A	1.20 A
Rated current (I_{MPP})	5.03 A	7.54 A	0.94 A

These different types of PV panels were discussed in order to make the correct choice of PV panel to be used in this research with regard to cost, durability and its application to solar power management systems. A SW220 poly-crystalline PV panel was subsequently chosen for this research owing to its lower cost and better performance in areas of direct solar radiation. The increasing efficiency, lowering cost and minimal pollution are the principal advantages of the photovoltaic systems that have led to a wide range of their application (Parida, Iniyar & Goic, 2011:1625–1636). In summary, PV panels, such as mono-crystalline, poly-crystalline and amorphous silicon thin film offer a wide range of characteristics in respect to their texture and mode of manufacture and they are used for alternative energy sources in building-integrated photovoltaic (BIPV) and roof-mounted PV structures (Parida *et al.*, 2011:1625-1636) although the system efficiency and the power output of BIPV systems proved better than roof-mounted PV structures (Yoo & Lee, 2002:615–623). They can be used for a desalination plant; this is already in practice in many countries in North Africa and the Middle East owing to localized water shortages (Lamei, Van Der Zaag & Von Münch, 2008:1748–1756) as well as for water pumping, powering remote buildings, communication systems, satellites and space vehicles, reverse osmosis plants and for MW power plants.

2.4 Power regulation circuits

Solar arrays should be operated at the maximum power point in order to reduce the overall cost of the system (Kim, Hyunmin & Deokjung, 1996:1673–1678). So power regulations circuits should be incorporated in the set-up of a PV system. Power regulation circuits used in PV systems include Maximum power point trackers, DC-DC converters and solar chargers.

2.4.1 Maximum power point tracker (principle of operation)

Maximum power point (MPP) is a single point, where the array provides the maximum power possible for environmental conditions (radiation and temperature), and so functions with the maximum performance (Enrique, Andújar & Bohórquez,

2010:79-89). Solar arrays are the most expensive components in PV power systems. To extract the maximum power from a solar array, it is necessary to know the peak power point at each instant. The use of a MPPT optimizes the electrical operation as well as energy yield of an array by about 97% (Hohm & Ropp, 2003:47-62). At present, there are numerous works aimed at designing MPPT systems (Enrique *et al.*, 2007:31–38). A MPPT is not a mechanical tracking system that ‘physically moves’ the modules to make them point more directly at the sun, but an electronic system that varies the electrical operating point of the modules so that they are able to deliver maximum power.

They can be used with a mechanical tracking system, but the systems are completely different, generally in a PV system if the load is directly coupled with the solar array, the operation point does not coincide with the maximum power point. To fulfill the load demand, direct connection of the load to the solar array leads to over sizing the solar panels thus increases the cost of the entire system. To solve the problem, a DC–DC converter with an automatic duty cycle control is usually inserted between the solar panel and the load. The MPP computing system will modify the duty cycle and input impedance of the converter until the system reaches the MPP (Petreuşa, Pătăraua, Dărăbana & Morley, 2011:588-600). For any PV system, the output power can be increased by two options;

- Increasing the incident solar radiation on the system.
- Tracking the MPP of the PV system.

The first option requires using a sun tracker to track the position of the sun, to increase the solar radiation received by the PV system while option (b) requires using a MPPT, that tracks the optimum power of the PV system (Bahgat, Helwa, Ahmad & El Shewany, 2005:1257-1268). For several years, research has been focusing on various MPPT control algorithms to draw the maximum power from the solar array. Among the ‘constant voltage control’ method, the ‘perturb and observe’ method with fixed and variable step sizes, the ‘incremental conductance’ method and the ‘fuzzy logic’ control have drawn attention (Yu, Jung, Choi & Kim, 2004:455-463).

The Perturbation and Observation (P&O) method is also known as the “hill climbing method” (Petreuşa *et al.*, 2001:588-600). The P&O method is probably the most frequently used in practice, mainly due to its easy implementation (Hohm & Ropp, 2002:29). However, operation with fixed size perturbations results in a trade-off between speed of response and maximum power yield in the steady-state (D'Souza, Lopes & Liu, 2010:296-305). The P&O method measures the derivative of power (Δp) and the derivative of voltage (Δv) to determine the movement of the operating point. If the sign of ($\Delta p/\Delta v$) is positive, the reference voltage is increased by some amount of value or vice versa.

The incremental conductance method can track the MPP voltage more accurately than the P&O method, by comparing the incremental conductance and instantaneous conductance of a PV array (Il-Song, 2007:405–414). However, it has limitations that reduce its tracking efficiency. When the light intensity decreases considerably, the P–V curve becomes very flat. This makes it difficult for the MPPT to locate the MPP, since the changes that take place in the power are small as regards perturbations occurred in the voltage (Hohm & Ropp, 2002:49).

Another disadvantage of the P&O algorithm is that it cannot determine when it has exactly reached the MPP. Thus, it remains oscillating around it, changing the sign of the perturbation for each ΔP measured. It has also been observed that this algorithm can show misbehaviour in fast changes in the radiation levels (Kawamura, Harada, Ishihara, Todaka, Oshiro & Imataki, 1997:155–165). Several improvements in the P&O algorithm have been proposed (Emslin, Wolf & Swiegers, 1997:769–773) and (Xiao, Dunford, Palmer & Capel, 2007:2539–2549). One of them is the addition of a waiting time if the system identifies a series of alternate signs in the perturbation, meaning that it is very close to the MPP. This allows reducing the oscillation around the MPP and improves the efficiency under constant radiation conditions. However, this algorithm causes the MPPT to be very slow, making its misbehavior more noticeable in partly cloudy days (Hohm & Ropp, 2002:51). When the energy storage device reaches the full charged state, the amount of power being transferred to it gradually decreases (float charging), thereby making use of pulse width modulation.

2.4.2 Solar chargers (principle of operation)

A solar charger employs solar energy to supply electricity to devices or charge batteries. The solar battery charger requires solar cell voltage and current, battery voltage and current for controlling solar cell and battery status (Il-Song, Pyeong, Un-Dong, Chin-Gook & Hong-Gyu, 2009:1-6). It is desirable to extract maximum power from solar cells under various isolation conditions; this is the main reason why power regulation circuits are employed in a PV system (Chang & Ng, 1994:105-108). If a PV module is directly connected to the storage batteries, then the output voltage of the PV module will be fixed to the voltage of the storage batteries, so the system cannot always operate at each optimum operating point. Therefore, it is necessary for the PV system to install a DC-DC converter between the PV modules and the storage batteries in order to always operate at the optimum operating point (Lamaison, Bordonau, Esquivel & Peracaula, 1999:463-468).

Solar chargers based on simple regulator architectures do not feature high efficiencies. During the first phase of the charging process, they deliver constant current to the battery. In the final phase, they regulate constant voltage on the battery side. They either drop the voltage difference between the panel and the battery, or they equalize the panel voltage to the battery voltage. The similarities of a solar charger to an MPPT is that they have a MPPT incorporated in them to keep the batteries from overcharging and also to allow the PV panels to operate at their optimum power output voltage increasing as much as 30%. The amount of time a solar charger uses in charging up a battery depends on the size of the battery and the amount of solar radiation received from the PV panel. Modern solar chargers that have MPPTs incorporated in them, monitor the battery voltage and opens the circuit, stopping the charging when the battery voltage rises to a certain level.

2.4.3 DC-DC converters (principle of operation)

DC-DC converters are power electronics devices employed to adapt the voltage and current levels between sources and loads, while maintaining a low power loss in the

conversion process (Olalla, Queinnec, Leyva & El Aroudi, 2011:688-699). Such devices are usually regulated with a control subsystem that maintains the desired levels of output current or voltage, despite the uncertainty of the system and the disturbances or parametric changes that might appear. DC-DC converters can be used to regulate the output voltage of a PV panel (Simon & Alejandro, 2011:496).

Switched Capacitor (SC) DC-DC: These converters are transformer and inductor less DC-DC converters that are used to step up, step down or invert a supply voltage where the power requirements are usually less than 5 W. The outputs of the currently available SC converters are referenced with respect to the input supply ground. SC converters are ideally suited for low power miniaturized industrial applications owing to their small size and lack of ground isolation (Peter & Agarwal, 2010:632-637).

Switched mode DC-DC Converters: DC-DC converters are used in PV systems as power regulation circuits to detect and track the MPP produced by the PV module, under different atmospheric conditions and connected load (Farahat, Metwally & Abd-Elfatah, 2012:393-402). They are the most popular devices to adapt voltage and current levels between DC sources and DC loads since they maintain a low power loss in the conversion process (Martinez, Angel & Jeffrey, 2011:1). A switched mode DC-DC converter is one of the three basic components of many MPPTs, being coupled basically alongside a control circuit and a tracking algorithm (Farahat *et al.*, 2012:393-402). They maintain a low power loss in the conversion process (Martinez *et al.*, 2011:1).

2.4.4 Summary of power regulation circuits (advantages, disadvantages and application)

Table 5 represents a comparison of the power regulation devices employed in PV systems (MPPTs, solar chargers and DC-DC converters). They are analysed with regard to their advantages, disadvantages and application. These power regulations devices were discussed in order to make a comparison between the MPPT, solar

charger and DC-DC converter, so as to identify the most appropriate power regulation device for this research.

Table 5: Power regulation devices (MPPTs, solar chargers, DC-DC converters)

Power regulation types	MPPTs	Solar chargers	DC-DC converters
Advantages	<ul style="list-style-type: none"> • The major advantage of using a MPPT is that it extracts the maximum power from a PV module • It helps to correct variations in the current-voltage characteristics 	<ul style="list-style-type: none"> • Easy to carry and store • Solar chargers are cost savers since they scale back the amount of electrical energy used 	<ul style="list-style-type: none"> • They maintain a tight regulation on the output • DC-DC converters maximize the bandwidth of the closed-loop response in order to reject disturbances • They satisfy desirable transient characteristics
Disadvantages	<ul style="list-style-type: none"> • Some MPPT methods take longer to reach the MPP because of the increased computation required • In the incremental conductance algorithm method, a MPPT has to incorporate compensation for a change in voltage whenever there is a corresponding change in current and MPP, increasing the entire cost of the system 	<ul style="list-style-type: none"> • Solar power chargers depend on the amount of sunlight, the usage of chargers is closely related to the weather • Due to the frequent change of the cloud layers, it is not stable when charging up the batteries 	<ul style="list-style-type: none"> • Local generation of heat, so cooling is needed • Conductive noise through cables
Applications	<ul style="list-style-type: none"> • They can be applied in PV systems for research purposes, small water turbines, wind-power turbines, etc. 	<ul style="list-style-type: none"> • They can be employed in PV systems • They can be used to charge cell phones and other small electronic devices 	<ul style="list-style-type: none"> • They can be employed in laboratory tests • In-vehicle instrumentation, mobile radio and portable PCs

A WELSEE (WS-MPPT 30) solar charger with an in-built MPPT was used in the main study of this research, as it improves the overall performance of the system by as much as 30%.

2.5 Energy storage devices

The generation of electric energy from renewable energy sources, like solar energy, is often difficult to predict due to the fluctuating nature of the climatic conditions, resulting in the generator output being neither deterministic nor dispatchable. This is the reason why PV systems often contain conventional storage devices for supplying the load whenever energy from the renewable source is not available (Koeppel & Korpas, 2008:2024-2036). Figure 11 represents a diagram of the non-even power generation from a PV panel, the balancing storage device and their combined network in feed supplied to the load. The generator on the graph represents the PV panel supplying an uneven power owing to climatic changes, air pollution and cloud movements and the energy storage device which can be a battery

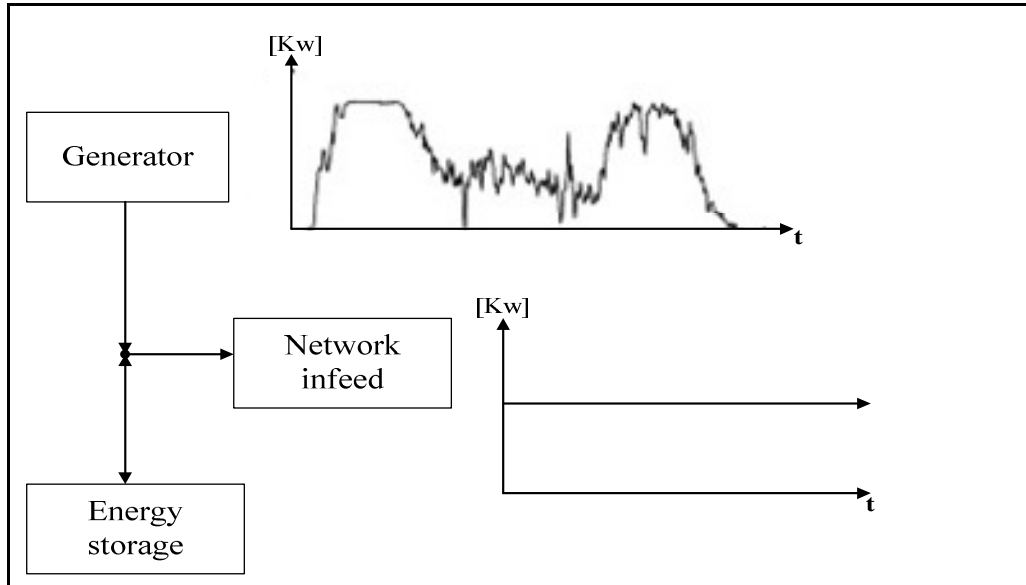


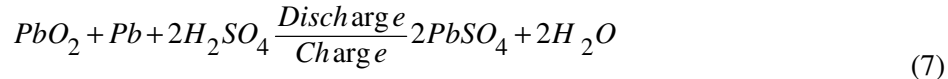
Figure 11: Symbolic representation of the non-even power generation, the balancing storage device and their combined network infeed (Koeppel & Korpas, 2008:2024-2036)

Energy storage systems are important components, especially when the harvested renewable energy is to be stored. Types of energy storage systems include batteries, super-capacitors and hydrogen storage (Pushparaj, Sreekala, Nalamsu, Ajayan, Yugang & John 2010:227-245). The fact is that energy generation from renewable energy is seldom constant over time and also electric energy demand is never constant. Therefore, using an energy storage technology in renewable energy systems is important (Zahedi, 2011:866-870).

There are a variety of different batteries that may serve as energy storage devices, but only three main types are discussed in this research.

2.5.1 Lead acid deep discharge batteries

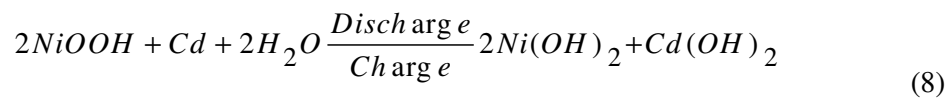
With ever-evolving information technology, it is becoming increasingly important to secure reliable back-up power supplies in solar systems, telecommunications networks and data-processing facilities (Nagashima, Takahashi, Yabumoto, Shiga & Watakabe, 2006:1166–1172). This is due to the fact that solar energy is not always available so an energy storage device (battery) is always necessary. Lead acid deep discharge batteries (LADDB) are suitable for a multitude of utility applications. They can be used for frequency regulation, load-leveling and back-up energy supply in solar power applications (Wagner, 1997:163-172). Its production and use will continue to grow because of its application for battery power in energy storage (Linden, 1995:24.1). The good performance, life characteristics and low price and ease of manufacturing on a local basis has led to the wide use of lead acid batteries in many designs and systems. The battery is more and more discharged at night as it keeps the system working and is recharged during the day due to solar radiation (Berndt, 1997:94). The active materials are lead dioxide (PbO_2) in the positive plate, sponge lead (Pb) in the negative plate, and a solution of sulfuric acid (H_2SO_4) in water as the electrolyte. The LADDB is manufactured in a variety of sizes and designs, ranging from less than 1 to over 10,000 Ah (Linden, 1995:24.2). The chemical reaction during discharge and recharge is normally written as (Linden, 1997:24.6):



Besides charging and discharging, a number of reactions are possible in a LADDB; these include hydrogen evolution, oxygen evolution, oxygen reduction and hydrogen oxidation (Berndt, 1997:98). In this research, a stationary LADDB was used as this type can be applied to PV and load-leveling environments when energy storage is needed (Linden, 1995:24.3)

2.5.2 Nickel-Cadmium (NiCad) batteries

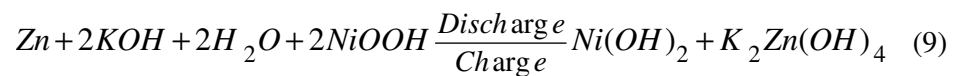
Nickel-Cadmium batteries (NiCad) have been in industrial production nearly as early as long as the lead-acid batteries (Berndt, 1997:174). NiCad batteries are particularly robust and behave better than many other electrochemical systems in extreme conditions such as overcharge, over discharge, and long-term storage in a wide range of temperature from -40°C to $+70^{\circ}\text{C}$ (Bernard, 2009:459–481). NiCad batteries can be classified in two types: vented (open) and sealed (Espinosa & Jorge, 2006:600-604). The vented nickel-cadmium batteries are older than the sealed nickel-cadmium batteries, are more reliable, sturdy and have a long life. This means they can be operated effectively at high discharge rates and in a wide temperature range (Linden, 1997:26.1). It has very good charge retention properties, and it can be stored for long periods of time in any condition without deterioration. The sealed nickel-cadmium batteries incorporate specific cell design features to prevent a buildup of pressure in the cell caused by gassing during overcharge. The active materials in NiCad cells are nickel hydrate (NiOOH) in the charged positive plate and sponge cadmium (Cd) in the charged negative plate. The electrolyte is an aqueous potassium hydroxide (KOH) solution in concentration of 20-34% by weight pure KOH. The basic electrochemical reaction is:



As a result, cells can be sealed and require no servicing or maintenance other than recharging. The characteristic feature of a NiCad battery is the charge/discharge reactions that are frequently repeated (Berndt, 1997:174). Nickel–cadmium batteries can be classified in two types: vented (open) and sealed. In order to maintain their capacity, cells need to be overcharged at a level of at least approximately 10% above their limit (Espinosa & Jorge, 2006:600-604).

2.5.3 Nickel-Zinc Battery

Zinc–nickel oxide battery is commonly called Nickel–Zinc (Cairns, 2009:528-533). The nickel-zinc battery is created by the combination of the nickel electrode as used in NiCad batteries and a zinc electrode (Linden, 1997:29.1). The electrolyte of this battery for both negative electrode and positive electrode is high concentration solutions of ZnO in aqueous KOH. The negative electrode is inert metal such as nickel foil, and the positive electrode is nickel oxide for secondary alkaline batteries (Cheng, Zhang, Yang, Wen, Cao & Wang, 2007:2639-2642). This combination sought to achieve the long-life characteristic of the NiCad battery with the capacity advantage of the zinc anode (Linden, 1997:29.1). The basic electrochemical reaction is:



Nickel-Zinc batteries are well suited for applications such as power tools because of their high specific power, relatively low cost, and reasonable cycle life zinc-nickel batteries have high practical discharge voltages; their theoretical electromotive force is above 1.70 V and practical specific energy is about 85 Wh/kg. (Cheng *et al.*, 2007:2639-2642). The nominal voltage is 1.6 V per cell and the battery holds an almost constant voltage during most of the discharge period and exhibits voltage stability at different discharge rates. In addition, nickel-zinc batteries can hardly complete more than 300–500 cycles during deep-discharge cycles before failing, and so, has not penetrated commercial markets. The failure is usually caused by the

negative electrode, which suffers from the following two main phenomena. The first phenomenon is the shape change of the negative electrode associated with non-uniform current distribution in zinc electrodes, and Zn dendrite resulting from concentration polarization. And the second phenomenon associated with nickel-zinc batteries is the presence of a non-uniform electrode position which occurs since the system is strongly non-linear and far from equilibrium, and is controlled by Poisson-type formulations. One method to bring the system closer to equilibrium is to change the mass transport of zincate from diffusion control to convection control by making use of flowing electrolyte and a single flow lead/acid battery (Ito, Nyce, Plivelich, Klein, Steingart & Banerjee, 2011:2340-2345).

2.5.4 Summary of energy storage devices (advantages, disadvantages and applications)

A comparison of the different energy storage devices (LADDB, NiCad and the Nickel-Zinc) batteries with regards their advantages, disadvantages and application is presented in Table 6. This was done so as to select the most appropriate battery for this research. A RITAR RA12-100 (100 Ah) LADDB was then selected to be used in this research, as it has a high storage capacity and an overall efficiency of about 70%, with a deep depth of discharge of 80% (Nakayama, Takahashi, Hirakawa & Yamaguchi, 2004:135-140). Figure 12 represents a picture of the LADDB used.

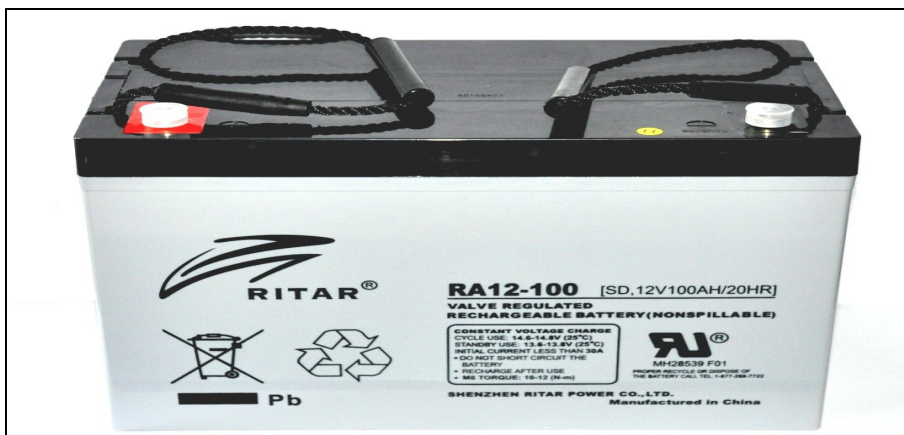


Figure 12: A RITAR RA12-100 (100 Ah) LADDB (Best batteries, 2008)

Table 6: Types of batteries

Battery type	Lead-Acid Deep Discharge	Nickel-Cadmium	Nickel-Zinc
Advantages	<ul style="list-style-type: none"> • Low-cost secondary battery due to high rate of production compared to other secondary batteries • Available in large quantities • Good high rate performance • Electrically efficient, with an efficiency of over 70% • High cell voltage with an open circuit voltage of >2.0V • Easy state-of-charge induction and it has a depth of discharge of 80% the depth of discharge of the battery gives the state of charge and they basically have 500-800 cycles 	<ul style="list-style-type: none"> • Long life cycle • When sealed, no maintenance required • Rapid recharge capability • Can withstand electrical and physical abuse • They have a depth of discharge of about 60%-80% and 1,500 cycles. 	<ul style="list-style-type: none"> • High Specific energy, 50-80 Wh/kg. • High power capability, >100W/Kg • Wide operating temperature range, -20 to 60°C • They have a depth of discharge of 80% and 100-500 cycles
Disadvantages	<ul style="list-style-type: none"> • Relatively low cycle life (50-500 cycles) • Poor charge retention • Long-term storage in a discharged condition can lead to irreversible polarization of electrodes (sulfation) 	<ul style="list-style-type: none"> • Higher cost than lead- acid batteries • Low energy density • Voltage depression in certain applications • Environmental 	<ul style="list-style-type: none"> • Low-cycle life, 100-300 cycles • Nickel-zinc cells have lower volumetric energy density.
Applications	<ul style="list-style-type: none"> • Energy storage device for charge retention and PV load-leveling • They can be used for stationary power in automotive, marine, aircraft, diesel engines in vehicles. • Standby emergency power in telephone exchange and signaling. 	<ul style="list-style-type: none"> • Used in light weight portable power (photography, toys, house wares) • As standby power (emergency lighting, alarm, memory backup) 	<ul style="list-style-type: none"> • Used in small electric-vehicle applications • They can also be used in small appliances, mine lamps, military aircraft etc.

The depth of discharge (DOD) is the percentage of the rated capacity drawn from the battery (Wenham & Stuart, 2007:103). The DOD is used to describe how deeply the battery is discharged. For instance, if a battery is 100% fully charged which is the state of charge (SOC), it means the DOD of the battery is 0%. However when the DOD of the battery is 75%, it means it has delivered 75% of its energy to the load,

then the SOC is 25% which is the battery energy that is remaining. The DOD and the SOC of a typical LADDB are represented in Figure 13.

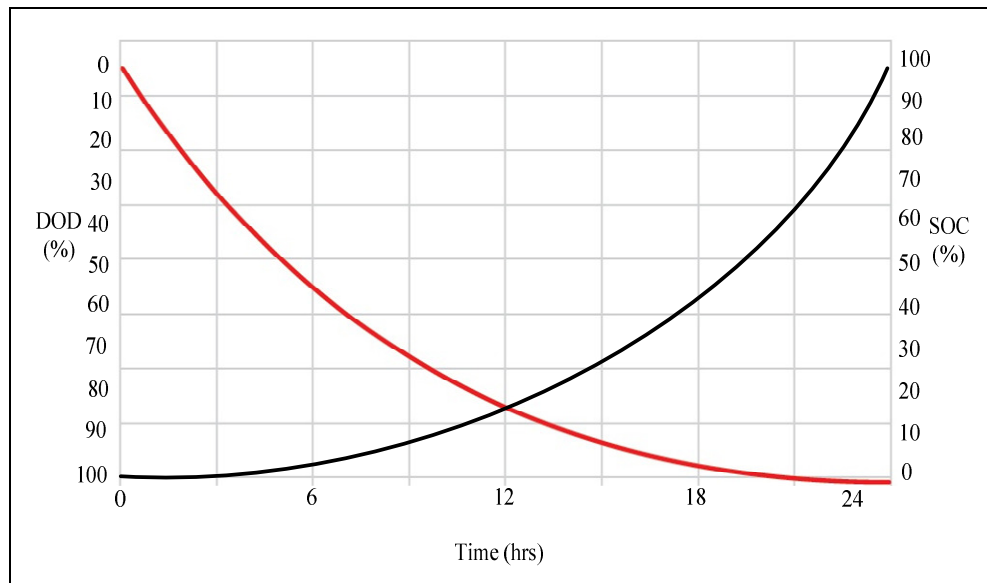


Figure 13: Depth of discharge for a LADDB (lead acid deep discharge battery)

DOD always can be treated as to how much energy that has been removed from the battery (Bestgopower, 2012). The SOC and the rated capacity of a battery determine the available current in the battery. For instance a battery of 100 Ah having a SOC of 25%, this means that the available current in the battery is 25 A. and 75% has been used up, rather discharged to the load. The cycle life of a battery is strongly influenced by the depth of discharge. When the DOD of a battery is exceeded continuously, the cycle life decreases dramatically (Zhang, Sharkh, Li, Walsh, Zhang & Jiang, 2011:3391-3398).

2.6 Summary

The different kinds of PV panels, power regulation circuits and energy storage devices have been discussed as well as their individual manufacturing process, advantages, disadvantages and applications. This was done in order to make a proper selection of the type of device that best suits this research. A SOLARWORLD SW

220 poly-crystalline, a WELSEE WS-MPPT 30 solar charger and a RITAR (RA 12-100) LADDDB was chosen for this research. Under energy storage devices, interest was directed to the LADDDB, NiCad and the Nickel-Zinc batteries as these batteries are most commonly used in PV application. This leads to the introduction of Chapter 3, which will consider the research methodology with regards to the use of software simulations in PV system designs, mathematical models and equations of latitude for PV panel installations that were used in the pilot and main studies.

Chapter 3 Research design and experimental set-up

3.1 Introduction

The previous chapter considered the types of PV panels that exist, power regulation devices and energy storage devices that can be employed in a basic PV system. Chapter 3 will thus consider the research design, data analysis method employed and simulation packages as used in this research in obtaining the results that are presented in Chapter 4.

3.2 Research design

In this research a quantitative data-collection study is used. Quantitative research tends to focus on measurement and proof. Inferential statistics are frequently used to generalize what is found about the study sample to the population as a whole. It also involves the collection and analysis of numerical data. Quantitative data-collection studies often employ measuring instruments and its concepts include (Hesketh & Laidlaw, 2002:1):

- Selecting and defining the research question;
- Deciding on a study type;
- Deciding on the data collection tools;
- Selecting the sample and its size; and
- Analysing, interpreting and validating findings.

The optimum output power available from a PV panel would be achieved through empirical testing using already existing equations of latitude, mathematical models and simulation packages for tilt and orientation angles. Empirical testing is done because little real experimental data or no real consistency exists with which to verify the suggested values for specific areas of latitude and longitude in South Africa. This proves problematic for the successful installation of PV panels for

optimum output power. This research aims to assist in identifying ways to improve the installation of PV panels for optimum output power as well as enabling a higher yield of solar energy, thereby reducing dependence on traditional energy sources such as fossil fuels. The sample size for the pilot study was 4 months while that of the main study was 12 months. The quantitative data-collection method involves a controlled experimental and correlation method, where an intervention is made under controlled conditions with the sole purpose of evaluating its effect (Hesketh & Laidlaw, 2002:5). The intervention made in the main study was the introduction of five identical PV panels using three of these panels and setting each set to a different tilt angle (16° , 26° or 36°) with a corresponding orientation angle of 0° while the other two PV panels were set to different orientation angles ($+15^{\circ}$ and -15°) with the same tilt angle of 36° . These are clearly shown in Figure 16. The correlation method is used to discover relationships between the various tilt and orientation angles.

3.3 Sampling, validity and data analysis

Sample size is important in quantitative research, as a sample size which is too big increases costs, and when it is too small it does not give sufficient data to reach a meaningful conclusion (Hesketh & Laidlaw, 2002:14). To obtain valid and reliable data requires that, before completing the research, the measurement procedures and measurement instruments must attain acceptable levels of reliability and validity.

Reliability of a measurement procedure is the stability or consistency of the measurement. To ensure an adequate sample size and reliability, the pilot study required at least two samples each of the PV panel with the tilt angle placed at 16° , 26° and 36° at an orientation angle of 0° .

The two samples ensured test-retest reliability of the measuring instrument which must be administered on at least two occasions (Welman, Kruger & Mitchell, 2005:146). This means that if the same variable is measured under the same conditions, a reliable measurement procedure will produce identical (or nearly identical) results. In other words, it refers to a measuring instrument's ability to yield

consistent numerical results each time it is applied; it does not fluctuate unless there are variations in the variable being measured. Basically, it is rare to have perfect reliability. Several procedures exist for establishing the reliability of an instrument, such as test-retest, alternate-form and the split-half methods (Georgekutty & Georgemathew, 2012:51-61). In summary, reliability refers in general to the extent to which independent administration of the same instrument (or highly similar instruments) consistently yields the same (similar) results under comparable conditions.

Validity was realized in this research by using content and criterion validity (Strydom, Jooste & Du Plessis, 2005:161). Content validity deals with the sampling adequacy of the data, while criterion validity involves multiple measurements and is established by comparing the results obtained from previous data with current data.

Data analysis is the process of inspecting, cleaning, transforming, and modelling data with the goal of highlighting useful information, suggesting conclusions, and supporting decision-making (Charles & Gary, 1989:1). In this research, the following methods of data analysis were employed. Firstly, filtering of data was done in order to extract useful information from the data.

The PV voltage was filtered to include all voltages greater than or equal to 25 V using MS EXCEL in the Filter Analysis Toolpak. A reference voltage of 25 V was chosen in order to fall within a 15% range of the MPP voltage of the PV panel (being 29.2 V). The DC-DC converter voltage was also filtered using a voltage 15% lower than the operating voltage of the device. This 15% range was chosen to account for any rapid fluctuations in voltages or slow recording responses of the data- logging equipment. Regression analysis (involving a linear regression and polynomial 6 value) may be used for process optimization (Montgomery & Runger, 2011:402).

The linear regression value (R^2) is used to represent the gradient of the straight line and establishes a relationship between the average on-time of the system and the direct solar radiation received from the sun, while the polynomial 6 value (R^2)

establishes a relationship between the average work-time per day and the direct solar radiation received from the sun. The on-time of the system interprets the availability of power and also indicates the period of time in which the PV panel was supplying power to the DC-DC converter. Basically the on-time is adversely affected by a number of factors these range from climatic conditions, air pollution and the amount of solar radiation available. The linear regression value (R^2) carried out in this research further indicates that the higher its value, the higher the on-time of the system which indicates a better tilt angle for the PV panel (Asowata, Swart & Pienaar, 2012:119-125).

3.4 Software simulation packages for PV system designs

Simulation software is the science of creating statistically accurate models to represent the behaviour of real life systems in order to subject them to predictive experimentation (Lanner, 2012). In this research, a correlation of the experimental results obtained to data obtained from a meteorological database software known as METEONORM was done. Table 7 presents a list of meteorological database that exist in the market today along with their source and region of applicability.

Amongst the meteorological database presented in Table 7, the METEONORM simulation software was chosen, because it contains data from stations worldwide, readily available on the internet and it is widely used for solar thermal, PV and building simulation (Remund & Müller, 2011:1-5). Another benefit of METEONORM is that it includes data covering a large time period from 1960 – 2005.

These software programs are used for calculating solar irradiation on any arbitrary oriented surface using data from meteorological databases based on monthly averages giving maximum solar irradiation values under clear sky conditions. They have become a valuable tool for estimating global solar irradiance, especially for where solar radiation data is missing or irregular (Hatwaambo, Jain, Perers & Karlsson, 2009:1394-1398).

Table 7: Simulation packages

Database	Region	Values	Source	Period	Availability
METEONORM	Worldwide	Monthly	1700 stations	1960-2005	Software free
Satellite	Europe	Hourly	Synthetic generation	1996-2000	Web free
US TMY2	USA	Hourly	239 stations	1960-1990	Web free
ISM-EMPA	Switzerland	Hourly	22 stations	1981-1990	Included in PV system
Helioclim (SoDa)	Europe & Africa	Hourly	Meteosat	From 2004	Web restricted
Solar GIS	Europe, Africa	Monthly	Meteosat	1994-1999	Web free
WRDC	Worldwide	Hourly	1195 stations	1964-1993	Web free
RETScreen	Worldwide	Monthly	WRDC-NASA	1961-1990	Software free

A meteorological software package was used to correlate the solar irradiance for latitude of 26° south, being the point of latitude where the Vaal University of Technology (VUT) is located. The correlation was done in order to establish reliability of both the software package and the empirical data. The METEONORM was chosen for this research as it contains meteorological database information of stations in the southern hemisphere as well as the Perez *et al.* mathematical model.

3.5 Mathematical models and equations of latitude for PV panel installations

There are numerous isotropic and anisotropic mathematical models along with equations of latitude that suggest specific optimum tilt and orientation angles for PV panels for given latitudes on earth. Some of these isotropic and anisotropic mathematical models are presented in Table 8, while Table 9 gives widely accepted equations of latitude. Anisotropic models concentrate on direct (beam) radiation which comes directly from the sun, thereby producing no sharp shadows of any

object and is dependent solely on the line of sight (The German Solar Energy Society, 2005: 10-21).

Table 8: Mathematical models (Noorian, Moradi & Kamali, 2008:1406-1412)

Model	Year	Type	Equation
Liu and Jordan	1962	Isotropic	$\frac{[1 + \cos(S)]}{2}$
Hay	1979	Anisotropic	$\frac{B_h}{G_{oh}} \times B_h + \left(\frac{B_h}{G_{oh}}\right) \frac{[1 + \cos(S)]}{2}$
Koronakis	1986	Isotropic	$\frac{1}{3[2 + \cos(S)]}$
Perez et al.	1986	Anisotropic	$0.5[1 + \cos(S)] \left[1 - F_1^1 - F_2^1\right] + F_1^1 \left(\frac{a}{c}\right) + F_2^1 \left(\frac{b}{d}\right)$
Skartveit and Olseth	1986	Anisotropic	$\frac{B_h}{G_{oh}} \times r_b + \Omega \cos(S) + \left(1 - \frac{B_h}{G_{oh}} - \Omega\right) \frac{[1 + \cos(S)]}{2}$ where $\Omega = \left\{ \max \left[0, \left(0.3 - 2 \frac{B_h}{G_{oh}} \right) \right] \right\}$
Perez et al.	1990	Anisotropic	$0.5 \left(1 - F_1^1\right) [1 - \cos(S)] + F_1^1 \left(\frac{a}{b}\right) + F_2^1 \sin(S)$
Stevnanad Unsworth	1990	Anisotropic	$\frac{0.51r_b + \{[1 + \cos(S)]\}}{2 - 1.74} \cos(S) - \pi \sin^2\left(\frac{S}{2}\right)$ $\frac{1.26\pi x \sin(S) - \left(\frac{Sx\pi}{180}\right)}$
Tian et al.	2001	Isotropic	$\frac{1 - S}{180}$
Badescu	2002	Isotropic	$\frac{[3 + \cos(2S)]}{4}$

Direct radiation is extremely important for concentrated solar collectors (CSP) which are used in solar thermal power plants, off-grid stand-alone PV systems and concentrated PV systems (Welman *et al.*, 2005:146). They can be computed by the relatively simple geometrical relationship between the horizontal and tilted surfaces

(Hatwaambo *et al.*, 2009:1394-1398). Amongst the anisotropic models, the Perez et al. model was chosen because it is an anisotropic model as this research focuses on direct beam radiation (which basically drives the DC-DC converter). Direct beam radiation is a major characteristic associated with anisotropic models and it is readily available in the METEONORM simulation package chosen for this research. Table 9 shows suggested equations of latitude for PV panel installations. This research concentrates on the Heywood and Chinnery equations of latitude for calculating the tilt angle of PV panels which are applied within the southern hemisphere (Armstrong & Hurleya, 2009:780-787). VUT (where this research was carried out) is in the southern hemisphere and lies on a latitude of 26°42'649" south and a longitude of 27°51'809" east. Substituting the value of 26° into alpha (Φ) gives the corresponding values of 16°, 26° and 36° tilt angles as shown in Table 10.

Table 9: Suggested equations of latitude

Author	Equation of latitude(ϕ)
Duffie and Beckmann	$(\phi + 15^\circ) \pm 15^\circ$
Heywood	$\phi - 10^\circ$
Lunde	$\phi \pm 15^\circ$
Chinnery	$\phi + 10^\circ$
Löf and Tybout	$\phi + (10^\circ \rightarrow 30^\circ)$
Garg	$0.9 \times \phi$
Heywood	Φ

Table 10: Calculation of tilt angles

Latitude	Equation	Calculation	Tilt angle
26°	$\Phi - 10$	$26^\circ - 10$	16°
26°	ϕ	26°	26°
26°	$\Phi + 10$	$26^\circ + 10$	36°

This research therefore concentrated on the following tilt and orientation angles as summarized in Table 11.

Table 11: Tilt and orientation angles of the PV panels used in the pilot and main studies of this research

Study	Tilt angle	Orientation angle
Pilot study (One PV panel system)	The tilt angle was changed each week between 16°, 26° or 36°	Fixed orientation angle of 0°
Main study (Five PV panel systems)	Three of the panels placed at 16°, 26° and 36°	Fixed orientation angle of 0°
	Two of the panels placed at 36°	Each PV panel placed at a different orientation angle of +15° and -15°

3.6 Pilot study

In this research, a pilot study was done in order to form the foundation for the main study. A pilot study is one way in which prospective researchers can be orientated to complete the main project at hand. A pilot study can also be defined as the process whereby the research design for a prospective survey is tested (Strydom *et al.*, 2005:205-206). Figure 14 represents the practical set-up of the pilot study carried out in this research. A SOLARWORLD (SW220 poly-crystalline PV panel) was used owing to its lower cost and better performance in areas of direct solar radiation. The PV panel was placed at a fixed orientation angle of 0° with the tilt angle varied to 16°, 26° and 36°.

One PV panel was used in the pilot study in order to ensure cost efficiency before purchasing unnecessary equipment for the main study. A sampling period of four months was done for the pilot study which was from April 2011 through July 2011. Five samples were gathered for each tilt angle for this particular period.

The five samples ensured test-retest reliability of the measuring instrument which must be administered on at least two occasions (Welman *et al.*, 2005:146) and the sampling time was on an interval of one minute for each respective tilt angle for a particular week. The PV panel was connected to a 12 V, 24 V and a 48 V MEANWELL DC-DC converter, which can be used for power conditioning (Chen *et al.*, 2007:1611-1622). A 12 V, 24 V and 48 V DC-DC were tested in this research

because they maintain a low power loss in the conversion process. A DLIC using hall-effect current sensors, LTS 6-NP (LEM product) connected the PV system to a DAQPRO 5300 data logger for recording input and output voltages and currents. The DAQPRO 5300 data logger has 8 analogue input channels and a 16 bit sampling resolution that makes it ideal for logging purposes in this type of empirical research (Zamir & Berman, 2004: 31). The DC-DC converter was connected to a fixed load resistance of 6 Ω .

The DLIC together with the data logger form the data collection tools in this research. The data logger records the data in its internal memory for downloading at a later stage. The rated open circuit voltage (V_{OC}) of the SW220 poly-crystalline PV panel is approximately 36 V.

The DLIC is subsequently required to condition the voltages (PV voltage and DC-DC converter voltage) to make it less than the maximum input voltage of 10 V required by the data logger. The DLIC must also be able to provide DC current monitoring using hall-effect current sensors. The advantages of the DLIC used in this research include the following:

- Steady and reliable power backup for the current sensors;
- Basic use for DC-DC converters, solar chargers and MPPTs;
- Dual channel monitoring on one-circuit board;
- Easy calibration using a multimeter;
- Protection for data loggers having a maximum input voltage of 10 V or less;
- and
- Current sensor interchange-ability according to current demands.

However, it is possible that these PV voltages could be as high as 29 V. Considering the 29 V parameter then reveals that the data loggers mentioned above will not be able to accommodate these high voltages, as most of them have a maximum input voltage of 2.5 V. A data logging interface (DLI) circuit is subsequently required to condition the voltage to make it less than the maximum input voltage required by the

data loggers. The DLI must also be able to provide DC current monitoring using hall-effect current sensors.

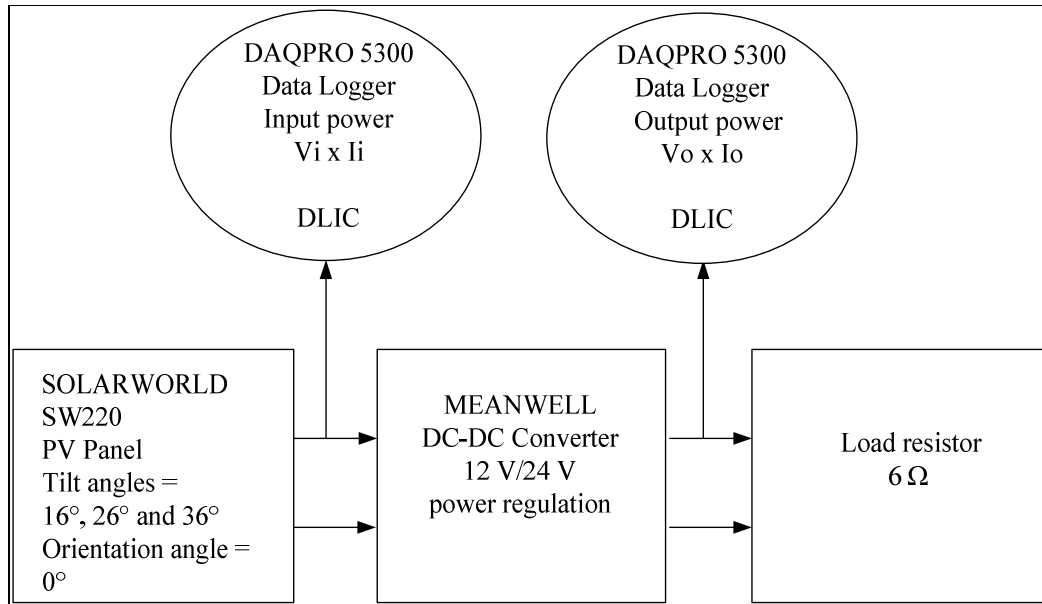


Figure 14: Practical set-up for pilot study

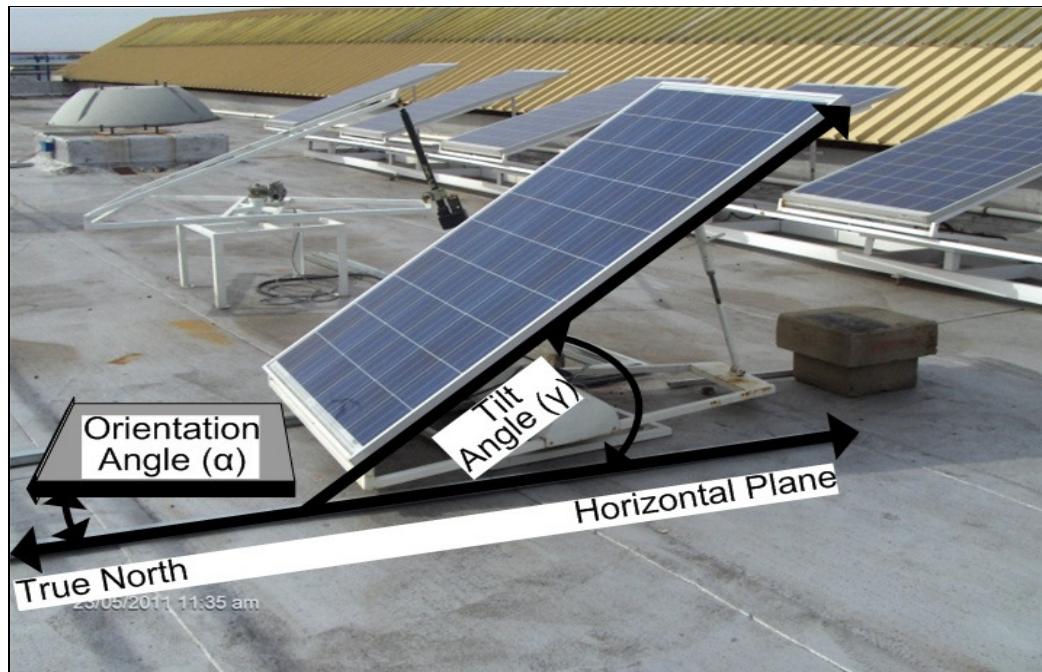


Figure 15: SW 220 poly-crystalline PV panel used in the pilot study

Figure 15 presents a picture of the PV panel used for the pilot study. The picture shows the tilt (γ) and orientation angles (α) and the horizontal plane of the PV panel. True north is determined using a GARMIN Etrex GPS handheld device.

The PV panel is orientated parallel to this direction resulting in an orientation angle of 0° . The exact longitude and latitude angles for the installation of the PV panel on the roof of the S-Block at VUT are obtained with this device and the PV panel is placed using the following co-ordinates (Latitude: $26^\circ 42, 649'$ S and Longitude: $27^\circ 51, 809'$ E).

3.7 Main study

The main study of this research builds on the results of the pilot study. Figure 16 represents the practical set-up of the main study done in this research showing the position of the sun relevant to the PV panels that are placed at different tilt and orientation angles.

In the pilot study, a singular stationary PV panel was used with a fixed orientation of 0° with the tilt angle being varied between 16° , 26° and 36° on a weekly basis. However, the main study features five identical SW 220 poly-crystalline PV panels connected to a DLIC via a circuit breaker (CB).

Five separate WELSEE (WS-MPPT 30) solar chargers were connected via five different channels of the DLIC. A PICOLOG 1216 data logger was connected on each corresponding channel of the DLIC where it was used to record specific data (PV voltage and PV current). A PICOLOG 1216 data logger was used as it has 16 analogue input channels that can accommodate all five PV panels (Zamir & Berman, 2004).

Five identical loads (21 W consisting of one RABTRON 10 W LED Lamp and five RADIANT 11 W fluorescent bulbs) were coupled to the MPPT along with five RITAR

(RA12-100) DCVRLA batteries. These totalled a number of five identical PV systems (see Figure 17 for the electrical design).

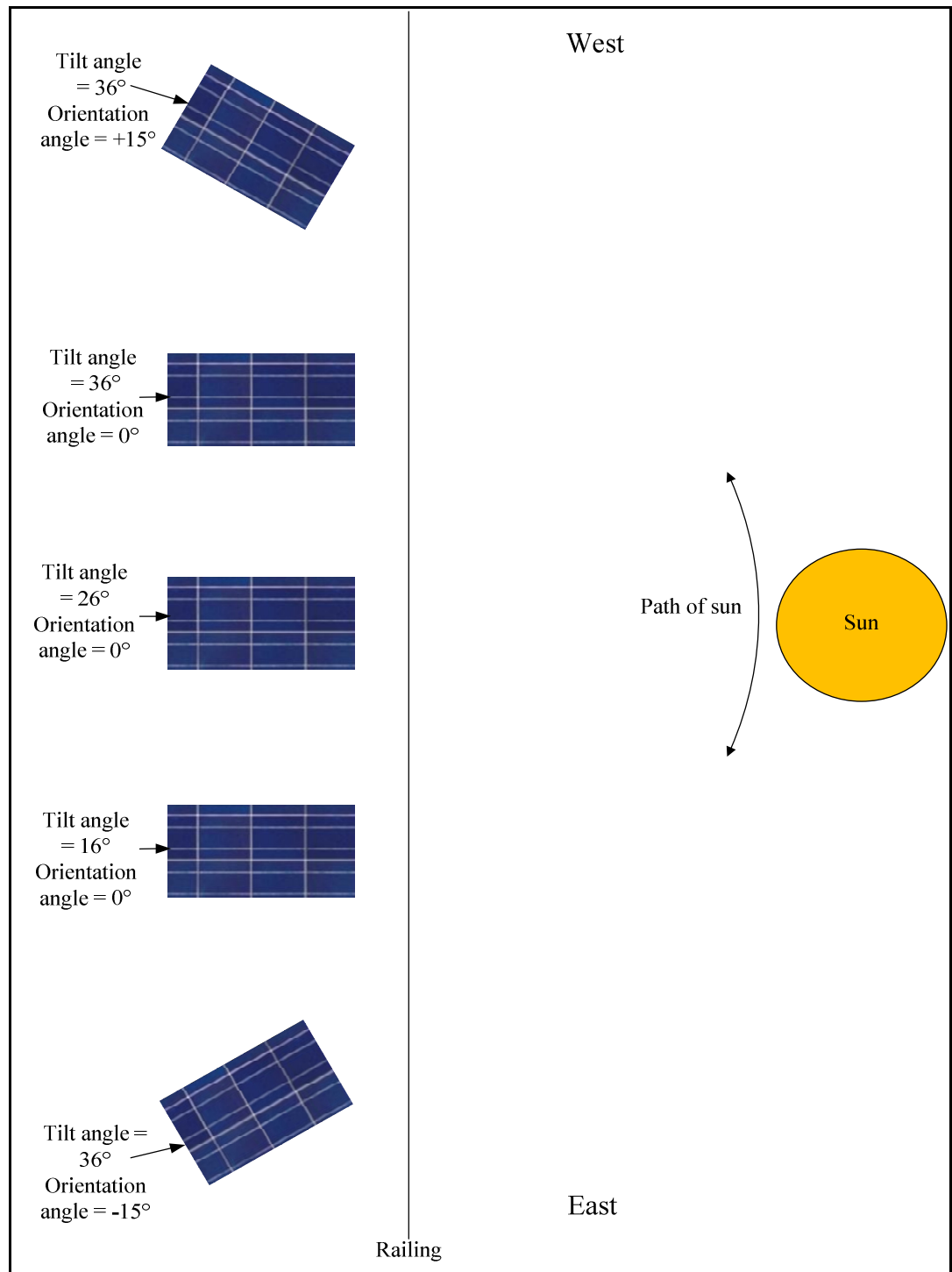


Figure 16: The practical set up for the main study

Three of the PV panels were set to 16°, 26° and 36° tilt angles with an orientation angle of 0°. The other two PV panels were set to a tilt angle of 36° with a corresponding orientation angle of +15° and -15° respectively. The 36° tilt angle was chosen as the reference tilt angle for these two PV panels owing to the results obtained in the pilot study which were published in 2012 (Asowata, Swart & Pienaar, 2012:1-5). The arc in the diagram indicates the path of movement of the sun in the sky.

Atmospheric conditions in terms of industrial pollution (Swart, Schoeman & Pienaar, 2011:1) and cloud movement affect the performance of PV panels, and therefore have a direct bearing on the total number of complete samples which must be collected (Mashorhor, Samsudin, Noor & Rahman, 2008: 269-273). The output voltage and current from the PV panel are of prime importance in this research, as they indicate the output power of the PV panel under specific conditions. These parameters are used to judge and evaluate the effectiveness of each of the five different PV systems, enabling a successful correlation as only one variable is changed.

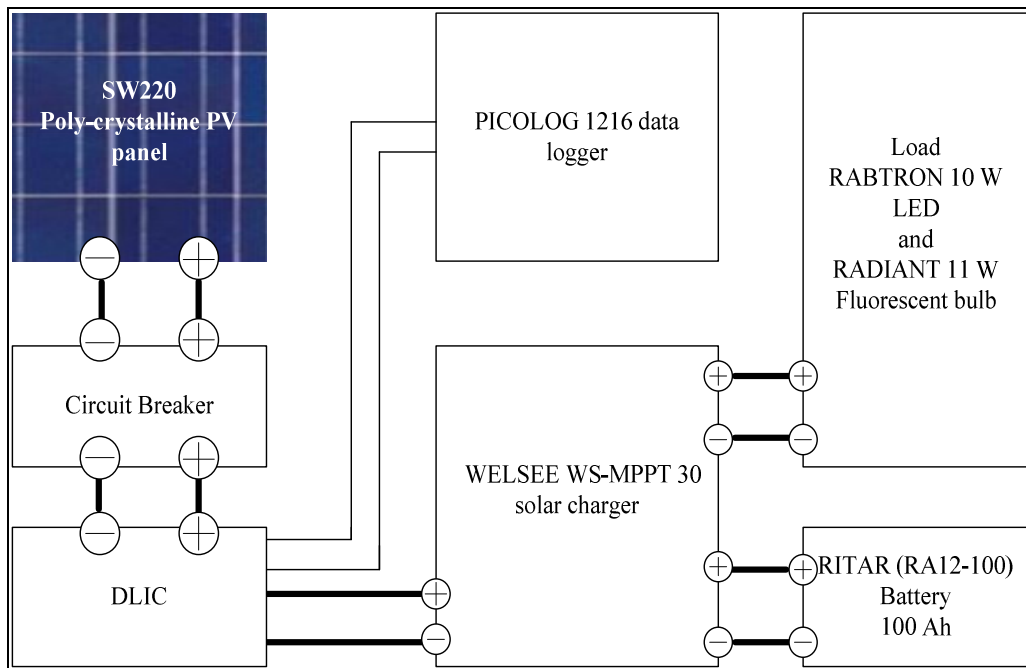


Figure 17: Electrical design of the main study

3.8 Summary

This chapter focused on the methodology and the simulation package which was used in the research and how the pilot study was done using a stationary SW220 poly-crystalline PV panel set to three different tilt angles suggested by Heywood and Chinnery. The main study was also addressed where five identical SW220 poly-crystalline PV panels were placed at different tilt angles (16° , 26° and 36°) with a corresponding orientation angle of 0° . The other two PV panels were placed at a tilt angle of 36° with orientation angles set to $+15^\circ$ and -15° . Chapter 4 will present the experimental results obtained from the data analysis as well as the correlation of the experimental results with the simulation package.

Chapter 4 Measurement and results

4.1 Introduction

Chapter 3 considered the methodology used in this research, as well as some mathematical models, equations of latitude and simulation packages that exist regarding PV installations. Priority is given to the Perez *et al.* model which is an anisotropic model as this research focuses on direct beam radiation. The Heywood and Chinnery equations of latitude were selected due to the fact that they are the suggested equations of latitude according to literature for calculating tilt and orientation angles in the southern hemisphere (Vanderbijlpark lies on a latitude of 26° south). This equation was recently validated and discussed at an international conference in China (Asowata *et al.*, 2012:1-6). Chapter 4 will now consider the experimental results (measured) of both the pilot and the main study. The results obtained from the equations of latitude, mathematical models and the correlation of the experimental results with the simulation package is also presented in the form of graphs and tables.

4.2 Pilot study results

In the pilot study of this research, data was collected over a four month period from April through July of 2011. The pilot study sought to differentiate between the on-time and off-time of a PV system, where the on-time can also be referred to as the power-conversion time where the PV panel is converting solar energy into electrical energy. The average on-time per week is further an indication of the availability of direct beam radiation incident on the PV panel. The average on-time per week, as well as the average on-time per day, is determined for a singular PV panel which was placed at three different tilt angles, being 16°, 26° and 36° with a fixed orientation angle of 0°. Figure 18 shows an example of the effect that different radiation conditions exert on the output of a DC-DC converter. The first portion of the graph (0% to 58%) indicates no output of the DC-DC converter as no solar radiation exists (attributed mainly to night time). The second portion of the graph (58% to 81%) is

where the DC-DC converter produces an output voltage which is not its stated operating voltage (12 V). This is due to the fact that diffused radiation exists and not direct beam radiation. Diffused radiation is basically the radiation from the surroundings of the PV panel which is not sufficient to drive the load successfully. The third portion of the graph (82% to 100%) indicates the effect of direct beam radiation on the DC-DC converter voltage.

The point at which power is delivered to the load is indicated by a triangle and represents the start of the conversion-time as a result of the direct beam radiation (100% - 82% equaling 18% for this given example). The triangle also indicates a voltage of about 12 V which coincides with the output voltage specification of the DC-DC converter. The R^2 Value is obtained by doing a regression analysis (Linear). It is basically a value that indicates the strength of the relationship between the average work-time per week of the system and the amount of solar radiation available for that particular week. This analysis was applied to each week of data collected between April and July of 2011.

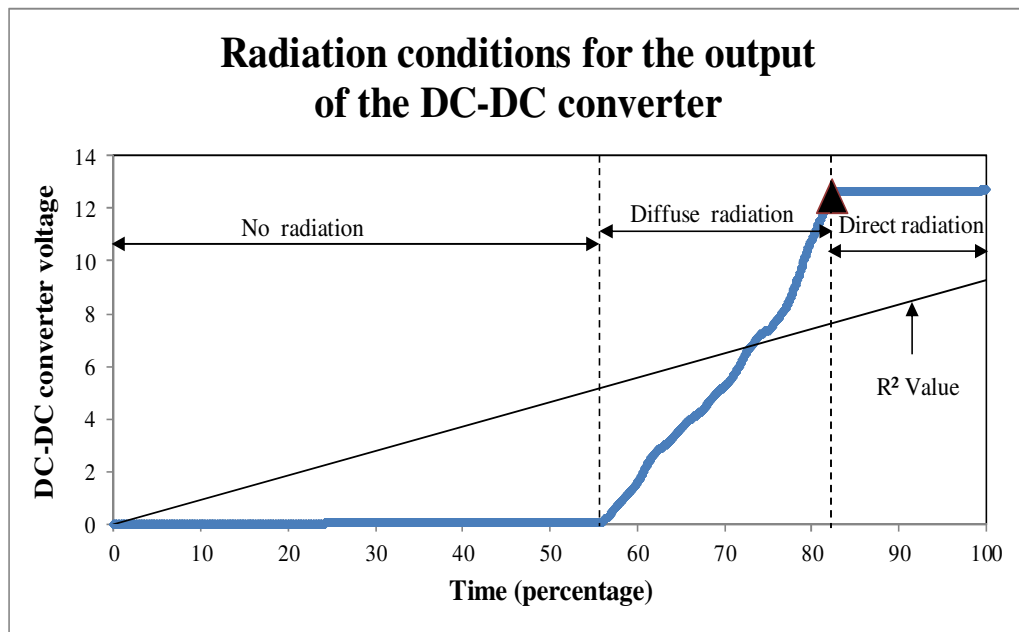


Figure 18: Radiation conditions for the output of the DC-DC converter (an example)

Figure 19 shows an example of the average work-time per day for the DC-DC converter, obtained from a residual plot using polynomial 6. The polynomial regression is a form of linear regression in which the relationship between the independent variable x (time) and the dependent variable y (voltage) is modeled. The dots below the polynomial curve indicate the effect of cloud movement on the set of data obtained. The work-time per day is the amount of time the PV panel was delivering power to the load (being from about 10:30 AM to approximately 15:30 PM). A regression analysis of the residual plot (polynomial 6) is further done to obtain the average work-time per day of different DC-DC converters (represented by the R^2 Value). This analysis was also done for each week of data collected from April through July of 2011.

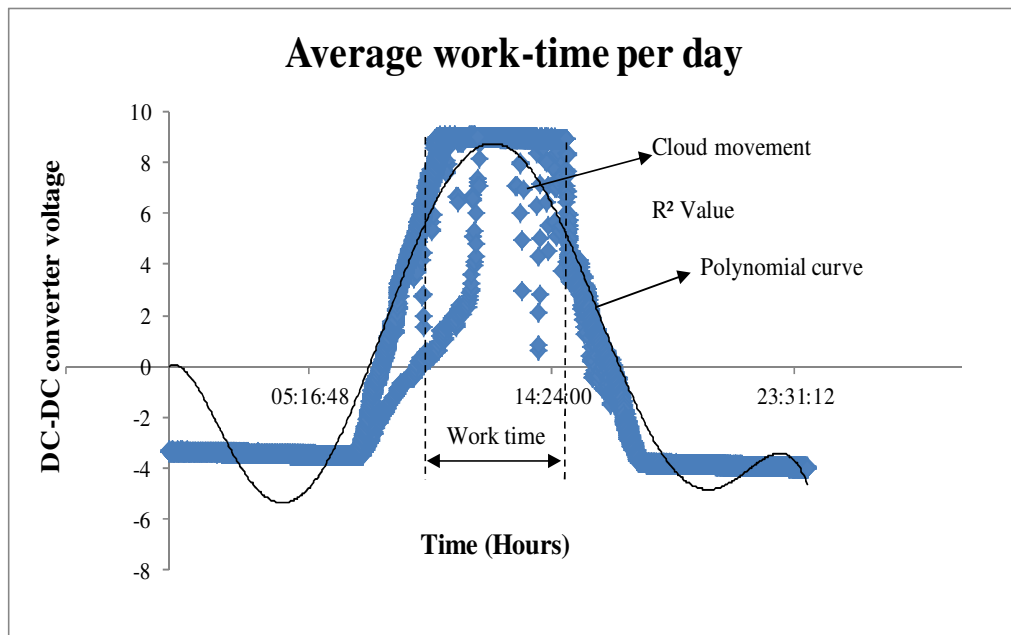


Figure 19: Average work-time per day of the DC-DC converter (an example)

Although a number of different polynomial orders exist in the Data Analysis Toolpak used in MS EXCEL, the polynomial 6 was chosen as its resulting line matches the original data points most effectively as compared to the other orders. The R^2 Value indicates how well the resulting line matches the original data points. It is also a statistical value that indicates the strength of the relationship between the average

work-time per day and the direct solar radiation received. Figure 20 represents a regression trend line representing the recorded output voltage of a DC-DC converter for the week of 8 – 15 July, 2011.

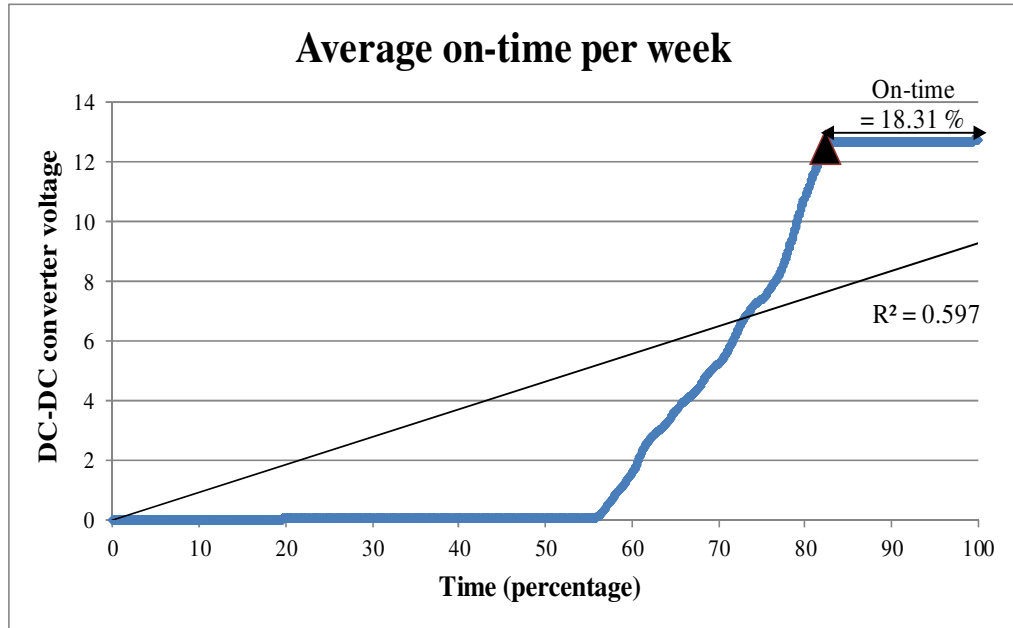


Figure 20: Regression analysis (linear) of the data obtained for the 8 – 15 July, 2011 (12 V DC-DC converter/PV panel placed at tilt angle = 16°

The average on-time and off-time for this week is plotted versus time. The DC-DC converter’s output voltage to a constant load is directly related to the input voltage from the PV panel. The point at which sufficient power is being delivered to the load is indicated by a triangle and represents the start of the on-time or power-conversion time. The triangle also indicates a voltage of about 12 V on the Y-axis which coincides with the output voltage specification of the DC-DC converter.

This analysis shows an average on-time per week of 18%, which equates to the percentage of available direct beam radiation for that specific week. No radiation, diffuse radiation and direct beam radiation can be deduced from this sketch using the example shown in Figure 18. A linear trend line indicates a statistical R^2 Value of 0.597. This value illustrates the strength of the relationship and the proportion of

variability between the average on-time per week and the available direct beam radiation received. Figure 20 shows that the DC-DC converter supplies power to the load for about 18% of the week which equates to the percentage of available direct beam radiation (direct sun hours) for that specific week. The amount of direct sun hours per day is therefore calculated as follows:

$$\text{Direct sun hours per day} = 24 \text{ hours} \times \text{AveOnTime} \quad (10)$$

$$\text{Direct sun hours per day} = \frac{24 \text{ hours} \times 18.31\%}{100}$$

$$\text{Direct sun hours per day} = 4.39 \text{ hours}$$

Figure 21 now highlights the average work-time per day for the week of 8 – 15 July, 2011.

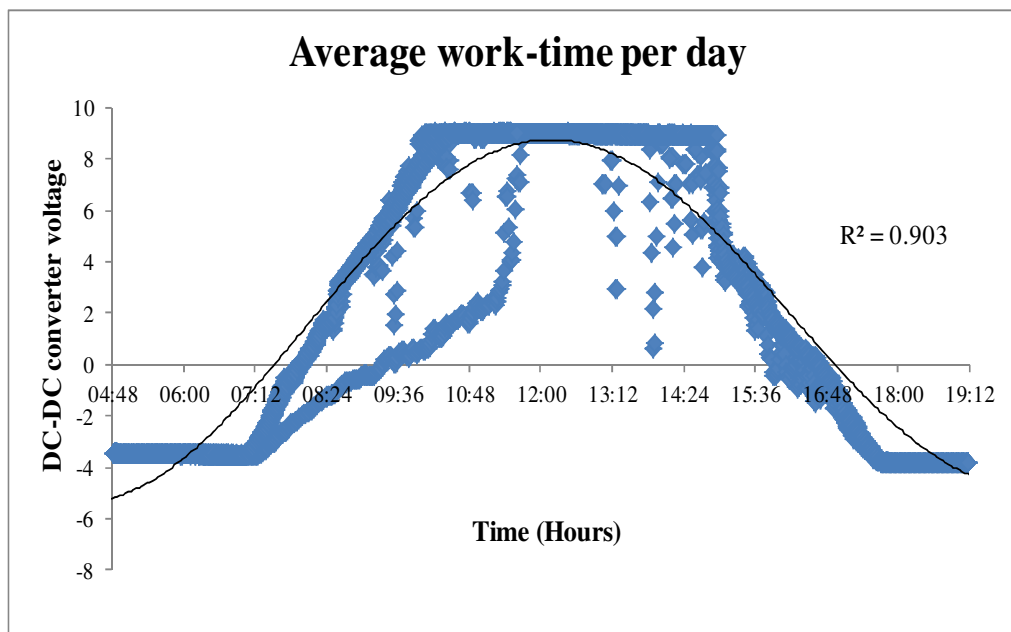


Figure 21: Average work-time per day 8 – 15 July, 2011 (12V DC-DC converter/ PV panel placed at tilt angle = 16°)

The work-time (illustrated in the example of Figure 21), in which the PV panel was delivering power to the load, is approximated between 10:00 AM and 15:18 PM. It

also shows that minimum cloud movement was present (lack of many dots below the polynomial curve) for this set of data, giving rise to a relatively clear-sky condition. The average on-time per week for the 17 – 24 June, 2011 and 10 – 17 June, 2011 are shown in Figures 22 and Figure 23 respectively.

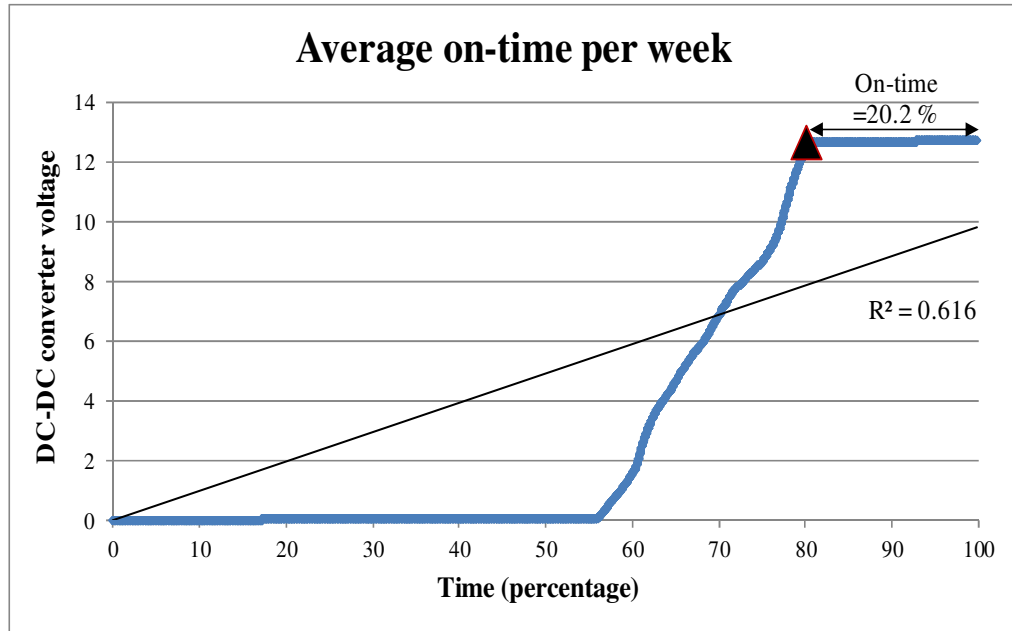


Figure 22: Regression analysis (linear) of the data obtained for the 17 – 24 June, 2011 (12 V DC-DC converter/PV panel placed at tilt angle = 26°

These data sets were taken for a 12 V DC-DC converter with the PV panel set to 26° and 36°. The average on-time of the system (the time in which power is being delivered to the load) is derived with a normal probability plot using MS EXCEL (Data Analysis Toolpak). The point at which power is delivered to the load is indicated by a triangle and represents the start of the conversion-time and is 20.2% and 19.74% respectively.

A linear trend line indicates a statistical R^2 Value of 0.616 and 0.632. Figures 22 and 23 indicate a higher on-time as compared to Figure 20 and subsequently a higher R^2 Value. Regression analysis can be used for process optimization (Montgomery &

Runger, 2011:402) which, in this case, suggests that the 36° tilt angle provides a better optimum PV system performance as compared to the 26° and 16° tilt angles.

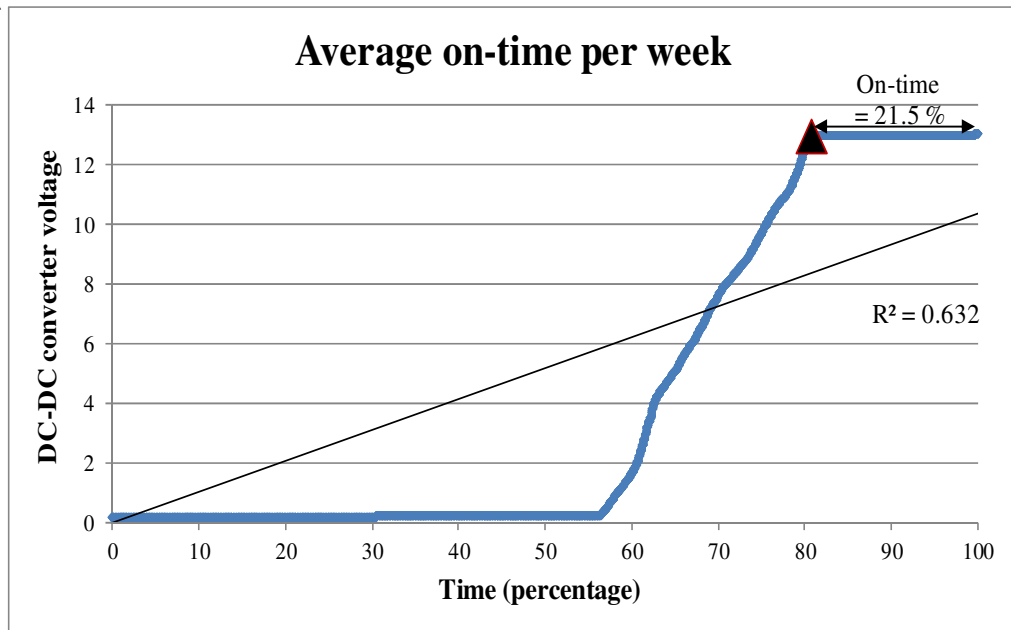


Figure 23: Regression analysis (linear) of the data obtained for the 10 – 17 June, 2011 (12 V DC-DC converter/PV panel placed at tilt angle = 36°)

Figure 24 and Figure 25 shows the average work-time per day for the week of 17 – 24 June, 2011 and 10 – 17 June, 2011. These data sets were taken for 12 V DC-DC converters with the PV panel set to 26° and 36° tilt angles. The R^2 Value in Figure 24 is 0.928, which shows how well the resulting line matches the original data points. It is also a statistical value that indicates the strength of the relationship between the average work-time per day and the direct solar radiation received from the sun.

Figure 24 further highlights the average work-time per day in which the PV panel was delivering power to the load (being from about 09:00 AM to approximately 15:19 PM) and also shows that no cloud movement was visible (lack of dots below the polynomial curve), giving rise to a clear-sky condition. Figure 25 represents the effect of cloud movement and air pollution on the average on-time of the system for a week. A regression analysis (Polynomial 6) for the residual plot shows a R^2 Value

of 0.910, which shows how well the resulting line matches the original data points. It is also a statistical value that indicates the strength of the relationship between the average work-time per day and the direct solar radiation received from the sun.

Figure 25 further highlights the average work-time per day in which the PV panel was delivering power to the load (being from about 09:36 AM to approximately 15:30 PM). It further shows that a lot of cloud movement was present (presence of dots below the polynomial curve), giving rise to a no clear-sky condition. A comparison between Figure 24 and Figure 24 reveals a wider response curve (higher average work-time) and subsequently a higher R^2 Value for Figure 24 (R^2 value of 0.928 as compared to a R^2 Value of 0.910).

Further analysis of the Figures shows that Figure 24 was taken under a clear sky condition (lack of dots under the polynomial curve) while Figure 25 indicates a lot of cloud movement (visible dots below the polynomial curve). Atmospheric conditions, in terms of industrial pollution (Swart *et al.*, 2011: 1) and cloud movement, affect the performance of PV systems, and therefore have a direct bearing on the total number of complete samples which must be collected (Mashorhor *et al.*, 2008: 269-273). The plot presented in Figure 24 and 25 was obtained using polynomial 6 under the data MS EXCEL (Data Analysis Toolpak).

A polynomial is basically defined as a term rather as a finite sum of terms, with only positive or zero integer exponents permitted on the variables. The product of a real number and one or more variables raised to powers is called a term. (Originlab, 2013) where X is the independent variable and Y is the dependent variable, a polynomial regression fits data to a model.

Other polynomials do exist but polynomial 6 was chosen in this research because the resulting line it produces matches the data points most accurately as compared to other polynomials. The DC-DC converter voltage is well represented on the Y-axis as well as the time in hours which the PV panel was supplying power to the DC-DC converter hence to the load is well represented on the X-axis.

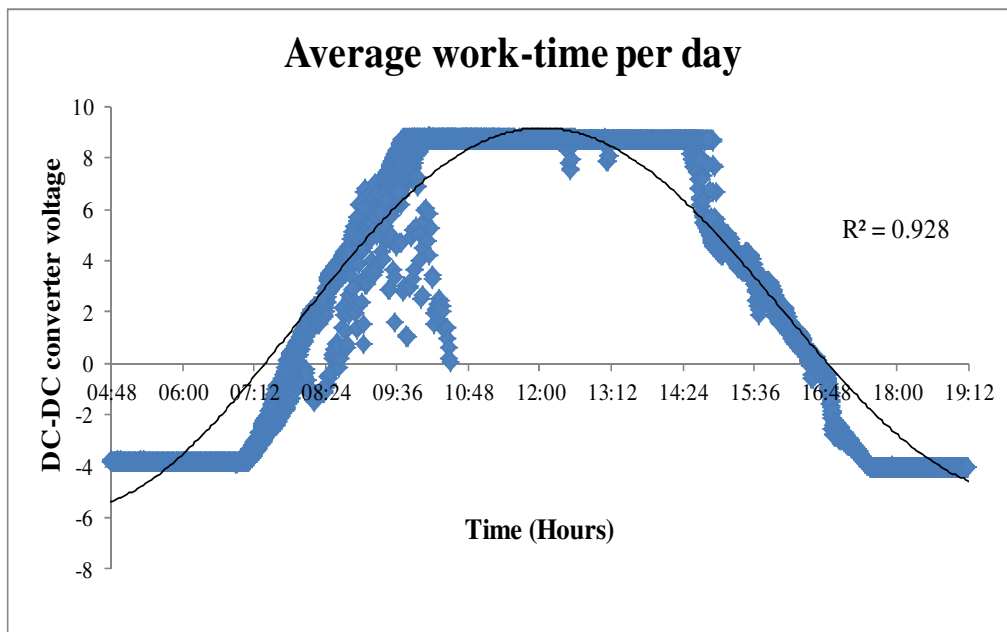


Figure 24: Average work-time per day 17 – 24 June, 2011 (12V DC-DC converter/ PV panel placed at tilt angle = 26°)

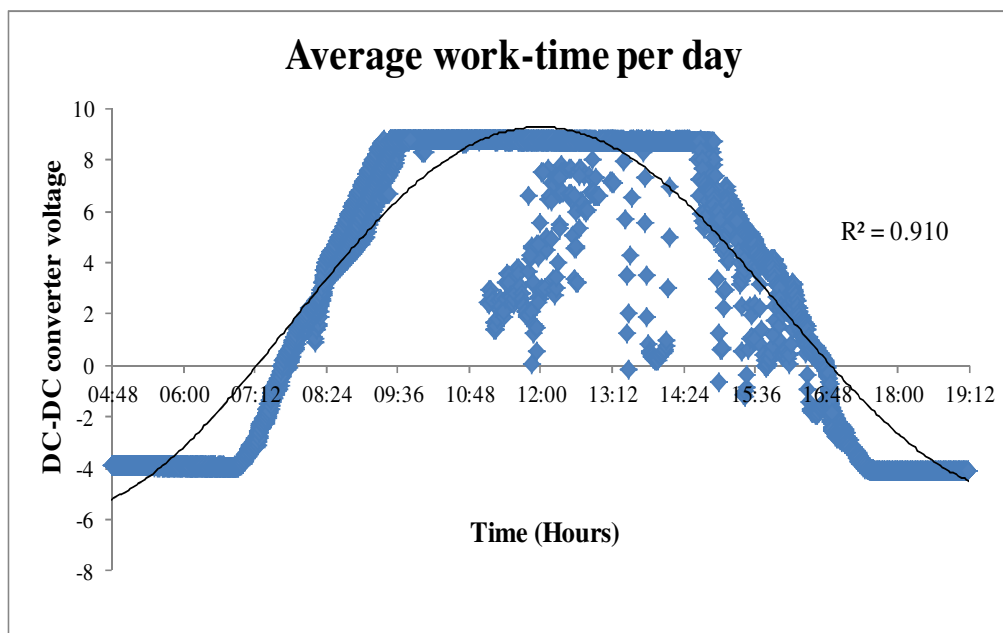


Figure 25: Average work-time per day 10 – 17 June, 2011 (12V DC-DC converter/ PV panel placed at tilt angle = 36°)

The individual results of the average on-time per week obtained from the regression analysis were collated with the other results obtained for each week of data collected over a four month period from April through July of 2011. Five samples for each tilt angle were collected and the analysis of this 15 week period is shown in Table 12, where the data is ranked according to the regression trend value. This regression trend line value (linear) indicates the relationship between the average on-time per week (actual direct solar radiation received by the PV panel for each week) and the output voltage of the DC-DC converter.

Table 12: Set of data for the months of April 2011 through July 2011 using 12 V, 24 V and 48 V DC-DC converters

Week starting	Tilt angle	On-time/week as a percentage	Regression trend line value (R^2)
20 th May	16°	2.84	0.567
29 th July	16°	11.53	0.573
13 th May	16°	1.84	0.577
15 th July	16°	18.31	0.597
22 nd July	16°	9.36	0.599
27 th May	36°	10.07	0.609
15 th April	36°	8.38	0.644
22 nd April	36°	8.76	0.611
24 th June	26°	20.2	0.616
6 th May	26°	16.19	0.623
1 st July	26°	19.81	0.629
10 th June	36°	14.94	0.631
17 th June	36°	21.5	0.632
29 th April	26°	19.68	0.656
8 th April	26°	17.89	0.657

From the results gathered in Table 12, it is generally observed that the 26° and 36° tilt angles indicated the highest regression trend value (linear) for these months. The higher average on-time per week results in a higher R^2 Value. A peak winter month in South Africa is June, which indicated some high regression trend values (linear) for 26° and 36° tilt angles (see Table 12). This coincides with earlier endeavours to calculate the correct tilt angle using mathematical and simulation models based on research done by Chinnery (Armstrong & Hurleya, 2009: 780-787).

These initial experimental results suggest validity and reliability of these mathematical and simulation models for winter months in South Africa. The efficiency of the different DC-DC converters was also calculated for the pilot study using the four months of collected data (see Tables 13, 14 and 15 for the three different DC-DC converters). The different tilt angles, PV voltage, current and power inputs, DC-DC converter voltage, current and power outputs, efficiency and on-time are shown. The input voltage (PV voltage) data was filtered below 27 V, while the DC-DC voltage was filtered 2 V below its specification (e.g. using a 24 V DC-DC converter resulted in a filtered voltage of 22 V). This was done in order to make allowance for the response time of the DAQPRO 5300 data logger responsible for recording the data. These individual PV and DC-DC voltages were averaged and the input and output powers were calculated as follows:

$$\text{Input power (PV power)} = \text{PV voltage} \times \text{PV current} \quad (11)$$

$$P_{in} = V_{in} \times I_{in}$$

$$P_{in} = 29.72 \times 2.81$$

$$P_{in} = 83.5 \text{ W}$$

$$\text{Output power (DC-DC power)} = \text{DC-DC voltage} \times \text{DC-DC current} \quad (12)$$

$$P_{out} = V_{out} \times I_{out}$$

$$P_{out} = 48.26 \times 1.404$$

$$P_{out} = 67.75 \text{ W}$$

The efficiency of the PV system for each week for the data obtained in the pilot study of this research was calculated using the efficiency formula which is presented in equation 19.

$$n(\%) = \frac{P_{out}}{P_{in}} \times 100 \quad (13)$$

$$\begin{aligned} n(\%) &= \frac{67.75}{83.5} \times 100 \\ &= 81.14 \% \end{aligned}$$

The significance of these tables is to contrast the efficiency of the different types of DC-DC converters applied in this research, hence ascertaining which DC-DC converter was most efficient when used with a 220 W poly-crystalline PV panel. From the results gathered in Tables 13 – 15, the 12 DC-DC converter was most efficient as it shows an overall efficiency of 89.27%.

Table 13: Data for a 48 V DC-DC converter

Week ending	Tilt angle (°)	PV voltage (Vin) (V)	PV current (Iin) (A)	Power in (W)	DC voltage (Vout) (V)	DC current (Iout) (A)	Power out (W)	Efficiency (%)	On-time/wk in hrs
11 th Mar	16°	29.72	2.81	83.5	48.26	1.404	67.75	81.14	81.9
18 th Mar	26°	30.67	2.81	86.1	48.81	1.404	68.52	79.51	77.73
25 th Mar	36°	30.52	2.81	85.8	48.75	1.404	68.44	79.80	37.19
1 st Apr	16°	30.74	2.81	86.3	48.05	1.404	67.46	78.09	33.11
8 th Apr	26°	31.01	2.81	87.1	48.31	1.404	67.82	77.83	30.05
15 th Apr	36°	29.63	2.81	83.3	48.54	1.404	68.15	81.85	14.07
Average		30.38	2.81	85.35	48.45	1.404	68.02	79.70	NA

Table 14: Data for a 24 V DC-DC converter

Week ending	Tilt angle (°)	PV voltage (Vin) (V)	PV current (Iin) (A)	Power in (W)	DC voltage (Vout) (V)	DC current (Iout) (A)	Power out (W)	Efficiency (%)	On-time/wk in hrs
22 nd Apr	36°	31.26	4.115	128.3	24.01	4.078	97.91	76.11	14.71
29 th Apr	26°	31.8	4.115	130.9	24.27	4.078	98.97	75.63	33.06
6 th May	26°	30.37	4.115	124.9	25.17	4.078	102.64	82.13	28.39
13 th May	16°	27.86	4.115	114.4	22.95	4.078	93.59	81.63	4.23
20 th May	16°	29.43	4.115	121.0	24.21	4.078	98.72	81.52	4.77
27 th May	36°	30.26	4.115	124.1	24.16	4.078	98.52	79.12	16.91
Average		30.16	4.115	123.93	24.12	4.078	98.39	79.35	NA

Table 15: Data for a 12 V DC-DC converter

Week ending	Tilt angle (°)	PV voltage (Vin) (V)	PV current (Iin) (A)	Power in (W)	DC voltage (Vout) (V)	DC current (Iout) (A)	Power out (W)	Efficiency (%)	On-time/wk in hrs
10 th Jun	36°	31.17	2.7	84.2	12.61	6.0	75.66	89.90	25.02
17 th Jun	36°	31.47	2.7	84.9	12.6	6.0	75.6	88.97	33.16
24 th Jun	26°	31.15	2.7	84.2	12.51	6.0	75.06	89.24	33.93
1 st Jul	26°	32.03	2.7	86.4	12.68	6.0	76.08	87.97	33.28
8 th Jul	26°	31.96	2.7	86.2	12.71	6.0	76.26	88.37	29.71
15 th Jul.	16°	31.35	2.7	84.7	12.44	6.0	74.64	88.18	30.76
22 nd Jul.	16°	29.62	2.7	79.9	11.95	6.0	71.7	89.65	15.72
29 th Jul.	36°	29.55	2.7	79.6	12.22	6.0	73.32	91.89	19.37
Average		31.03	2.7	83.76	12.46	6.0	74.79	89.27	NA

The 12 V, 24 V and 48 V DC-DC converters were applied in this research. The similarity of these converters is that they provide an output voltage that rightly matches their specification at points when the PV voltage was optimum (29 V). In DC-DC buck (step-down) converters, the output voltage magnitude is always lower than the input voltage magnitude (Taghvaei, Radzi, Moosavain, Hizam & Marhaban, 2013:216-227) and is directly proportional to the duty cycle (Van Rensberg, 2012:102).

This indicates that the 12 V and the 24 V DC-DC converters are buck (step down) converters. In like manner, in a boost (step-up) converter the output voltage magnitude is higher than the input voltage magnitude, making the 48 V a boost (step-up) converter. The inductance in DC-DC buck converters basically reduces with the increased current corresponding to increased incident solar irradiation. This contributes to a 75% smaller inductor as the stable step response changes in respect to the input solar power (Taghvaei *et al.*, 2013:216-227).

The disadvantage of the boost DC-DC converter over the buck DC-DC converter is that under low irradiation condition, a boost converter cannot track the MPP as this point is in the non-operating region. All three types of DC-DC converters start delivering power to the load (start of the on-time) when their output voltage reaches their rated specification which is attributed to effect of direct beam radiation incident on the PV panels.

The pilot study has been introduced where the availability of power was interpreted with a couple of tables and graphs showing the average work-time per week and average work-time per day. A comparison of the different types of DC-DC converters that were used in this research, was discussed. The best power efficiency came from the 12 V DC-DC converter. The R^2 Values indicated that the 26° and 36° were the better tilt angles for PV installations in South Africa during winter months. The pilot study's results match closely the results obtained from the main study, which is presented next.

4.3 Main study results

In the main study, data was collected over a year period from the 1st of January to the 31st December 2012. As mentioned in Chapter 3, the main study consisted of five identical PV panels with three of the PV panels placed at tilt angles of 16°, 26° and 36° respectively with a corresponding orientation angle of 0°. The other two PV panels were placed at a tilt angle of 36° but with orientation angles of +15° and -15° respectively. This was done in order to compare and establish validity of the obtained results with regard to a 0° orientation angle.

All data parameters should remain identical except for one parameter, in order to arrive at an outright and valid comparison. Data was collected from the two PV panels set to different orientation angles from August to December 2012, owing to a delay in the supply of research materials. The results were sectioned into quarters (as four quarters exist per year) in order to simplify the analysis and presentation of the data. The quarters were arranged as shown in Table 16.

Table 16: Quarters of the year as structured for the main study

Quarter	Months
1 st Quarter	January-March
2 nd Quarter	April-June
3 rd Quarter	July-September
4 th Quarter	October-December

A total of 1440 samples were collected daily, as the sampling interval was set to one minute in the PICOLOG data logger. These samples were exported to a MS EXCEL sheet for further analysis. The sampled output PV voltages were used to determine the following charge states of a Lead Acid Valve Regulated Battery (LAVRB used as the main storage device):

- Case A: The percentage (%) of time when the system was not charging the batteries (which maybe night time or significant cloud movement). A reference voltage of 10 V was chosen due to the fact that the system draws

less than 100 mA of current from the PV panels for voltages less than 10 V, and is seen as insignificant in charging the system (see Figure 26 for the 10 V point). It is mathematically calculated as:

$$\text{Not Charging} = \frac{(\text{Sum of number of PV voltages, "<10V"})}{1440} \times 100\% \quad (14)$$

- Case B: The percentage (%) of time when the system was fully charged (when the batteries have reached 100% SOC or 13.8 V). PV voltages were filtered using a reference voltage of 18 V. Voltages greater than 18 V were selected as this is the voltage at which point the MPPT enters a pulse width modulation stage (PWM), indicating that the battery banks are fully charged (see Figure 26 overleaf). It is mathematically calculated as:

$$\text{Fully Charged} = \frac{(\text{Sum number of PV voltages, ">18V"})}{1440} \times 100\% \quad (15)$$

The percentage (%) of time when the system was discharging can now be calculated by subtracting 100 % from the addition of Case A (not charging) and Case B (fully charged). Table 17 shows a concise breakdown of data collected, discharging, charging and fully charged states (hours and percentages) of the PV system for the week starting the 19th of January 2012.

The preceding equations were used in calculating the data for each day, and were further applied to all 365 days of 2012 (1440 samples per day) and was averaged for each quarter of the year as 365 data points could not be shown.

This analysis shows that the 36° tilt angle completed a faster charging time (8.6 hours) and stayed fully charged for a longer period of time (5.4 hours) when compared to the 26° and 16° tilt angles. The analysis further shows that all three tilt angles had the same discharging time (10 hours). The total analysis of the different quarters of the year is shown in Tables 18 and 19.

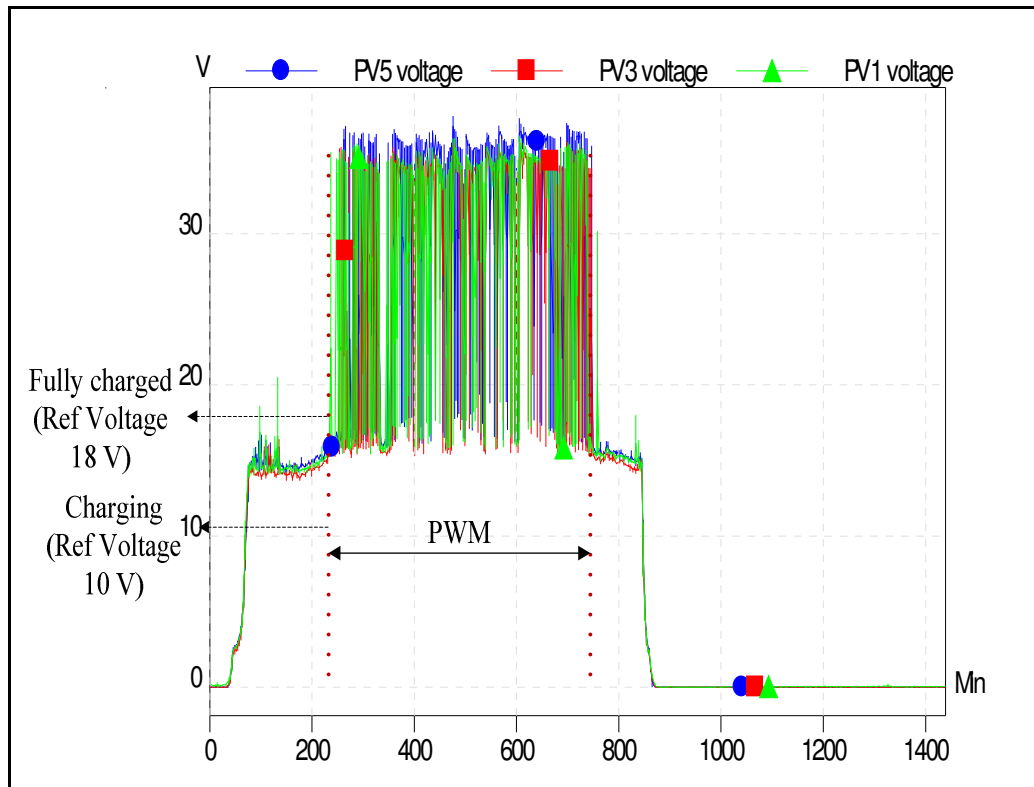


Figure 26: Data showing reference voltages of 10 V and 18 V for the 19 February 2012.

Table 17 further presents the time and percentages in which the system was fully charged, charging and discharging for that particular day with respect to the different tilt angles (36° , 26° and 16°) with all PV panels placed at the same orientation angle of 0° .

Table 17: Charge conditions of data taken for the week starting 19 January 2012

	36 Degrees	Hours	26	Hours	16 Degrees	Hours
Discharging	42.0%	10.1	41.9%	10.1	42.0%	10.1
Charging	35.7%	8.6	36.1%	8.7	36.6%	8.8
Fully charged	22.3%	5.4	21.9%	5.3	21.4%	5.1
Total	100.0%	24.0	100.0%	24.0	100.0%	24.0

Table 18: The average fully charged percentages for the five PV systems

Months/ Quarters	Average percentage fully charged for different tilt angles with a fixed orientation angle of 0°		
	36 Degrees	26 Degrees	16 Degrees
1 st quarter (January-March)	14.03%	12.96%	13.68%
2 nd quarter (April-June)	7.06%	5.63%	3.30%
3 rd quarter (July-September)	21.34%	18.29%	14.66%
4 th quarter (October-December)	18.08%	17.74%	16.90%

Of prime importance in this research is the percentage of time in which the system was fully charged. This assists in identifying the best tilt angle to place the PV panels, as a higher fully charged percentage indicates that the MPPT charges the system within a shorter time period as optimum output power is received from the PV panel. Figure 27 represents a graph of the 1st quarter of the main study which comprises data collected from January – March 2012.

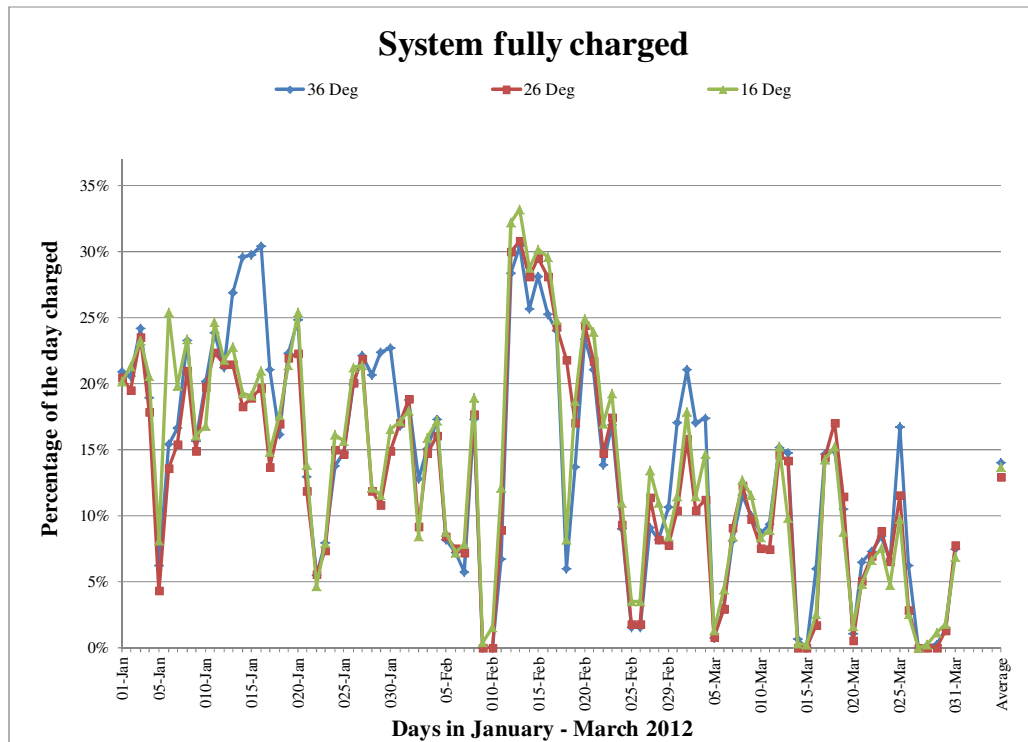


Figure 27: Average percentage when the system was fully charged (January – March 2012)

The average fully charged percentage for the 36° tilt angle was 14.03%, the 26° tilt angle 12.96% and the 16° tilt angle 13.96% and these are clearly represented in Figure 27.

The first quarter reveals that the PV system with a tilt angle of 36° outperforms the other two PV systems, as it enjoys a longer fully charged state, indicating that it has received more energy within a shorter time period than the other two systems. Recall that the discharging state is constant for all five PV systems, with the charging states depending on the amount of energy received from the PV panel.

Figure 28 represents the second quarter of the data obtained in the main study of this research which spans from April – June 2012. In this case the 36° tilt angle revealed an average fully charged percentage of 7.06%, the 26° tilt angle 5.63% and the 16° tilt angle 3.30%. Again the PV system with a tilt angle of 36° proves superior.

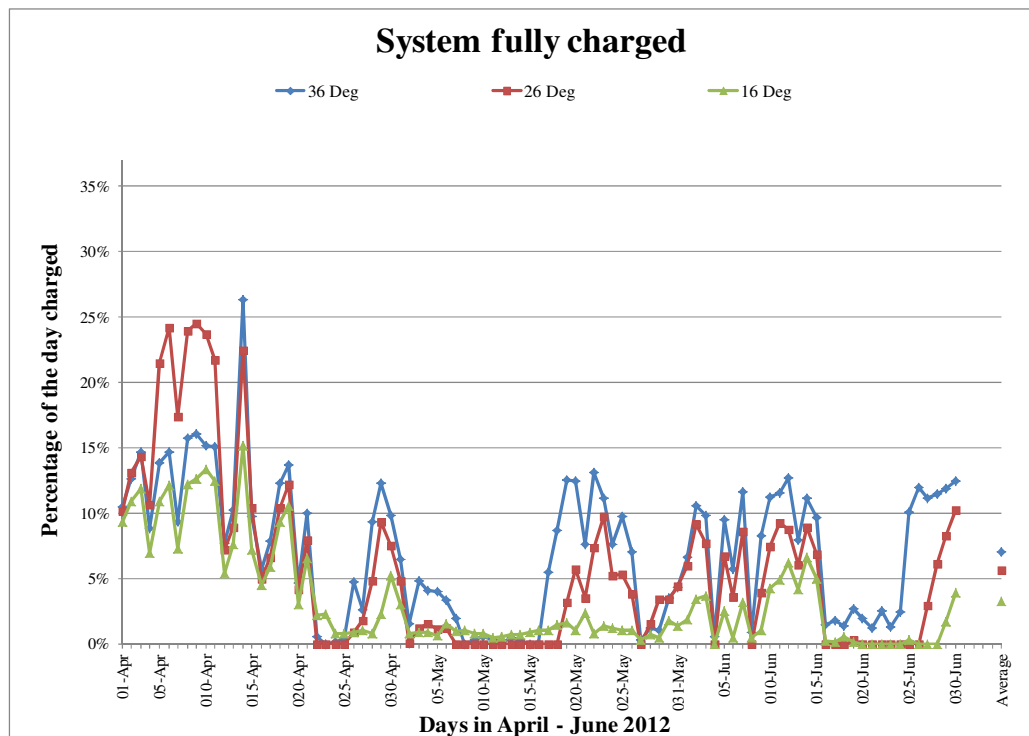


Figure 28: Average percentage when the system was fully charged (April –June 2012)

Figure 29 represents the third quarter of 2012 (July – September). From the analysis obtained in this quarter the 36° tilt angle reveals an average fully charged percentage of 21.34%, the 26° tilt angle 18.29% and the 16° tilt angle 14.66%. Again the PV system with a tilt angle of 36° proves superior.

Recall that the discharging state is constant for all three PV systems, with the charging states depending on the amount of energy received form the PV panel. Figure 30 represents the fourth quarter of the year (October – December 2012). In this case the 36° tilt angle produced an average fully charged percentage of 18.08%, the 26° tilt angle 17.74% and the 16° tilt angle 16.90%. Again the PV system with a tilt angle of 36° proves superior.

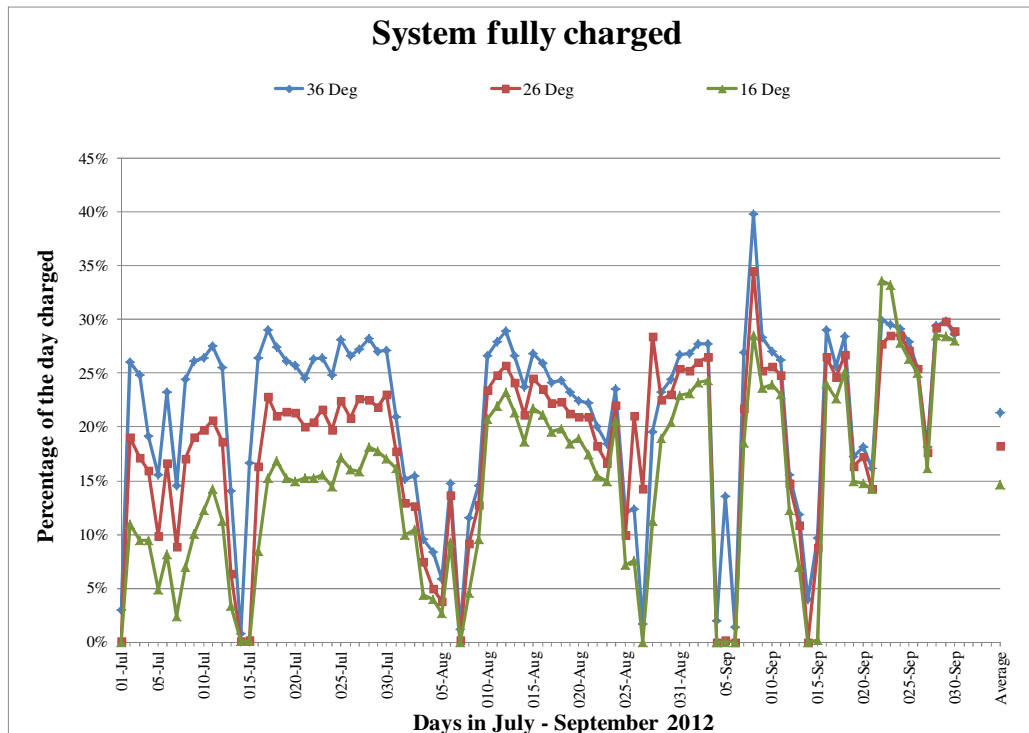


Figure 29: Average percentage when the system was fully charged (July – September 2012)

Average percentage when the system was fully charged (October – December 2012) is presented in the next figure.

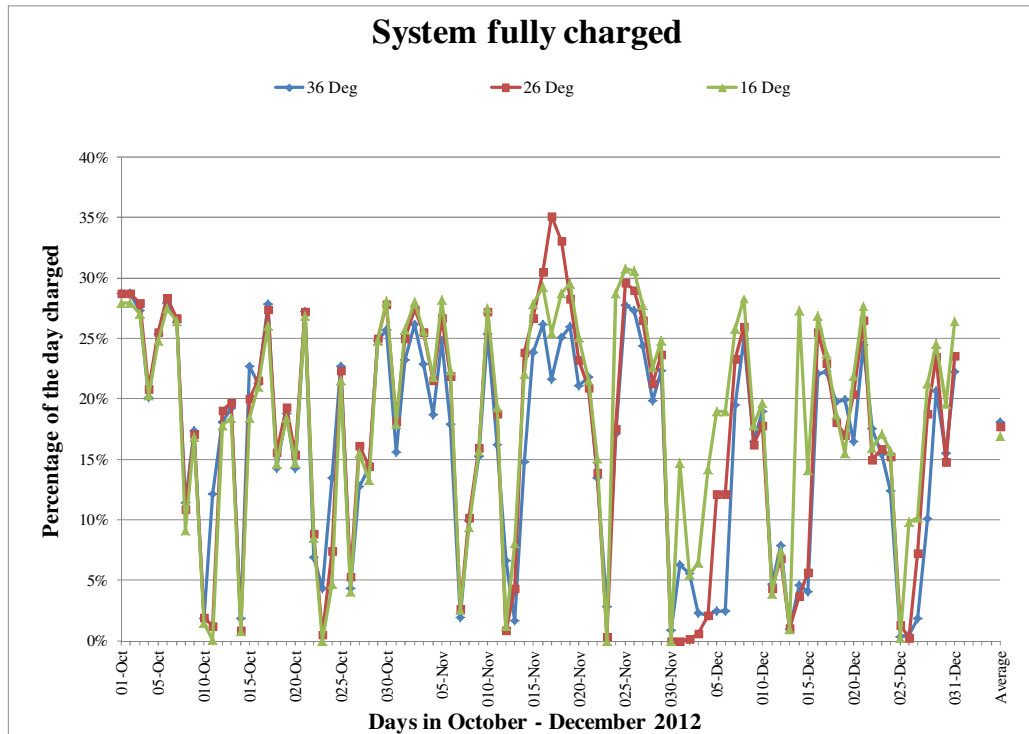


Figure 30: Average percentage when the system was fully charged (October – December 2012)

A similar regression analysis that was carried out in the pilot study (using a regression trend line value (linear or R^2 Value)) proved the 36° to be the best tilt angle for PV panel installation, when compared to the 16° and 26° tilt angles. Since regression analysis is a very vital tool in data analysis to establish validity, it was therefore also employed in the main study. This was done to establish and to prove the availability of power in the different PV systems.

The availability of power as well as the R^2 Value of a set of data of the week of 7th January 2012 is shown in Figures 31 – 33. The graphs of the data of the 7th January 2012 are an example taken from the data taken for the one year period. The graphs are a plot of the voltage versus time obtained for each week. This regression analysis, with an example shown in Figures 31 – 33, was done for the 52 weeks (sampling period of the main study). The R^2 values as well as the voltage from the PV panel when the MPPT enters the PWM stage of each week are presented in Table 19.

Table 19: R² values and PV voltages for the start of the PWM stage for each week of 2012

Week in	36°	Input voltage from the PV panel at MPPT (PWM stage)	26°	Input voltage from the PV panel at MPPT (PWM stage)	16°	Input voltage from the PV panel at MPPT (PWM stage)
7 th January	0.7668	17.821	0.7614	16.641	0.7528	16.432
14 th January	0.7785	17.179	0.7692	17.070	0.7783	19.103
21 st January	0.7732	17.070	0.7577	16.575	0.7658	17.729
28 th January	0.7455	17.271	0.7400	16.282	0.7432	16.740
4 th February	0.7548	17.436	0.7452	16.630	0.7514	16.850
11 th February	0.7172	16.978	0.7138	16.007	0.7250	16.245
18 th February	0.7710	17.234	0.7683	16.154	0.7594	16.374
25 th February	0.7117	16.520	0.7142	16.007	0.7278	16.154
3 rd March	0.7020	15.696	0.6890	15.678	0.6962	15.788
10 th March	0.7076	15.733	0.6976	15.604	0.6978	16.044
17 th March	0.6959	15.513	0.6883	15.458	0.6888	15.678
24 th March	0.6872	15.623	0.6851	15.586	0.6895	15.714
31 st March	0.6928	15.201	0.6842	15.275	0.6868	15.201
7 th April	0.6839	15.788	0.6882	15.586	0.6803	15.568
14 th April	0.7048	16.245	0.6928	15.971	0.6936	16.722
21 st April	0.6951	15.604	0.6884	15.458	0.6935	15.495
28 th April	0.6736	15.220	0.6909	15.055	0.7034	14.782
5 th May	0.6888	15.018	0.6633	15.110	0.6543	15.403
12 th May	0.7370	14.396	0.7049	14.945	0.6898	13.883
19 th May	0.6866	14.725	0.7136	14.249	0.6602	13.919
26 th May	0.6862	15.348	0.6370	15.147	0.6388	15.018
2 nd June	0.6307	15.549	0.6152	15.055	0.6541	15.014
9 th June	0.6830	15.183	0.6427	15.311	0.6403	15.678
16 th June	0.6324	15.440	0.6283	15.531	0.6365	16.099
23 rd June	0.6934	14.505	0.6965	14.872	0.6672	15.092
30 th June	0.6847	15.256	0.6416	15.568	0.6431	16.282
7 th July	0.6353	15.751	0.6112	15.659	0.6124	15.330
14 th July	0.6451	15.897	0.6328	15.513	0.6384	15.385
21 st July	0.6475	15.806	0.6389	15.586	0.6425	15.513
28 th July	0.6551	15.842	0.6430	16.044	0.6398	15.641
4 th August	0.6555	16.044	0.6459	16.044	0.6408	15.714
11 th August	0.6905	17.062	0.6839	16.821	0.6829	17.145
18 th August	0.7447	16.699	0.7406	16.610	0.7401	18.160
25 th August	0.7461	17.482	0.7430	16.832	0.7432	15.858
1 st September	0.7499	17.064	0.7486	16.554	0.7439	15.549
8 th September	0.7412	16.956	0.7295	16.753	0.7307	16.512
15 th September	0.7645	16.913	0.7596	16.817	0.7553	16.571
22 nd September	0.7747	16.885	0.7698	16.634	0.7651	16.449
29 th September	0.7584	16.857	0.7547	16.506	0.7525	16.129
6 th October	0.7925	16.898	0.7900	16.524	0.7885	16.099
13 th October	0.7839	16.966	0.7783	16.284	0.7762	16.049
20 th October	0.7937	16.637	0.7891	16.367	0.7860	15.726
27 th October	0.7911	16.817	0.7871	16.265	0.7848	15.575
3 rd November	0.8126	16.676	0.8105	16.329	0.8084	16.286
10 th November	0.7972	16.869	0.7958	16.674	0.7942	15.853
17 th November	0.8098	16.925	0.8064	17.614	0.8087	16.842
24 th November	0.8162	17.002	0.8133	17.346	0.8171	16.389
1 st December	0.8193	16.927	0.8131	16.830	0.8184	15.921
8 th December	0.8065	16.961	0.8121	18.109	0.8196	16.628
15 th December	0.8037	16.978	0.7990	16.984	0.7991	16.402
22 nd December	0.8351	17.771	0.8334	18.168	0.8321	16.122
31 st December	0.8293	16.462	0.8265	16.564	0.8292	15.969

In Figures 31 – 33 the triangle in each respective graph represents the output voltage of the PV panel where the energy storage device is fully charged and the MPPT enters a PWM stage. The analysis shown in Table 19 reveals that for all tilt angles the PV system reaches a fully charged state for PV output voltages between 15 V – 19 V, giving rise to the 18 V reference voltage that was applied in filtering the data. Another vital reason why a regression analysis was done is to obtain the tilt angle that produced the highest R^2 Value, indicating a faster charging time and optimum output power from the PV panel. The regression analysis to obtain a regression trend line value (linear or R^2 value) for Figures 31, 32 and 33 are 0.7668, 0.7614 and 0.7528 respectively. This value illustrates the strength of the relationship and the proportion of variability between the average voltage fully charged for a week and the available solar radiation received. Also the voltage fully charged on each graph corresponds to the value on the Y-axis.

From the regression analysis done of the data obtained in the main study with an example taken from the 1 – 7 January, 2012, which are presented in graphs (see Figures 31 – 33) as well as the data obtained for the 52 week period (see Table 19). The graphs and the values in Table 19 clearly shows that the 36° tilt had the highest R^2 value hence faster charging time and optimum output power from the PV panel.

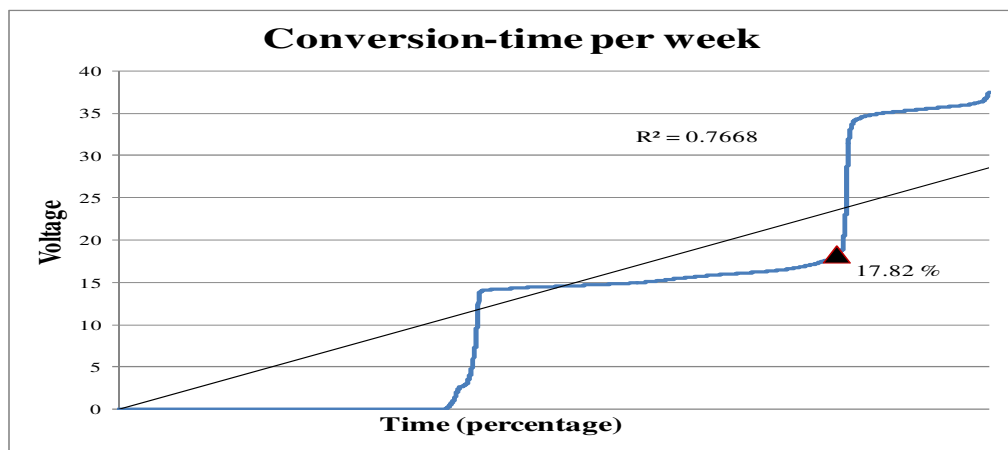


Figure 31: Regression analysis (linear) for the 1 – 7 January, 2012 (tilt angle = 36°)

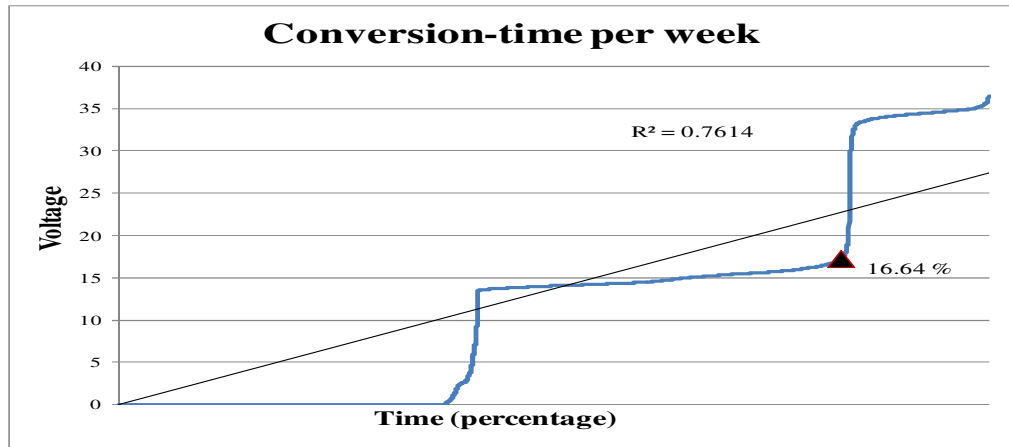


Figure 32: Regression analysis (linear) for the 1–7 January, 2012 (tilt angle = 26°)

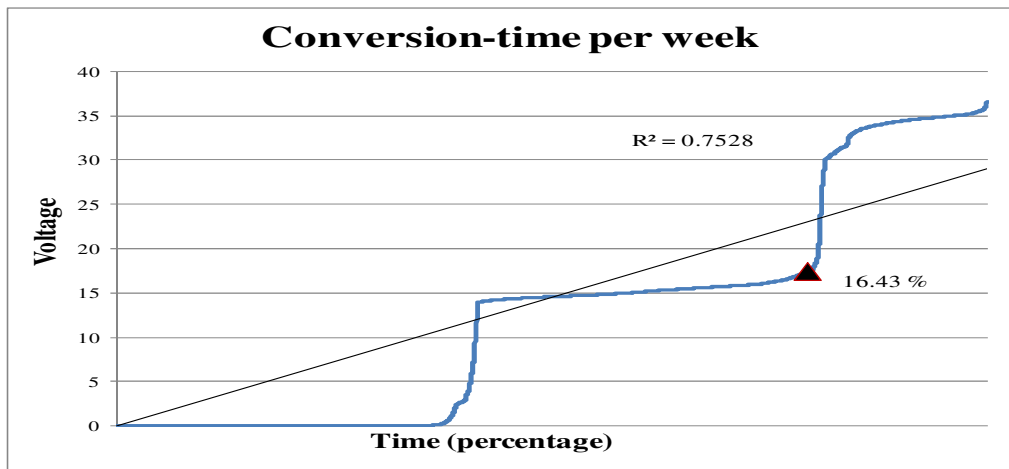


Figure 33: Regression analysis (linear) for the 1 –7 January, 2012 (tilt angle = 16°)

A contrast of the average of the +15°, -15° and 0° orientation angles using the same tilt angle of 36° is presented in Table 20 and shown as a graph in Figure 34. The percentage where the system was fully charged was calculated and averaged for the last quarter of the year. This was done in order to establish a reasonable comparison and establish which one of the three PV panels was producing more output power whilst being exposed to the same amount of direct beam solar radiation. From the graph it is clearly shown that the 36° tilt angle with an orientation of 0° (facing true north) gave the best result which corresponds to earlier endeavours suggested by

Heywood and Chinnery equations of latitude for calculating tilt and orientation angles for PV panel installations in South Africa. The 0° orientation angle produced a percentage fully charged of 11.93%, the +15° and -15° orientation angles produced corresponding values of 9.88% and 7.82%.

Table 20: Average of the 0°, +15° and -15° orientation using 36° tilt angle

Average percentage fully charged using 36° tilt angle with orientation angles of 0, +15 and -15°		
October – December 2012		
0°	+15°	-15°
11.93%	9.88%	7.82%

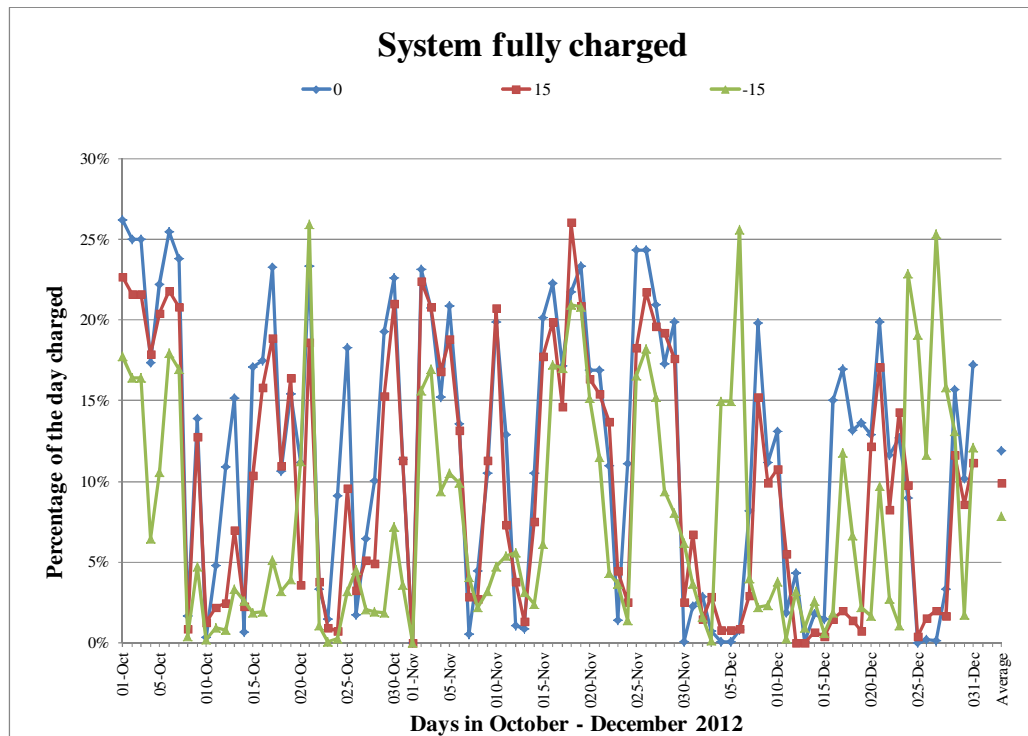


Figure 34: A comparison of +15°, - 15° and 0° orientation angles with the tilt angle placed at 36°

The simulation model results obtained in this research is presented next.

4.4 Simulation model results

A correlation of the experimental data collected from April through December 2011 to the Perez *et al.* mathematical model that exists in METEONORM was carried out. METEONORM simulation package is used for calculating solar irradiation on any arbitrary oriented surface using simulated meteorological databases (Hatwaambo *et al.*, 2009:1394-1398). It has become a valuable tool for estimating global solar irradiance, especially for where solar radiation data is missing or irregular.

The METEONORM simulation package was chosen as it contains the Perez *et al.* model which is an anisotropic model as this research focuses on direct beam radiation. The purpose of the correlation is to analyze the effect of power conversion of a PV panel for a specific point of latitude (26° South) in South Africa and to correlate it to the global solar irradiance obtained from METEONORM for that same point of latitude.

This will establish an experimental platform in support of the simulation software (METEONORM), as little or no real experimental data exists for the specified point of latitude (26° South) with regard to solar radiation. METEONORM was used to simulate the solar irradiance for a latitude of 26° South, being the point of latitude where VUT is located in Vanderbijlpark. This was done for three different tilt angles of 16°, 26° and 36° respectively. METEONORM calculations are based on monthly averages and gives maximum solar irradiation values under clear sky conditions.

The sophisticated interpolation models inside METEONORM allow a reliable calculation of solar radiation, temperature and additional parameters at any site in the world (Meteonorm, 2013). From the monthly values (station data, interpolated data or imported data), METEONORM calculates hourly values of all parameters using a stochastic model. The resulting time series correspond to 'typical years' used for system design. Figure 35 shows the simulation results from the Perez *et al.* model using METEONORM software and data obtained from meteorological databases for the time period of 1996 through 2005. These results indicate that the solar irradiance

available in Vanderbijlpark tends to fluctuate through the year, with a peak in August and a trough in June.

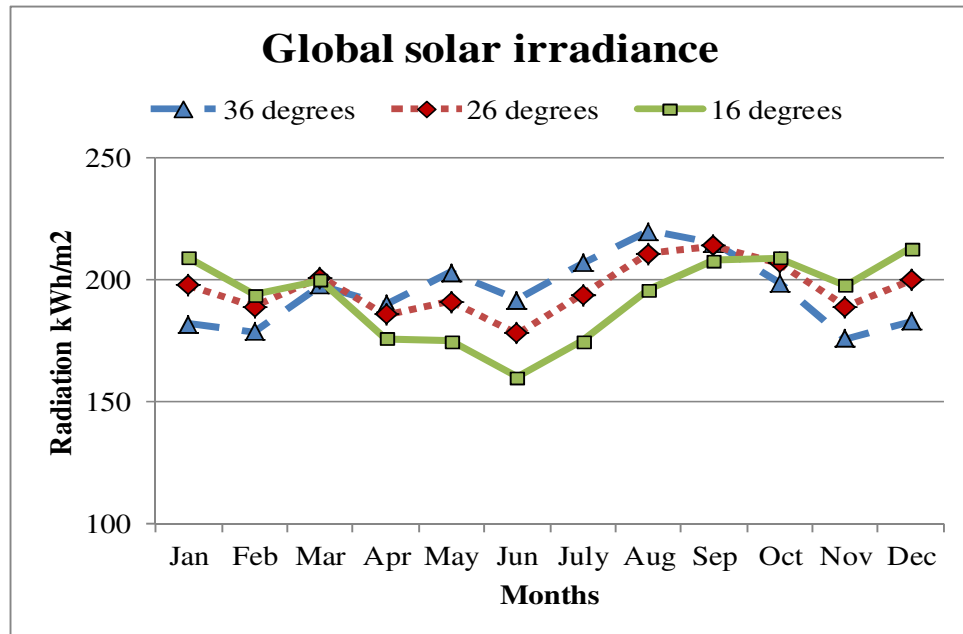


Figure 35: Simulation results of 16°, 26° and 36° tilt angles obtained from the METEONORM software for the 1996 – 2005 time period.

The individual results gathered from the regression analysis of the experimental data as presented in Figures 22 and 23 were collated with the other results obtained for each week of data collected over a nine month period from April through December 2011. The data (conversion-time per week) obtained from the experimental results are presented in percentages as they basically illustrate the on-time of the system (time which the system was converting incident solar energy into electrical energy) while the data obtained from the METEONORM software are presented in kWh/m².

A regression analysis was also carried out on the data obtained in the experimental result for the months of April through December and are presented in Table 21. The regression analysis once again proved that the higher the conversion time per week the higher the R² value. The results from the experimental data and that obtained

from METEONORM for the different tilt angles for each month for the 9 year period were also averaged. The analysis of this period is shown in Table 21.

Table 21: Set of average data from the experimental results and the solar irradiation results for the months of April through December.

Week ending	Regression analysis	Conversion-time / week as a percentage	Conversion-time/ month as a percentage	Average solar irradiation from Meteornorm (kWh/m ²)
8-April	0.657	17.89%	13.68%	January = 196.33
15-April	0.644	8.380%		February = 187.33
22-April	0.610	8.760%		March = 199.66
29-April	0.656	19.68%		April = 184.00
6-May	0.623	16.19%	18.41%	189.66
13-May	0.577	25.53%		
20-May	0.567	21.84%		
27-May	0.609	10.07%	18.29%	176.66
10-June	0.630	14.94%		
17-June	0.632	19.74%		
24-June	0.616	20.20%	14.26%	192.00
1-July	0.629	19.81%		
8-July	0.583	17.69%		
15-July	0.597	18.31%		
22-July	0.599	9.530%		
29-July	0.573	11.53%	16.32%	209.00
5-August	0.635	19.26%		
12-August	0.620	19.40%		
19-August	0.574	11.70%		
26-August	0.678	14.90%	18.0%	212.33
2-September	0.669	19.57%		
9-September	0.676	21.52%		
16-September	0.809	14.57%		
23-September	0.679	18.35%		
30-September	0.670	14.90%	10.11%	205.00
7-October	0.691	13.93%		
14-October	0.787	21.51%		
21-October	0.699	1.360%		
28-October	0.719	3.110%	6.23%	187.66
4-November	0.720	2.380%		
11-November	0.695	7.930%		
18-November	0.634	9.730%	7.94%	198.66
25-November	0.713	4.880%		
2-December	0.711	8.360%		
9-December	0.717	6.900%		
16-December	0.716	8.020%		
23-December	0.709	10.45%		
30-December	0.657	5.990%		

The data obtained from the empirical test and that from the Perez *et al.* model that exists in the METEONORM software is ranked according to the month of the year and presented in Table 21. The values presented in Table 21 were plotted on a graph

along with the simulation results from Figure 35 to illustrate that a correlation indeed exists between these two unique data sets

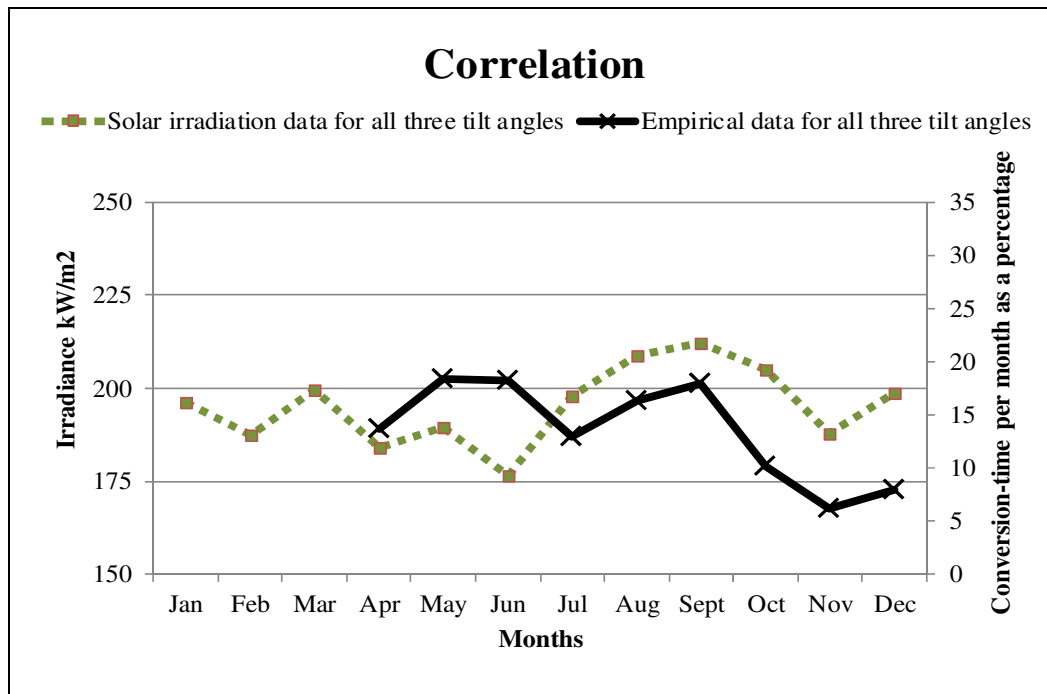


Figure 36: Correlation between the simulation data obtained from METEONORM and the empirical data obtained from the practical set-up (Asowata *et al.*, 2013: 1-6)

Figure 36 shows a slight variation exists for the month of June, where the empirical data suggest a small change from the previous month while the simulation data suggests a definite drop in solar irradiance. This small variation is normal and can be attributed to the fluctuating atmospheric conditions which vary somewhat from year to year.

4.5 Summary

The measurements and results of the pilot study and the main study have been comprehensively covered in this particular chapter. The average on-time per week, indicating the time in which the DC-DC converter was supplying power to the load,

was statistically represented by a R^2 Value that illustrates the strength of the relationship and the proportion of variability between the average on-time per week and the direct beam solar radiation. The average work-time per day showed the average hours in which the PV panel was supplying power to the system.

A peak winter month in South Africa is June, which indicated some of the highest regression trend values for 26° and 36° tilt angles (see Table 12). This coincides with earlier endeavours to calculate the proper choice of tilt angles using mathematical models based on the research done by Chinnery (Armstrong & Hurleya, 2009:780-787). These initial experimental results suggest the validity and reliability of these mathematical models for winter months in South Africa. Results gathered from the main study also indicated that a 36° tilt angle produces a quicker fully charged condition than the other two tilt angles (see Figures 27 – 30). A further analysis of the different orientation angles showed that the 0° orientation angle proves superior (see Figure 34).

The monthly averages of the empirical data obtained from the practical setup were contrasted to the monthly averages of solar irradiance as given by METEONORM (see Figure 36). This contrast proves that the METEONORM software is reliable as regards its solar irradiance curve, which is similar to the conversion-time curve obtained from the empirical data, except for the month of June.

The variation in June could be attributed to varying atmospheric conditions which are not always constant for each repetitive year, or it could be attributed to a higher solar output owing to solar flares. However, a moderate correlation does exist between the power conversion of a PV panel and the global solar irradiance obtained from METEONORM for a specific point of latitude in South Africa (being 26° South).

The final chapter of this research will consider the conclusions and recommendations reached with regard to the pilot and main study.

Chapter 5 Conclusions and recommendations

5.1 Introduction

The final chapter of this research presents the conclusions reached with regard to optimising the output power available from a PV panel through empirical testing. This research was aimed at optimizing the available output power from a stationary PV panel, by using mathematical models and simulation packages in combination with the experimental data to evaluate the optimum orientation and tilt angles. This will assist in identifying ways to improve the installation of PV panels for optimum output power as well as enable a higher yield of solar energy particularly in South Africa, thereby reducing dependence on traditional energy sources, such as fossil fuels. Recommendations for future research will conclude this chapter.

5.2 Brief overview

Chapter 1 discussed the background and provides a brief overview of the history of energy with particular focus on electrical energy and PVs. The purpose, methodology, delimitations and significance of the research were discussed.

Chapter 2 focused on PV panels, power regulation and energy storage devices that can be employed in a renewable energy system. The types of PV panels that exist (mono-crystalline, poly-crystalline and amorphous) were discussed as well as their manufacturing process, advantages, disadvantages and relevant applications. A SW220 poly-crystalline PV panel is selected owing to its lower cost and better performance in areas of direct solar radiation (sub-heading 2.3.4).

Power regulation circuits, including solar chargers, DC-DC converters and MPPT, were presented in terms of their basic principle of operation, advantages, disadvantages and possible applications. A WELSEE (WS-MPPT 30) solar charger with an in-built MPPT was used in the main study of this research, as it improves the

overall performance of the system by as much as 30% (sub-heading 2.4.4). Energy storage devices, including lead acid deep discharge, Nickel-Cadmium and Nickel-Zinc batteries, were discussed along with their advantages, disadvantages and possible applications. A RITAR RA12-100 (100 Ah) LADDB was used in this research, as it has a high storage capacity and an overall efficiency of about 70%, with a deep depth of discharge of 80% (sub-heading 2.5.4). The importance of the SOC and DOD of a battery was further explained as this research encompassed the use of a lead acid deep discharge battery as the energy storage device.

The research design, data analysis and experimental set-up of the pilot and the main study were presented in Chapter 3. A quantitative data-collection study is used in this research. The sampling, validity and data analysis employed in the analysis of the data obtained in this research is also discussed. The Perez *et al.* model and the Heywood and Chinnery equations of latitude for PV panel installations in the southern hemisphere were selected and addressed (sub-heading 3.5).

Chapter 4 presented the results obtained for the pilot and the main study. Regression analyses, represented by a statistical R^2 value were presented in a number of graphs. The regression analysis was used to obtain the gradient of the straight line, the average work-time per day and the average work-time per week for the data obtained from three different tilt angles stipulated by the literature.

The main study results presented a number of graphs where the data obtained from January through December 2012 were averaged into quarters showing three different percentages for the PV system (charging, fully charged and discharging). The simulation result of data obtained from METENORM, representing the mathematical model, and the empirical result is further analysed.

5.3 Conclusions

One of the most notable conclusions that can be made from this research is the flexibility, cost effectiveness, efficiency and reliability of the DLIC. The DLIC can

be incorporated in a PV system for energy consumption for both domestic (homes) and commercial purposes e.g. Telecommunication companies (Sentech), power generation companies (Eskom) for grid purposes). PV voltages for domestic usage basically have a maximum input DC voltage of 66 V to the inverter although it could be as high as 400 V for commercial usage depending on the large number of PV panels. For a typical domestic usage, DC-AC inverters used for energy consumption accommodate a maximum DC voltage of 66 V which is basically higher than the input voltage specification of the data loggers that can accommodate 2.5 V. A DLIC is required to condition the voltage to make it less than the maximum input voltage required by the data loggers. The DLIC must also be able to provide DC current monitoring using hall-effect current sensors, such as the LTS 6-NP (LEM product) or the ACS756 (ALLEGRO product). The overall cost of the DLIC is about R 480.

The pilot study was carried out over a period of four months (April – July, 2011). The pilot study was done in order to form the foundation for the main study. The availability of power in the test system was interpreted in a number of regression analysis graphs, where the average work-time time per week and average work-time per day was calculated. The effect of atmospheric/ climatic conditions on the output power of a PV panel was also mentioned.

A regression analysis to validate the availability of power in the system as well as to obtain the average work-time per day was shown in Table 12. The conclusion drawn from the regression analysis proved that a 36° tilt angle with an orientation angle of 0° (facing true north) yielded optimum output power from the PV panel. The efficiency of the power regulation device (DC-DC converter) that was used in the pilot was also analysed. This was done to ascertain the most effective DC-DC converter to be employed with this type of PV system. The 12 V DC-DC converter proved the most efficient (see Tables 13, 14 and 15).

The main study of this research presented three identical PV panels which were placed at the same orientation angle of 0°, but at different tilt angles of 16°, 26° and 36°. The data obtained from the main study was taken over a 12 month period

(January – December 2012) for identical PV systems featuring identical PV panels, solar chargers, energy storage devices and associated components (cabling, protection, etc.). All the PV systems were exposed to the same climatic/atmospheric conditions in order to establish validity and reliability of the data. The results obtained were analysed into four quarters in the year and their averages were presented in table form (see Tables 16 and 18). The results included percentages when the system was charging, fully charged and discharging (see Figures 27 – 30). A comparison of the different graphs revealed the 36° tilt angle to be the best tilt angle for optimum output power.

The results obtained from the two PV panels placed at orientation angles of +15° and -15° with a tilt angle of 36° were compared to the results obtained from the PV panel placed at 0° and a corresponding tilt of 36°. The comparison proved that the PV panel placed on orientation angle of 0° with a tilt angle of 36° provided the highest output power (see Figure 34). Although the two PV panels placed at +15° and -15° were installed from October - December which was the later part of the year 2012. The lateness of the installation was due to late supply of the PV panels by the suppliers.

A correlation of the solar irradiance data obtained from the Perez *et al.* model in the METEONORM simulation software was obtained to try and establish a correlation with the experimental results. The solar irradiance data from the Perez *et al.* model, an anisotropic model, was obtained for the time period from 1996 – 2005. The data obtained from the METEONORM software was averaged and contrasted to the experimental data (see Table 21). These results indicate that the solar irradiance available in Vanderbijlpark (South Africa) tends to fluctuate throughout the year, with a peak in August and a trough in June. The contrast proved that the METEONORM software is reliable as regards its solar irradiance curve, which is very similar to the conversion-time curve obtained from the empirical data (see Figure 36) except for the month of June.

The variation in June could be attributed to varying atmospheric conditions which are not always constant for each repetitive year. However, a moderate correlation of 90% does exist between the power conversion of a PV panel and the global solar irradiance obtained from METEONORM for a specific point of latitude in South Africa (being 26° South). This validates the literature that states that the METEONORM has become a valuable tool for estimating global solar irradiance, especially for where solar radiation data is missing or irregular.

5.4 Recommendations

A number of regression analyses have been carried out in the pilot and main study which has helped to verify suggested equations of latitude and validate a specific mathematical model for PV installations in the southern hemisphere. For a stationary PV panel, the 36° tilt angle facing true north (0°) provides optimum output power in the southern hemisphere throughout the year. It is recommended that solar companies and PV installers should go by the 36° tilt angle facing true north (0°) in the Vaal Triangle (South Africa).

In stand-alone PV systems, if a DC-DC converter is to be used as the power conditioning device, a 12 V DC-DC converter is recommended due to its efficiency. Rather than using a DC-DC converter, solar chargers with MPPT are recommended for optimum output powers as they improve the overall efficiency. Proposed additional research can be done in South Africa in the installation of solar pool heaters, solar geysers, solar pumps for domestic and commercial usage with the tilt angle set to 36° facing true north (0°) and the results observed. It is recommended that a DLIC in combination with a data logger should be used to record these results.

BIBLIOGRAPHY

ABDELKADER, M. R., AL-SALAYMEH, A., AL-HAMAMRE, Z. & SHARAF, F. 2010. A comparative analysis of the performance of mono-crystalline and multi-crystalline PV cells in semi-arid climate conditions: The case of Jordan. *Jordan Journal of Mechanical and Industrial Engineering*, Vol. 4: 543-552.

ALI, N. C. 2006. Present status of photovoltaic energy in Turkey and life cycle techno-economic analysis of a grid-connected photovoltaic-house, *Renewable and Sustainable Energy Reviews*, Vol. 10: 370-387.

ARMSTRONG, S. & HURLEYA, W. G. 2009. A new methodology to optimise solar energy extraction under cloudy conditions. *Renewable energy*, 35(4):780-787.

ASOWATA, O., SWART, A. J. & PIENAAR, C. 2012. Optimum tilt angles for photovoltaic panels during winter months in the Vaal Triangle, South Africa. *Smart Grid and Renewable Energy*, Vol. 3: 119-125.

ASOWATA, O., SWART, A. J. & PIENAAR, C. March, 2012. Optimum Tilt Angles for Photovoltaic Panels during Winter Months in the Vaal Triangle. *Asia-Pacific Power and Energy Engineering Conference*, Grand Mercure Baolong Hotel, Shanghai, China, pp 1-6.

ASOWATA, O., SWART, A. J. & PIENAAR, C. February, 2013. Correlating the power conversion of a PV panel to the solar irradiance obtained from meteorology. *International Conference on Industrial Technology*, Cape Town, South Africa, pp 1-6.

BAHGAT, A. B. G., HELWA, N. H., AHMAD, G. E. & EL SHEWANY, E. T. 2005. Maximum power point tracking controller for PV systems using neural networks, *Renewable Energy*, Vol. 30: 1257-1268.

BARTELS, J. R., PATE, M. B. & OLSON, N. K. 2010. An economic survey of hydrogen production from conventional and alternative energy sources. *International Journal of Hydrogen Energy*, 35(16): 8371-8384.

BENCHMARKS, S. 2007. Data analysis. London: SAGE publications.

BERNDT, D. 1997. Maintenance-free batteries, lead-acid, nickel-cadmium, nickel-metal hydride: A handbook of battery technology. 2nd ed. New York: Tauton Research Studies Press, Wiley.

BESTBATTERIES, 2012. [Online] Available at: <<http://bestbatteries.co.nz/categories/agm-sealed-vrla-batteries/ritar-deep-cycle-agm-sla-valve-regulated-batteries/12v-100ah-ra100sd-ritar.html>>. Accessed 21/03/2011

BESTGOPOWER, 2012. [Online] Available at: <http://www.bestgopower.com/faq/frequently-asked-questions/depth-of-discharge.html>>. Accessed on 2012-12-14.

BOXWELL, M. 2010. Solar electricity handbook: A simple practical guide to solar energy-designing and installing photovoltaic solar electric systems. United Kingdom: Code Green Publishing.

CAIRNS, E. J. 2009. SECONDARY BATTERIES NICKEL SYSTEMS | Nickel Zinc. In *Encyclopedia of Electrochemical Power Sources*. Amsterdam: Elsevier, pp. 528-533.

CÁRABÉ, J. & GANDIA, J. J. 2004. Thin-film-silicon solar cells. *Opto-electronics Review*, 12(1): 1–6.

CHANG, L. & NG, C. 1994. A solar battery charger with improved energy utilization. *Canadian Conference on Electrical and Computer Engineering*. Vol. 1: pp. 105-108.

CHANG, Y. P. 2010. Optimal tilt angles for photovoltaic modules using PSO method with nonlinear time-varying evolution, *Energy*, Vol. 35: pp. 1954-1963.

CHARLES, M. J. & GARY, H. M. 1989. Data analysis. A model-comparison approach. San Diego: Harcourt Brace Jovanovich Publisher.

CHEN, W., SHEN, H., SHU, B., QIN, H. & DENG, T. 2007. Evaluation of performance of MPPT devices in PV systems with storage batteries. *Renewable Energy*, Vol. 32: 1611-1622.

CHENG, J., ZHANG, L., YANG, Y. S., WEN, Y. H., CAO, G.P. & WANG, X. D. 2007. Preliminary study of single flow zinc nickel battery. *Electrochemistry Communications*, Vol. 9: 2639-2642.

DHARIWAL, S. R. & SMIRTY, M. 2006. On the sensitivity of open-circuit voltage and fill factor on dangling bond density and Fermi level position in amorphous silicon p-i-n solar cell. *Solar Energy Materials and Solar Cells*, Vol. 90: 1254-1272.

DIXON, R. K., MCGOWAN, E., ONYSKO, G. & SCHEER, R. M. 2010. US energy conservation and efficiency policies, challenges and opportunities. *Energy Policy*, Vol. 38: 6398-6408.

DORIN, P., TOMA, P., STEFAN, D., CRISTINA, M. & BRIAN, M. 2011. A novel maximum power point tracker based on analog and digital control loops. *Solar Energy*, Vol. 85: 588-600.

D'SOUZA, N. S., LOPES, L. A. C. & LIU, X. 2010. Comparative study of variable size perturbation and observation maximum power point trackers for PV systems. *Electric Power Systems Research*, Vol. 80: 296-305.

EINSTEIN, A. 1879-1995. Albert Einstein quotes. [Online]. Available at: <http://www.phnet.fi/public/mamaa1/einstein.htm>. Accessed: 2011-05-30.

EL CHAAR, L., LAMONT, L. A. & EL ZEIN, N. 2011. Review of photovoltaic technologies. *Renewable and Sustainable Energy Reviews*, Vol. 15: 2165-2175.

EL-HAWARY, M. 2008. Introduction to electrical power systems. New Jersey: John Wiley press.

EMSLIN, J. H. R., WOLF, M. & SWIEGERS, W. 1997. Integrated photovoltaic maximum power point tracking converter, *IEEE Transactions on Industrial Electronics*, 44(6), pp. 769–773.

ENRIQUE, J. M., ANDÚJAR, J. M. & BOHÓRQUEZ, M. A. 2010. A reliable, fast and low cost maximum power point tracker for photovoltaic applications. *Solar Energy*, Vol. 84: 79-89.

ENRIQUE, J. M., DURÁN, E., SIDRACH-DE-CARDON, M. & ANDÚJAR, J. M. 2007. Theoretical assessment of the maximum power point tracking efficiency of photovoltaic facilities with different converter topologies. *Solar Energy*, Vol. 81: 31-38.

ESPINOSA, D. C. R. & JORGE, A. S. T. 2006. Recycling of nickel cadmium batteries using coal as reducing agent. *Journal of Power Sources*, Vol. 157: 600-604.

FARAHAT, M. A., METWALLY, H. M. B. & ABD-ELFATAH, M. A. 2012. Optimal choice and design of different topologies of DC-DC converter used in PV systems, at different climatic conditions in Egypt. *Renewable Energy*, Vol. 43: 393-402.

FARRET, F. A. & SIMOES, M. G. 2006. Integration of alternative sources of energy. New Jersey: John Wiley Press.

FURKAN, D. E. 2010. The analysis on photovoltaic electricity generation status, potential and policies of the leading countries in solar energy. *Renewable and Sustainable Energy Reviews*, Vol. 15: 713-720.

GANGOPADHYAY, U., KIM, K., DHUNGEL, S. K., BASU, P. K. & YI, J. 2006. Low-cost texturization of large-area crystalline silicon solar cells using hydrazine mono-hydrate for industrial use. *Renewable Energy*, Vol. 31: 1906-1915.

GEORGEKUTTY, C. K. & GEORGEMATHEW. 2012. Hall marks in construction material management: A literature review. *Journal of Mechanical and Civil Engineering (IOSRJMCE)*, Vol. 2: 51-61.

GRIMES, C. A., OOMAN, K. V., SUDHIR, R. 2008. Light, water and hydrogen: The solar generation of hydrogen by water photoelectrolysis. New York, USA: Springer science+Business media LLC.

HAHN, C. 2008. Doing qualitative research using your computer. London: SAGE Publications.

HATWAAMBO, S., JAIN, P. C., PERERS, B. & KARLSSON, B. 2009. Projected beam irradiation at low latitudes using Meteonorm database. *Renewable Energy*, Vol. 34: 1394-1398.

HESKETH, E. A. & LAIDLAW, J. M. 2002. Quantitative research. [Online]. Available at: http://www.nes.scot.nhs.uk/nes_resources/ti/QuantativeResearch.pdf. Accessed: 2012-07-10.

HOHM, D. P. & ROPP, M. E. 2003. Comparative study of maximum power point tracking algorithms Electrical Engineering Department, South Dakota State University. Brookings, USA, pp. 47-62.

HUANG, J. Y., LIN, C. Y., SHEN, C. H., SHIEH, J. M. & DAI, B.T. 2012. Low cost high-efficiency amorphous silicon solar cells with improved light-soaking stability. *Solar Energy Materials and Solar Cells*, Vol. 98: 277-282.

IL-SONG, K. 2007. Robust maximum power point tracker using sliding mode controller for the three-phase grid-connected photovoltaic system. *Solar Energy*, Vol. 81: 405-414.

IL-SONG, K., PYEONG, S. J., UN-DONG, H., CHIN-GOOK, L. & HONG-GYU, K. 2009. State estimator design for solar battery charger. *IEEE International Conference on Industrial Technology, ICIT 2009*, pp. 1-6.

INCROPERA, F. P. & DEWITT, D. P. 2002. Fundamentals of heat and mass transfer. 5th Ed. New York: John Wiley and Sons.

ITO, Y., NYCE, M., PLIVELICH, R., KLEIN, M., STEINGART, D. & BANERJEE, S. 2011. Zinc morphology in zinc nickel flow assisted batteries and impact on performance. *Journal of Power Sources*, Vol. 196: 2340-2345.

JINSU, Y. 2010. Solar cell fabrication using edge-defined film-fed growth (EFG) silicon wafers. *Applied Surface Science*, Vol. 257: 1612-1615.

KAWAMURA, T., HARADA, K., ISHIHARA, Y., TODAKA, T., OSHIRO, H. N. & IMATAKI, M. 1997. Analysis of MPPT characteristics in photovoltaic power system. *Solar Energy Materials and Solar Cells*, Vol. 47: 155-165.

KIM, H. S., KIM, J. H., MIN, B. D., YOO, D. W. & KIM, H. J. 2009. A highly efficient PV system using a series connection of DC-DC converter output with a photovoltaic panel. *Renewable Energy*, Vol. 34: 2432-2436.

KIM, Y., HYUNMIN, J. & DEOKJUNG, K. August, 1996. A new peak power tracker for cost-effective photovoltaic power system. *Energy Conversion Engineering Conference. IECEC 96*, Vol.3: 1673-1678.

KOEPEL, G. & KORPAS, M. 2008. Improving the network infeed accuracy of non-dispatchable generators with energy storage devices. *Electric Power Systems Research*, Vol. 78: 2024-2036

KRAUTER STEFAN. 2006. Solar electric power generation - photovoltaic energy systems, modeling of optical and thermal performance, electrical yield, energy balance, effect on reduction of greenhouse gas emissions. Berlin: Springer.

KRUPA, J. & BURCH, S. 2011. A new energy future for South Africa. The political ecology of South African renewable energy. *Energy Policy*, Vol. 39: 6254-6261.

LAMAISON, R. M., BORDONAU, J., ESQUIVEL, A. & PERACLAULA, J. 1999. Analysis and design of a resonant battery charger for photovoltaic systems. *IEEE International Symposium on Industrial Electronics*, Vol.2: pp. 463-468.

LAMEI, A., VAN DER ZAAG, P. & VON MÜNCH, E. 2008. Impact of solar energy cost on water production cost of seawater desalination plants in Egypt. *Energy Policy*, Vol. 36: 1748-1756.

LANNER. 2012. Simulation and simulation software explained. [Online]. Available at: <http://www.lanner.com/en/simulation-explained.cfm>. Accessed: 2012-05-16.

LINDEN, D. 1995. Handbook of batteries. 2nd Ed. New York: McGraw-Hill.

LOVEGROVE, K. & DENNIS, M. 2006. Solar thermal energy systems in Australia. *International Journal of Environmental Studies*, 63(6):791-802.

LUIS, C. & SANTIAGO, S. 2002. Modelling photovoltaic systems using PSpice. Chichester: John Wiley.

MACKINTOSH, B., SEIDL, A., OUELLETTE, M., BATHEY, B., YATES, D. & KALEJS, J. 2006. Large silicon crystal hollow-tube growth by the edge-defined film-fed growth (EFG) method. *Journal of Crystal Growth*, Vol. 287: 428-432.

MADEHOW. Solar Cell. 2012. [Online]. Available at:<http://www.madehow.com/Volume-1/Solar-Cell.html#b>. Accessed: 2012-08-21.

MARKVART, T. & CASTANER, L. 2005. Practical handbook of photovoltaic fundamentals and application. Oxford: Elsevier Press.

MARTINEZ, W. L., ANGEL R. M. & JEFFREY, L. S. 2011. Exploratory data analysis with MATLAB. 2nd Ed. Florida: CRC Press.

MASHORHOR, S., SAMSUDIN, K., NOOR, A. M. & RAHMAN, A. R. A. 2008. Evaluation of Genetic Algorithm based solar tracking system for Photovoltaic panels in Sustainable Energy Technologies. *IEEE international Conference. ICSET2008*, pp. 269-273.

METEONORM. 2013. [Online]. Available at: <http://meteonorm.com/products/meteonorm-software/>. Accessed: 2013-01-15.

MÖLLER, H. J., FUNKE, C., RINIO, M. & SCHOLZ, S. 2005. Multicrystalline silicon for solar cells. *Thin Solid Films*, Vol. 487: 179-187.

MONTGOMERY, C. D. & RUNGER, C. G. 2011. Applied statistics and probability for engineers. New York: John Wiley and Sons Press.

M0UKD.COM. 2011. Information about different types of solar panels. [Online]. Available at: <http://www.moukd.com>. Accessed: 2011-10-30.

MUTHMANN, S. & GORDIJN, A. 2011. Amorphous silicon solar cells deposited with non-constant silane concentration. *Solar Energy Materials and Solar Cells*, Vol. 95: 573-578.

NAGASHIMA, S., TAKAHASHI, K., YABUMOTO, T., SHIGA, S. & WATAKABE, Y. 2006. Development and field experience of monitoring system for valve-regulated lead acid batteries in stationary applications. *Journal of Power Sources*, Vol. 158: 1166-1172.

NAKAYAMA, Y., TAKAHASHI, S., HIRAKAWA, K., & YAMAGUCHI, Y. 2004. Development of a long life 35Ah capacity VRLA battery for load-levelling applications. *Journal of Power Sources*, Vol. 125: 135-140.

NASSAR, Y. F. & SALEM, A. A. 2007. The reliability of the photovoltaic utilization in southern cities of Libya. *Desalination*, Vol. 209: 86-90.

NOORIAN, A. M., MORADI, I. & KAMALI, G. A. 2008. Evaluation of 12 models to estimate hourly diffuse irradiation on inclined surfaces. *Renewable Energy* 33(6): 1406-1412.

OLALLA, C., QUEINNEC, I., LEYVA, R. & EL AROUDI, A. 2011. Robust optimal control of bilinear DC-DC converters. *Control Engineering Practice*, Vol. 19: 688-699.

ORIGINLAB. 2013. [Online]. Available at: http://www.originlab.com/www/helponline/origin/en/UserGuide/Polynomial_Regression_Results.html. Accessed: 2013-02-03

PARIDA, B., INIYAN, S. & GOIC, R. 2011. A review of solar photovoltaic technologies. *Renewable and Sustainable Energy Reviews*, Vol. 15: 1625-1636.

PAUL, A. L. 2010. Electricity from sunlight: An introduction to photovoltaics. Chichester: Wiley.

PETER, P. K. & AGARWAL, V. 2010. Analysis and design of a ground isolated switched capacitor DC-DC converter. *IEEE International Symposium on Industrial Electronics (ISIE)*, pp. 632-637.

PETREUȘA, D., PĂȚĂRĂUA, T., DĂRĂBANA, S. & MORLEY, B. 2011. A novel maximum power point tracker based on analog and digital control loops, *Solar Energy*, Vol. 85: 588-600.

PUSHPARAJ, V. L., SREEKALA, S., NALAMSU, O., AJAYAN, P. M., YUGANG, S. & JOHN, A. R. 2010. Semiconductor nanomaterials for flexible technologies. *Flexible Energy Storage Devices Using Nanomaterials*. Oxford: William Andrew, pp. 227-245.

REMUND, J. & MÜLLER, S. C. Solar radiation and uncertainty information of meteonorm7. [Online]. Available at:http://meteonorm.com/fileadmin/user_upload/publications/PVSEC_11_mn7_p.pdf. Accessed: 2012-09-02.

SALOUX, E., TEYSSEDOU, A. & SORIN, M. 2010. Explicit model of photovoltaic panels to determine voltages and currents at the maximum power point. *Solar Energy*, Vol. 85: 713-722.

SARMA, M. & GLOVER, J. 2002. Power system analysis and design. California: Thomas learning academic resource center.

SIMON, A. & ALEJANDRO, O. 2011. Power-switching converters. 3rd Ed. Boca Raton: CRC Press.

SOLANKI, C. S. 2009. Solar photovoltaics: Fundamentals, technologies and applications. 1st Ed. New Delhi, India: PHI Learning.

SOLAR ALWAYS. [Online]. Available at: <http://www.solaralways.com/types/solar-panels>. Accessed: 2011-10-30.

STEFAN, K. 2009. Solar electric power generation: Solar photovoltaics (Fundamentals, technologies and applications), New-Delhi, India: Rajkarmal Electric Press.

STRYDOM, J. W., JOOSTE, C. J. & DU PLESSIS, P. J. 2005. Applied strategic marketing. 2nd ed. Sandton, South Africa: Heinemann.

STUART, R. W., MARTIN, A. G., MURIEL, E. W. & RICHARD, C. 2007. Applied photovoltaics. Virginia, USA: James and James.

STURGES, S. & HEWITT, J. 1995. Progress of a policy experiment: Climate challenge interim report card. *The Electricity Journal*, Vol. 8: 60-70.

SWART, A. J., SCHOEMAN, R. M. & PIENAAR, H.C. 2011. Assessing the effect of variable atmospheric conditions on the performance of photovoltaic panels: A case study from the Vaal Triangle. *Southern African Energy Convention*, p. 1.

TAGHVAEE, M. H., RADZI, M. A. M., MOOSAVAIN, S. M., HIZAM, H. & MARHABAN, H. M. 2013. A current and future study on non-isolated DC-DC converters for photovoltaic applications. *Renewable and Sustainable Energy Reviews*, Vol. 17:216-227.

THE GERMAN SOLAR ENERGY SOCIETY (Ecofys). 2005. Planning and installing photovoltaic systems, a guide for installers, architects and engineers. London: James and James.

USDOE. US. Energy Information Administration. 2008. [Online]. Available at: <http://www.eia.doe.gov/emeu/iea/popgdp.html>. Accessed: 2011-03-23.

VAN RENSBURG, J. F. J. 2012. Industrial power electronics, 2nd edition. Vanderbijlpark: Lerato.

WAGNER, R. 1997. Large lead/acid batteries for frequency regulation, load levelling and solar power applications. *Journal of Power Sources*, Vol. 67: 163-172.

WELMAN, C. KRUGER, F. & MITCHELL, B. 2005. Research Methodology. South-Africa: Oxford University Press.

WENDY, L. M., ANGEL, R. M. & JEFFREY, L. S. 2011. Exploratory data analysis with MATLAB. 2nd ed. Boca Raton, FL: CRC Press.

WENHAM, S. R & STUART, R. 2007. Applied photovoltaics. 2nd ed. London: Earthscan.

WILLIAM, B. S., SHARON, R. S. & MICHAEL, G. Power from the sun. 1986. [Online]. Available at: <http://www.powerfromthesun.net/Book/chapter06/chapter06.html>. Accessed: 2013-01-17.

XIAO, W., DUNFORD, W. G., PALMER, P. R. & CAPEL, A. 2007. Application of centered differentiation and steepest descent to maximum power point tracking. *IEEE Transactions on Industrial Electronics*, 54(5): 2539–2549.

YAFAOUI, B. W. & CHEUNG, R. 2007. Implementation of maximum power point tracking algorithm for residential photovoltaic systems. *2nd Canadian Solar Buildings Conference*, Calgary, pp. 1-6.

YOO, S. H. & LEE, E. T. 2002. Efficiency characteristic of building integrated photovoltaics as a shading device. *Building and Environment*, Vol. 37:615-623.

YU, G. J., JUNG, Y. S., CHOI, J. Y., & KIM, G. S. 2004. A novel two-mode MPPT control algorithm based on comparative study of existing algorithms. *Solar Energy*, Vol. 76: 455-463.

ZAHEDI, A. 2011. Maximizing solar PV energy penetration using energy storage technology. *Renewable and Sustainable Energy Reviews*, Vol. 15: 866-870.

ZAMIR & BERMAN. 2004. Fourier Systems Data Acquisition Solutions for Industry. [Online]. Available at: http://www.fouriersystems.com/pdf/fourier_catalogue.pdf. Accessed 2012-06-17.

ZHANG, C. P., SHARKH, S. M., LI, X., WALSH, F. C., ZHANG, C. N. & JIANG, J. C. 2011. The performance of a soluble lead-acid flow battery and its comparison to a static lead-acid battery. *Energy Conversion and Management*, Vol. 52: 3391-3398.

ANNEXURES PAGE NUMBERS

ANNEXURE A	Hall-effect current sensor, LTS 6-NP data sheet	101
ANNEXURE B	Specification of the DAQ PRO-5300 data logger	103
ANNEXURE C	Picture of the data logging interface circuit (DLIC)	105
ANNEXURE D	PICOLOG 1216 data logger data sheet	106
ANNEXURE E	Specification of the WELSEE (WS-MPPT 30) solar charger	108
ANNEXURE F	Specification of the RITAR RA12-100 (100 Ah) LADDB	110
ANNEXURE G	Specification of the SW 220 poly-crystalline PV panel	112
ANNEXURE H	Specification of the RADIANT 11 W fluorescent bulb	114
ANNEXURE I	Specification of the RABTRON 10 W LED Lamp	117



Current Transducer LTS 6-NP

For the electronic measurement of currents: DC, AC, pulsed, mixed with galvanic isolation between the primary circuit (high power) and the secondary circuit (electronic circuit).

$$I_{PN} = 6 \text{ At}$$



16065

Electrical data

I_{PN}	Primary nominal current rms	6	At
I_{PM}	Primary current, measuring range	0 .. ± 19.2	At
I_p	Overload capability	250	At
V_{OUT}	Output voltage (Analog) @ I_p	$2.5 \pm (0.625 \cdot I_p / I_{PN})$	V
	@ $I_p = 0$	2.5 ¹⁾	V
G	Sensitivity	104.16	mV/A
N_s	Number of secondary turns (± 0.1 %)	2000	
R_L	Load resistance	≥ 2	kΩ
R_M	Internal measuring resistance (± 0.5 %)	208.33	Ω
TCR_M	Temperature coefficient of R_M	< 50	ppm/K
V_C	Supply voltage (± 5 %)	5	V
I_C	Current consumption @ $V_C = 5 \text{ V}$	Typ	$28 + I_s^{2H} \cdot (V_{OUT} / R_L)$ mA

Accuracy - Dynamic performance data

X	Accuracy @ I_{PN} , $T_A = 25^\circ\text{C}$	± 0.2	%
	Accuracy with R_M @ I_{PN} , $T_A = 25^\circ\text{C}$	± 0.7	%
ϵ_L	Linearity error	< 0.1	%
TCV_{OUT}	Temperature coefficient of V_{OUT} @ $I_p = 0$	-10°C .. +85°C	Typ 80, Max 200 ppm/K
		-40°C .. -10°C	250 ppm/K
TCG	Temperature coefficient of G	-40°C .. +85°C	50 ²⁾ ppm/K
V_{OM}	Magnetic offset voltage @ $I_p = 0$, after an overload of	$3 \times I_{PN}$	± 0.5 mV
		$5 \times I_{PN}$	± 2.0 mV
		$10 \times I_{PN}$	± 2.0 mV
t_m	Reaction time @ 10 % of I_{PN}	< 100	ns
t_r	Response time to 90 % of I_{PN} step	< 400	ns
di/dt	di/dt accurately followed	> 15	A/μs
BW	Frequency bandwidth (0 .. -0.5 dB (-0.5..-1 dB))	DC .. 100	kHz
		DC .. 200	kHz

General data

T_A	Ambient operating temperature	-40 .. +85	°C
T_S	Ambient storage temperature	-40 .. +100	°C
m	Mass	10	g
	Standards	EN 50178: 1997	

Features

- Closed loop (compensated) multi-range current transducer using the Hall effect
- Unipolar voltage supply
- Isolated plastic case recognized according to UL 94-V0
- Compact design for PCB mounting
- Incorporated measuring resistance
- Extended measuring range.

Advantages

- Excellent accuracy
- Very good linearity
- Very low temperature drift
- Optimized response time
- Wide frequency bandwidth
- No insertion losses
- High immunity to external interference
- Current overload capability.

Applications

- AC variable speed drives and servo motor drives
- Static converters for DC motor drives
- Battery supplied applications
- Uninterruptible Power Supplies (UPS)
- Switched Mode Power Supplies (SMPS)
- Power supplies for welding applications.

Application domain

Notes: ¹⁾ Absolute value @ $T_A = 25^\circ\text{C}$, $2.475 < V_{\text{out}} < 2.525$

²⁾ $I_S = I_P/N_S$

³⁾ Only due to TCR_{BR}



Current Transducer LTS 6-NP

Isolation characteristics

V_d	Rms voltage for AC isolation test, 50 Hz, 1 min	3	kV
\hat{V}_w	Impulse withstand voltage 1.2/50 μs	> 8	kV
		Min	
V_p	Rms voltage for partial discharge extinction @ 10pC	> 1.5	kV
dCp	Creepage distance ¹⁾	15.5	mm
dCI	Clearance distance ²⁾	6.35	mm
CTI	Comparative Tracking Index (group IIIa)	175	

Notes: ¹⁾ On housing


²⁾ On PCB with soldering pattern UTEC93-703.

Applications examples

According to EN 50178 and IEC 61010-1 standards and following conditions:

- Over voltage category OV 3
- Pollution degree PD2
- Non-uniform field

	EN 50178	IEC 61010-1
dCp, dCI, \hat{V}_w	Rated insulation voltage	Nominal voltage
Single insulation	600 V	600 V
Reinforced insulation	300 V	300 V




FACTORIES
Monitoring product quality throughout the entire manufacturing cycle




TESTING STANDARDS
Ensuring quality control and compliance with safety standards



RESEARCH & DEVELOPMENT
Academic and industrial laboratory research measuring multiple parameters



MILITARY
Storage, equipment maintenance, machinery and production testing



AUTOMOTIVE
Compatibility tests, electronics, control panels and engine operating temperatures

DaqPRO Solution

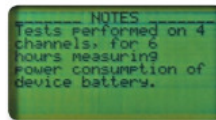
ALL IN ONE SOLUTION FOR DATA LOGGING AND ANALYSIS



DaqPRO provides truly independent data acquisition with full setup, data display and analysis all on the DaqPRO screen.



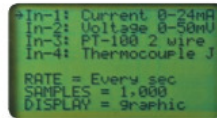
- High-end data acquisition hand-held mobile solution
- 8 channels each capable of measuring seven popular parameters
- Setup on every port makes it viable for all industries
- Standalone operation: Display and keyboard for field programming and analysis (graph/table)
- Rechargeable 7.2 V battery with over 500 charging cycles
- High sampling rate – up to 4,000 samples/second
- Large data storage 512 KB RAM
- Fast communication channels: USB
- Multiple logging storage of up to 100 sampling sessions
- Scales readings into meaningful engineering units e.g. bar, ppm
- Built-in clock and calendar keeps track of time and date for each data recording
- On screen text editing to annotate collected data
- Value for money



Notes



Numeric & graphic displays



Setup



File storage

DaqLab Software

Together with the comprehensive data analysis software, the DaqPRO is the perfect choice for remote data acquisition and monitoring whether off-site or inside any industrial environment

Analysis Wizard
Scientific functions statistics

Sensor calibration

Online logger setup

Online graph & table view

Export to Excel



About fourtec

fourtec – Fourier Technologies Ltd. is a recognized leader in data-logging and monitoring solutions for controlled industrial environments, such as food, pharmaceutical, medical, storage and transportation industries. Our solutions enable our customers to deliver higher quality products, ensure consumer safety, comply with regulatory requirements and increase profitability. Innovation, expertise and a commitment to quality are the values

Specifications

Inputs (DaqPRO 5300)

Selectable type for each input: 0 to 24 mA, 0 to 50 mV, 0 to 10 V, NTC, PT-100, Thermocouple, Pulse and Frequency (Input 1 only)

0 to 24 mA
Range: 0 to 24 mA
Resolution: 4.76 μ A
Accuracy: $\pm 0.5\%$
Loop impedance: 21 Ω

0 to 50 mV
Range: 0 to 50 mV
Resolution: 3 μ V
Accuracy: $\pm 0.5\%$

0 to 10 V
Range: 0 to 10 V
Resolution: 200 μ V
Accuracy: $\pm 0.5\%$
Input impedance: 125 k Ω

Temperature NTC
NTC: 10/100 k Ω resistor
Range: -25 to 150 $^{\circ}$ C
Resolution: 0.05 $^{\circ}$ C
Accuracy: $\pm 0.5\%$

Temperature PT-100
Range: -200 to 400 $^{\circ}$ C
Resolution: 0.1 $^{\circ}$ C (7 m Ω)
Accuracy: -200 to -50 $\pm 0.5\%$
50 to 400 $\pm 0.5\%$
-50 to 50 $\pm 0.5\%$

The DaqPRO offers up to 8 PT-100 2 wire channels or 4 PT-100 3 wire channels

Temperature Thermocouple J
Range: -200 to 1200 $^{\circ}$ C
Resolution: 0.1 $^{\circ}$ C (1 μ V)
Accuracy: -200 to -50 $\pm 0.5\%$
50 to 1,200 $\pm 0.5\%$
-50 to 50 $\pm 0.5\%$
Cold junction compensation error: $\pm 0.3\%$

Temperature Thermocouple K
Range: -250 to 1,200 $^{\circ}$ C
Resolution: 0.1 $^{\circ}$ C (1 μ V)
Accuracy: -250 to -50 $\pm 0.5\%$
50 to 1,200 $\pm 0.5\%$
-50 to 50 $\pm 0.5\%$
Cold junction compensation error: $\pm 0.3\%$

Temperature Thermocouple T
Range: -200 to 400 $^{\circ}$ C
Resolution: 0.1 $^{\circ}$ C (1 μ V)
Accuracy: -200 to -50 $\pm 0.5\%$
50 to 400 $\pm 0.5\%$
-50 to 50 $\pm 0.5\%$
Cold junction compensation error: $\pm 0.3\%$

Internal Temperature
Range: -25 to 70 $^{\circ}$ C
Resolution: 0.1 $^{\circ}$ C (1 μ V)
Accuracy: $\pm 0.5\%$

Pulse Counter (Input 1 only)
Optocoupler input
Range: 0 to 65,000
Input signal: 0 to 5 V
Input impedance: 470 Ω
Bandwidth: 0 to 25 Hz

Frequency Meter (Input 1 only)
Optocoupler input

General A to D Specifications

Noise: 30 μ V rms
Internal linearity error: $\pm 0.08\%$ of FSR
Offset error: 0.1 $\%$

Open Collector Output (Output 8)
Maximum current sink: 50 mA (fuse protected)
Maximum input voltage: 5 V
Input impedance: 50 Ω

Communication

USB 1.1 compliant

Sampling

Capacity: 512 KB
Analog sampling rate: Variable, 1 sample/hour to 4,000 samples/sec, 1 channel
Analog sampling resolution: 16-bit
Channel separation: 80 dB

Man Machine Interface

- Full keyboard operation - enables manual programming of the logger
- Graphic LCD 64 x 128 pixels

Power Supply

- Internal rechargeable 7.2V NiMH battery
- Built-in battery charger
- External 9 to 12 V DC input
- Battery life: 25 hours between charges

Operating Temperature Range

0 to 50 $^{\circ}$ C

Casing

Plastic ABS box
Dimensions: 182 x 100 x 28 mm
Weight: 450 gr

Standards Compliance

CE, FCC

DaqLAB Analysis Software

- Windows OS: 2000 SP3/2003/XP SP2/Vista/7 32-bit
- Fast data download from the DaqPRO
- Data displayed in numeric or graphical display forms
- Graphical analysis tools such as Zoom and Cursors
- Storage of selected data on disk files
- Hard copy printing of the collected data
- Direct data export to EXCEL
- On-line retrieval and display of data in real-time
- Incorporating data processing functions
- Setting up the DaqPRO
- Calibrating the DaqPRO
- Defining new sensors

Accessories

- Carrying case
- Solar cell and battery for field data logging
- Weather box complying with the IP-67 standard for protecting the DaqPRO while working in field applications

Ordering Information

P/N	Description
DBS301	DaqPRO data logger, carrying case, AC/DC adapter, DaqLab analysis software CD (including user guide), communication cable, calibration certificate
11460A	Weather box

Picture of the data logging interface circuit (DLIC)

ANNEXURE C





PicoLog® 1000 Series

Multi-channel Voltage Data Loggers



- Up to 16 unipolar analog input channels
- Up to 12-bit resolution with 0.5% accuracy
- Up to 4 software configurable digital output lines
- Up to 1 MS/s sample rate
- USB connected and powered
- Includes API and examples for C/C++/C#, VB, LabVIEW VIs
- Complete with ready-to-go data logging software



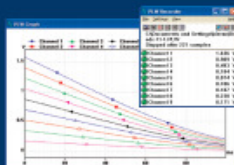
All you need

Designed to meet the needs of a wide range of general-purpose voltage, sensor and transducer logging applications. The PicoLog 1216 and 1012 feature independent software-configurable channels, ranges, scaling and control outputs, an optional external terminal board for easy range extension and ease of terminating wires.



Ready-to-go

The PicoLog 1000 Series multi-channel voltage data loggers include everything needed for immediate use and are complemented by a full suite of software including the PicoLog data logging package, the PicoScope oscilloscope package and an SDK for writing user programs.



Flexible sampling modes

Both loggers feature 3 sampling modes to meet most data logging needs: streaming, real-time continuous and block mode. Streaming allows channel voltage readings to be logged continuously at 1 kS/s on any number of channels, while real-time continuous provides averaged, time-accurate readings with automatic measurements available in PicoLog. Block mode captures at the full 1 MS/s sample rate of the logger for the duration of the 8k sample buffer.

www.picotech.com

SPECIFICATIONS

		PicoLog 1216	PicoLog 1012
Inputs	Analog inputs	16 channels	12 channels
	Resolution (bits)	12 bits	10 bits
	Sampling rate – streaming	1 kS/s per channel in PicoLog, 100 kS/s using API	
	Sampling rate - block mode	1 MS/s using PicoScope and API	
	Sampling rate – real-time continuous	1 kS/s or greater	
	Buffer memory	8k samples shared by all channels	
	Input type	Single-ended, unipolar	
	Voltage range	0 - 2.5 V	
	Accuracy	0.5% @ 12 bits	1.0% @ 10 bits
	Overload protection	±30 V	
	AC/DC coupling	DC coupling	
	Input impedance	1MΩ fixed – buffered inputs	
	Outputs	Digital outputs	4 digital outputs
Output power for sensors		2.5 V @ 10 mA. Current-limited	
Other outputs		PWM output (PicoScope 6 and API)	None
Physical and general	Power requirements	Powered from USB port, <200 mA operating, <100 mA on startup	
	PC connectivity	USB 2.0 full speed	
	Input/output connector	25-way D Type, female (pin-compatible with USB ADC-11)	
	Dimensions	45 mm x 100 mm x 140 mm (1.77" x 3.94" x 5.51")	
	Weight	<200 g (7.05 oz)	
	Compliance	CE (EMC) Class A emissions & immunity. FCC emissions	
	Software	Compatibility	Windows XP (SP2 or greater) and Vista (32 and 64 bit)
- PicoLog	Multiple views	View data as a graph, spreadsheet or text	
	Parameter scaling	Convert raw data into standard engineering units	
	Math functions	Use mathematical equations to calculate additional parameters	
	Alarm limits	Program an alert if a parameter goes out of a specified range	
- PicoScope 6	Capture modes	Oscilloscope, spectrum and persistence modes	
	Channel maths	Calculate the sum, difference, product, inverse or create your own custom function using standard arithmetic, exponential and trigonometric functions	
	Automated measurements	15 scope measurements and 11 spectrum measurements	
- Development kit	Driver and examples	C/C++/C#, Visual Basic and LabVIEW	
	Compatibility mode	Drop-in replacement of USB ADC-11	

ORDER CODES and PRICES

ORDER CODE	DESCRIPTION	PRICE
PP547	PicoLog 1216 with terminal board	£159
PP544	PicoLog 1216	£149
PP546	PicoLog 1012 with terminal board	£105
PP543	PicoLog 1012	£95
PP545	Terminal board only	£15

Contact Pico Technology or your distributor for up-to-date US dollar and euro prices. Errors and omissions excepted.

PicoScope, PicoLog and Pico Technology are trademarks of Pico Technology. Windows XP and Vista are trademarks of Microsoft Corporation.



Pico Technology, James House, Colmworth Business Park, St Neots, Cambridgeshire, PE19 8YP, UK
 T: +44 (0) 1480 396 395 F: +44 (0) 1480 396 296 E: sales@picotech.com

www.picotech.com

DO163-1

Copyright © 2009 Pico Technology

Specification of the WELSEE (WS-MPPT 30) solar charger

ANNEXURE E

MPPT solar charge controller



WELSEE WS-MPPT30 20A 48V Solar Battery Charge Controller

WELSEE MPPT30 battery charger controller

This WS-MPPT battery charger controller(also known as WELSEE intelligent solar charge controller, solar charge controller, PV controller) can intellige working voltage of solar panels, letting the solar panels always work at Maximum Power Point of V-A curve. Compared with ordinary solar controller, it increase the efficiency of PV modules by 10%-30%. WELSEE WS-MPPT solar controllers 10A--60A include 12V series, 24V series and 48V series.

MPPT advantage:

Maximum Power Point Tracking (MPPT in short) system is a system which allows PV panels to outputs more Power by adjusting working condition of it. Figure 1 A indicates that the ordinary controller, which makes PV battery work on 12V ,only outputs a power point of 53W (a general power point), B controller makes PV battery always work at the maximum power point, thus outputs the power point of 75W (the maximum power point).

Product features:

- Applicable to various types of batteries,
- MPPT function
- Temperature sensor battery charging compensation
- Overload protection (automatic restoration)
- Overcharge protection
- Short circuit protection (automatic restoration) ,
- Thunder protection
- Reverse discharge protection
- Reverse polarity connection protection (automatic restoration)
- Under voltage protection

MPPT principle:

The maximum power point is mainly affected by the ambient temperature and the intensity of sunshine. The intensity of sunshine being constant, the power decreases with the rise of the temperature. The temperature being constant, when the sunshine intensifies, the open circuit voltage of PV batti unchanged. But the short circuit current increases substantially, thus the maximum output power increases substantially.

This WS-MPPT battery charger controller can intelligently regulate the working voltage of solar panels, letting the solar panels always work at Maximum curve. Compared with ordinary solar controller, this MPPT controller can increase the efficiency of PV modules by about 30%.

However, due to many different factors, such as the difference in solar panel making, the change the Sun illuminance, change in temperature, the effic etc., the actually available increased rate is 10%-30%.

Model	WS-MPPT30 20A	WS-MPPT30 30A
-------	---------------	---------------

www.tradeage.com/sale/mppt-solar-charge-controller-welsee-ws-mppt30-30a-48v-battery-charger-controller-ce978320

1/5


4/19/13

MPPT solar charge controller, WELLSEE WS-MPPT30 30A 48V battery charger controller Wholesale at tradeage.com

Rated Voltage	12V / 24V / 48V	
Max Load current	20A	30A
Input voltage range	12V~20V / 24V~40V / 48V~80V	
Length≤1m Charge loop drop	0.25V	
Length≤1m Discharge loop drop	0.05V	
Over voltage protection	17V / 34V / 48V	
Full charge cut	13.7V / 27.4V / 54.8V	
Low voltage cut	10.5~11V / 21V~22V / 42V~43V	
Temperature compensation	-3mV/ °C/ cell	
No load loss	≤10mA	≤20mA
Max wire area	4 mm ²	4 mm ²
Ambient temperature	-25°C~+55°C	




WELLSEE




RA12-100S (12V100Ah)


RA12-100S is a general purpose battery with 10 years floating design life, meet with IEC, JIS .BS and Eurobat standard. With heavy duty grid, thickness plates, special additives, RA series battery have long and reliable standby service life. Our RA series batteries keep high consistent for better performance in series usage.




Specification	
Cells Per Unit	6
Voltage Per Unit	12
Capacity	100Ah@10hr-rate to 1.80V per cell @25°C
Weight	Approx. 29.0 Kg
Max. Discharge Current	1000A (5 sec)
Internal Resistance	Approx. 4.8 mΩ
Operating Temperature Range	Discharge: -20°C~60°C Charge: 0°C~50°C Storage: -20°C~60°C
Normal Operating Temperature Range	25°C ±5°C
Float charging Voltage	13.6 to 13.8 VDC/unit Average at 25°C
Recommended Maximum Charging Current Limit	30 A
Equalization and Cycle Service	14.6 to 14.8 VDC/unit Average at 25°C
Self Discharge	RITAR Valve Regulated Lead Acid (VRLA) batteries can be stored for more than 6 months at 25°C. Self-discharge ratio less than 3% per month at 25°C. Please charge batteries before using.
Terminal	Terminal F12/F15
Container Material	A.B.S. (UL94-HB), Flammability resistance of UL94-V1 can be available upon request.





MH28539



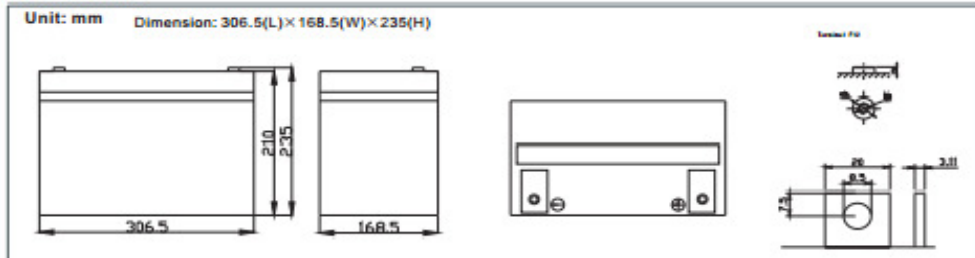
GEM3208-0110-E-15



ISO9001:2000 Certificate

Dimensions



Constant Current Discharge Characteristics: A (25°C)

F.V/Time	5MIN	10MIN	15MIN	30MIN	1HR	2HR	3HR	4HR	5HR	8HR	10HR	20HR
9.60V	320.7	226.9	181.4	112.7	65.00	38.89	26.88	22.03	18.03	12.42	10.50	5.777
10.0V	311.4	215.8	177.7	110.8	64.70	38.60	26.78	21.93	17.93	12.32	10.40	5.672
10.2V	302.2	208.2	174.9	109.8	64.10	38.31	26.57	21.83	17.82	12.22	10.30	5.567
10.5V	271.3	192.1	166.5	107.1	63.50	38.02	26.47	21.62	17.61	12.12	10.20	5.462
10.8V	244.9	175.2	153.5	102.4	62.00	37.33	25.75	21.11	17.29	11.92	10.10	5.357
11.1V	209.1	156.6	137.7	95.91	58.90	35.68	24.62	20.09	16.55	11.41	9.796	5.041

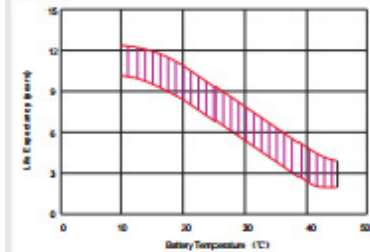
Constant Power Discharge Characteristics: W(25°C)

F.V/Time	5MIN	10MIN	15MIN	30MIN	1HR	2HR	3HR	4HR	5HR	8HR	10HR	20HR
9.60V	3317	2416	1996	1284	751.1	458.4	319.9	262.6	215.1	148.3	125.5	69.26
10.0V	3251	2342	1964	1269	749.3	456.0	320.0	262.3	214.6	147.6	124.7	68.06
10.2V	3214	2280	1941	1260	743.5	453.3	318.6	261.7	213.9	146.6	123.6	66.80
10.5V	2926	2123	1852	1230	736.8	450.0	317.4	259.3	211.3	145.4	122.4	65.54
10.8V	2665	1957	1712	1179	723.2	444.2	308.7	253.4	207.5	143.0	121.2	64.28

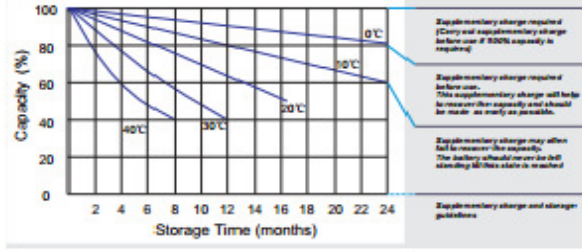
RA12-100S

12V 100Ah 

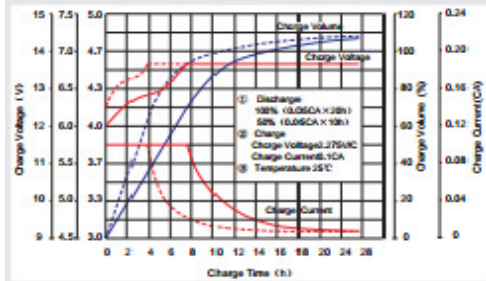
Effect of temperature on long term float life



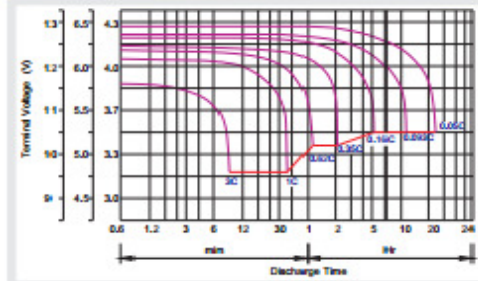
Storage characteristic



Charge characteristic Curve for standby use



Discharge characteristic Curve



Capacity Factors With Different Temperature

Battery Type		-20°C	-10°C	0°C	5°C	10°C	20°C	25°C	30°C	40°C	45°C
GEL Battery	6V&12V	50%	70%	83%	85%	90%	98%	100%	102%	104%	105%
	2V	60%	75%	85%	88%	92%	99%	100%	103%	105%	106%
AGM Battery	6V&12V	46%	66%	76%	83%	90%	98%	100%	103%	107%	109%
	2V	55%	70%	80%	85%	92%	99%	100%	104%	108%	110%

Discharge Current VS. Discharge Voltage

Final Discharge Voltage V/cell	1.75V	1.70V	1.60V
Discharge Current (A)	(A) ≤0.2C	0.2C < (A) < 1.0C	(A) ≥ 1.0C

Charge the batteries at least once every six months, if they are stored at 25°C.

Charging Method:

Constant Voltage	-0.2Cx2h+2.4-2.45V/cellx24h, Max. Current 0.3CA
Constant Current	-0.2Cx2h+0.1CAx12h
Fast	-0.2Cx2h+0.3CAx4.0h

Maintenance & Cautions

Float Service:
※ Every month, recommend inspection every battery voltage.
※ Every three months, recommend equalization charge for one time.
Equalization charge method:
Discharge: 100% rate capacity discharge.
Charge: Max. current 0.3CA, constant voltage: 2.4-2.45V/Cell charge 24h.
※ Effect of temperature on float charge voltage: -3mV/°C/Cell.
※ Length of service life will be directly affected by the number of discharge cycles, depth of discharge, ambient temperature and charging voltage.

Specification of the SW220 poly-crystalline PV panel ANNEXURE G

429113 SolarWorld Sunmodule SW220 Poly 220W 20V Solar Panel



[MY SHOWCASE](#) | [MY ACCOUNT](#) | [LOG IN](#)
 877-211-8192

[BUY](#) | [LEARN](#) | [INSTALL](#) | [SHARE](#)

Search Products

We are no longer offering this product.
 The below information is presented for informational purposes only. You may also find similar items in the category.

[SHOP ALL PRODUCTS](#) Store / Solar Panels

SOLARWORLD SUNMODULE SW220 POLY 220W 20V SOLAR PANEL



[SHARE](#)
[FEEDBACK](#)

[DETAILS](#) | [DOCUMENTS](#) | [REVIEWS](#)

Item code	Model number	Volts	Watts	Cell Tech	Connector Type
SQW220SW220POLY	SW 220 Poly V2	20V	220W	Polycrystalline	MC4 (Solarline 2 locking)

Please Note: Pricing is only valid for SolarWorld modules sold within the USA

SolarWorld Sunmodule SW 220 Poly / Version 2.0 220W Polycrystalline Solar Panel

The SolarWorld Sunmodule SW 220 solar panels herald an innovative new module concept. The Plus-sort (based on a SolarWorld flash report) and five watt model stepping ensures true, highest system efficiency and dispenses with the time-consuming task of sorting the modules on site. The fully automated production process at the SolarWorld factories creates a module quality that is consistently high, which in turn will ensure high yields for the long term.

High-quality, high performance, and high reliability – the SolarWorld Sunmodule is designed and built for long-term yield stability and ease of use. Every module is factory flashed at standard test conditions (STC) to determine the power output and then sorted in 5 watt increments. Only modules with a flashed power that is greater than or equal to the nameplate rated power are delivered. Flash report data is provided with every order.

The patented box channel frame design provides extraordinary stiffness in bending and torsion. The laminate with 4mm glass is set deep in the frame channel and secured with precision applied adhesive. The frame is assembled by press fit to maximize strength and longevity. The result is an extremely robust package that can be mounted in any orientation and can withstand static loads of up to 113 psf.

SolarWorld provides a 5-year workmanship warranty* and 25-year linear performance guarantee*.
 *See warranty statement in the Product Documentation section above for details.

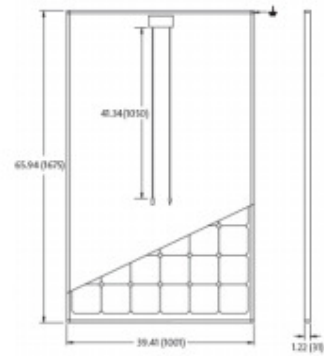



SolarWorld Sunmodule SW220 Poly 220W 20V Solar Panel

- SolarWorld is the largest manufacturer of solar photovoltaic panels in the USA since 1977 and is a \$1 billion world wide solar manufacturer.
- MultiYear Independent testing by Photon magazine confirms that Sunmodules generate up to 10% more kWh per rated kW than other major brands. More kWh means more money in your pocket.
- Sunmodules are tested to withstand hail, extreme heat, high winds and heavy snow loads.
- Sunmodules meet or exceed the latest electrical codes for safety and durability.
- Sunmodules are manufactured in ISO 9001:2000 certified factories and feature:
 - Silicone sealant
 - Tempered glass
 - EVA embedding
 - Solar cell
 - Back sheet
 - High-strength frame
- The Sunmodule's tight +/- 3% power tolerance assures that you get the output you're paying for.

Rated power	P_r	220.20
Peak power	P_{MPP}	220W
Peak power voltage	V_{MPP}	29.2V
Peak power current	I_{MPP}	7.54A
Open circuit voltage	V_{oc}	36.6V
Short circuit current	I_{sc}	8.06A
Max Series Fuse		15A

Dimensions



- VERSION 2.0 FRAME**
- Compatible with "Top-Down" mounting methods
 - Grounding Locations: 4 corners of the frame

Due to continuous research and product improvement the specifications in this Product Information Sheet are subject to change without notice. Specifications can vary slightly. For installation and operation instructions, see the applicable manuals. No rights can be derived from this Product Information Sheet and SolarWorld AG assumes no liability whatsoever connected to or resulting from the use of any information contained herein.



BBB Rating: A+ as of 4/29/2013

[Click for Review](#)

MEMBER

MEMBER

TESTED DAILY 28-JUN

CUSTOMER CERTIFIED 04/26/13 by SolarW

Secured by

Specification of the RADIANT 11 W fluorescent bulb ANNEXURE H


4/29/13 Cool white 3U series energy-saving lamp (CE/EMC),New(E27/B22) 3U series energy-saving lamp (CE/EMC),YS-Lighting Product Details from Jian...

A global marketplace for online sourcing and shopping [A quick guide to using Alibaba.com](#)

Over 2 million supplier storefronts Safe and simple trade solutions Easily access verified suppliers

[Join Free](#) | [My Alibaba](#)

1st year


 **Jiangsu Yongshi Lighting Co., Ltd.**

Home **Products** Company Profile Contacts

Home Products 2U-3U CFL lamp 3U CFL Lamp Cool white 3U series energy-saving lamp (CE/EMC)

search our products

Verified Company


 Jiangsu Yongshi Lighting Co., Ltd.
[Jiangsu, China (Mainland)]
Business Type: Manufacturer, Trading Company
[Onsite Check](#)
No substantiated complaints in last 90 days
Supplier's last login time: **Within 24 hours**
[View Contact Details](#)

[Add Company to Favorites](#)

Products (4803)

- New Products (38)
- 8U CFL Lamp (300)
- 6U CFL lamp (398)
- 5U CFL Lamp (172)
- 4U CFL lamp (818)
- 2U-3U CFL lamp (270)
 - 2U CFL Lamp (104)
 - 3U CFL Lamp (165)
- spiral CFL lamp (1379)
- Halogen lamp (21)
- Lotus and other of lamp (180)
- Flower lamp (25)
- mosquito repellent light (149)
- Plant growing lamp (77)
- PL energy saving lamp (15)
- 2D Lamp (45)
- Glass tube (85)
- LED Spot Lamp (281)
- LED Bulb Lamp (451)
- LED Ceiling Lamp (155)
- LED T5/T8 Tube (128)

Cool white 3U series energy-saving lamp (CE/EMC) Language Option



Cool white 3U series energy-saving lamp (CE/EMC)
[Report Suspicious Activity](#)
[Add to My Favorites](#)

Product Details:

Place of Origin	Jiangsu, China (Mainland)
Brand Name	YS-Lighting
Model Number	YS-4-3U-15W
Principle	CFL
Shape	U
Brand	YONGSHI
Powder	Tri-colour powder
Voltage(V)	110-130/230-240/270~V
Wattage(W)	15
Power factor	0.6
Colour temp(K)	5500-6000
CR	80
Base	E27/B22
Tube dia(mm)	9
Lifespan(h)	10000

Payment & Shipping Terms:

FOB Price:	US \$ 0.92-2.43/Piece Get Latest Price
Minimum Order Quantity:	3000 Piece/Pieces
Port:	Lianyungang
Packaging Details:	1)Color gift box 2)Cartons 3)Packing according to your requirements
Delivery Time:	30days
Payment Terms:	T/T
Supply Ability:	10000 Piece/Pieces per Week

[Place Order via](#) [Buyer Protection](#) ensure your transaction safety

 ...

Detailed Product Description

1)power factor more than 0.75 2)E55lm/W 3) Certification: CE/EMC/ROHS 4)lower light attenuation 5)High lumens efficiency

Product name: **Cool white 3U series energy-saving lamp (3U series lamp)**

Life Time: 10000h
Housing Dia.: 40mm
Lamp size: 40mm*40mm*160mm
Qty/Ctn: 50pcs
Meas.: 42.5cm*22cm*19.5cm

3U series energy-saving lamp(3U series lamp) can be customized according your requirements.
Your enquiry about Large 3U series energy-saving lamp(3U series lamp) will be welcomed and please feel free to contact us.

More 3U series energy-saving lamps

Model	YSL-9-3U-8W	YSL-9-3U-12W	YSL-9-3U-15W	YSL-12-3U-20W	YSL-12-3U-26W	YSL-12-3U-36W	YSL-17-3U-40W	YSL-17-3U-45W
Wattage(W)	8	12	15	20	26	28	40	45
Base	E27/B22	E27/B22	E27/B22	E27/B22	E27/B22	E27/B22	E27/B22	E27/B22
Tube Dia. (mm)	9	9	9	12	12	12	17	17
Color Temp. (K)	2700-6800	2700-6800	2700-6800	2700-6800	2700-6800	2700-6800	2700-6800	2700-6800
Lumens(lm)	520	780	975	1300	1690	1820	2600	2925
Life time(h)	10000	10000	10000	10000	10000	10000	10000	10000
Lamp size(cm3)	40*40*120	40*40*150	40*40*160	50*50*168	50*50*185	50*50*195	65*65*260	65*65*270
Qty/Ctn(pcs)	50	50	50	50	50	50	50	50
MOC(pcs)	5000	5000	5000	5000	5000	5000	5000	5000

Our factory

We are the factory in Jiangsu Province and we are specialized in **LED lamps** and high power **energy-saving lamps**, which is more than 200W.

We can manufacture energy-saving lamps, ranging from **1U to 9U spiral**.

We also make **LED lamps**, such as **LED spot lamps**, **LED ceiling lamps**, **LED bulb lamps**, **LED down lights**, **LED daylight**, **LED street lamps** and so on.

Our service

- Our products can be customized according to your requirement!
- The lumen maintenance rate of our product is up to 95% after 2000h and 80% after 6000h.
- If there is something I can do for you, please contact with me! I will give you the reply within 24 hours.
- Welcome to your inquiry! Thx a lot!



More similar products



Testing equipment

Specification of the RABTRON 10 W LED Lamp

ANNEXURE I



[Contact Us](#) | [Forum](#) | [Home](#) | [How to order online](#) | [Online Catalog](#) | [Products](#)

Online Catalog

For full ranges of Products please visit our Online Catalog www.shop.rabtron.co.za

Components Menu

- ▶ Accessories
- ▶ Adaptors/Power supply
- ▶ Alarms/Security
- ▶ Batteries
- ▶ Cables
- ▶ Connectors & Sockets
- ▶ Electro-Chemicals
- ▶ Electronic Kits
- ▶ Electronic Literature
- ▶ Enclosures
- ▶ Fans
- ▶ Fuses
- ▶ Hardware/Fixings
- ▶ HeatSinks
- ▶ Inductors
- ▶ Light / Sound
- ▶ Motors
- ▶ Opto-Electronics
- ▶ Panel Meters
- ▶ Passive Components
- ▶ PC Boards/Projects
- ▶ PIC Programmers
- ▶ Potentiometers
- ▶ Relays
- ▶ Semiconductors
- ▶ Switches
- ▶ Test And Measurement
- ▶ Tools/Equipment
- ▶ Transformers

LED Floodlights

LED Floodlights

LED Flood Lights look just like the normal halogen flood lights you are used to seeing around car parking lots, stadiums, farms, factories, storage areas, night construction and security lighting.

- Comparing with traditional HPS or Mercury flood lights, our LED flood lights save 50% - 70% electricity cost.
- Comparing with halogen lamps, it saves over 80% electricity cost.
- Lifespan is 3 - 5 times than lifespan of HPS, metal halide and halogen floodlight.
- No maintain cost.
- Eco-friendly - no UV, IR, lead, mercury or air pollution.
- These LED Flood lights are designed for use in many applications from lighting up billboards to shops, factories, agriculture and various other applications.
- The LED Flood light generates significantly less heat and has a much longer life span.
- Use these floodlights for improved visibility. The lights offers a cool and pure light
- Electricity savings with the use of LED Floodlights are huge and of course another way to make South Africa Greener and more environment friendly.

Materials

1. Die-casting aluminium crust
2. High intensity toughened glass cover
3. High-purity aluminum reflector
4. Single high powerful LED light source
5. High efficiency LED driver

Application

1. Factories
2. Gymnasiums
3. Yards
4. Advertising boards
5. Buildings
6. Lawns
7. Garden designs
8. Some other outdoor places where need flood lighting and lights decoration

Search

Use keywords to find the product you are looking for. [Advanced Search](#)

Navigation

- ◆ Home
- ◆ About Us
- ◆ Online Catalog
- ◆ Products
- ◆ Download
- ◆ Contact Us
- ◆ Forum
- ◆ Links
- ◆ Manufacturers
- ◆ Newsletter
- ◆ Query Form
- ◆ Site Map
- ◆ Technical

Newsletter

Subscribe to our mailing list

* indicates required

Email Address



LED Floodlight 10W White - 220VAC

- Input Voltage: 220V AC
- LED Power: 1 piece 10W LED Floodlight
- Colour: White
- Material: Die-cast housing
- IP65
- Angle: 120°
- Chip: Bridgelux



LED Floodlight 30W White - 220VAC

- Input Voltage: 220V AC
- LED Power: 1 piece 30W LED Floodlight
- Colour: White
- Material: Die-cast housing
- IP65
- Angle: 120°
- Chip: Bridgelux